School of Electrical Engineering, Computing and Mathematical Sciences

Thermoelectric Generator Modeling and Power Maximization in Non-Uniform Heat Distribution

Miftah Yama Fauzan

0000-0002-4462-0397

This thesis is presented for the Degree of

Master of Philosophy

of

Curtin University

July 2021

DECLARATION

To the best of my knowledge and belief this thesis contains no material previously published by any other person except where due acknowledgment has been made.

This thesis contains no material which has been accepted for the award of any other degree or diploma in any university.

Miftah Yama Fauzan

July 2021

Statement of Contribution by Others

This thesis is based on the research journals "Experimental Modelling of Grid-tied Thermoelectric Generator from Incinerator Waste Heat", published in International Journal of Smart Grid and Clean Energy, 2020, and "Enhanced Power Extraction from Thermoelectric Generators Considering Non-uniform Heat Distribution," Journal of Energy Conversion & Management, Elsevier, 2021, and it is my own work except following contributions of co-authors:

Prof. S.M. Muyeen – Conceptualisation, supervision and critical revision of paper.

Syed M. Islam – Conceptualisation, supervision and critical revision of paper.

Signature of Candidate Miftah Yama Fauzan

Signature of Principle Supervisor S.M. Muyeen

ACKNOWLEDGEMENTS

I am truly thankful to my supervisor, Assoc. Prof. S.M. Muyeen and co-supervisor, Prof. Syed Islam for their guidance, patience and constant encouragement throughout my master's study. Without their support, it would be very difficult to complete this thesis.

I would also like to thank the rest of my thesis committee and all the staff members of the Department of Electrical Engineering and Computing and Mathematical Sciences, Curtin University, for their help and support in my thesis.

Finally, I would like to thank my mother, Rosi Indarjani, my father, Mochamad Ashari, and my beloved wife Dinsa Celia Putri for always providing me with endless support, love, and continuous encouragement throughout the years of my master study, writing journal papers and this thesis.

Miftah Yama Fauzan

July 2021

ABSTRACT

The non-uniform heat distribution of a thermoelectric generator is equivalent to the partial shading event of the photovoltaic system, and hence, it is identified as a critical aspect in maximizing electrical output. In this thesis, a technique to enhance the performance of the thermoelectric generator under non-uniform heat distribution is developed. A large area of heat source is needed when the thermoelectric generator is used for high power applications such as powering air conditioners, household appliances, and distributed generation systems. Non-uniform heat distribution is a natural phenomenon in the large surface of the heat source, which results in the voltage diversity of each thermoelectric generator; therefore, the output power of the arrays drops significantly. One of the objectives of this study is to model the thermoelectric generator system for high-power applications under non-uniform temperature distribution. The parameters of the model, including the internal voltage source in series with an equivalent resistance, are determined from experimental analysis. The model has successfully demonstrated the performances of a thermoelectric array connected to the grid under uniform and non-uniform heat distribution conditions. A method of maximizing power, i.e., developing a specialized maximum power point tracker (MPPT) along with blocking diodes, is proposed to overcome the effects of non-uniform heat distribution. The proposed MPPT uses a modified perturbed and observed technique to extract the peak power under the change of partial surface temperature, as well as the change of loads. A prototype of a thermoelectric generator

is developed for verification purposes. A rigorous comparative study is conducted as well between the model outputs and the experimental scenarios.

TABLE OF CONTENTS

Declaration i

Statement of Contribution by Others ii

Acknowledgements iii

Abstract iv

Table of Contents vii

List of Figures viii

List of tables xiii

List of Abbreviations xiv

CHAPTER I : INTRODUCTION 3

1.1 Research Goal 3
1.2 Contribution of the Thesis 5
1.3 Thesis Organization 6
CHAPTER 2 : LITERATURE REVIEW 8

2.1 Introduction 8
2.1.1 Wearable TEG 8
2.1.2 Ground and Ambient Temperature TEG 14
2.1.3 Solar Dish Concentrator TEG 15
2.1.4 Waste Heat Recovery TEG 16
2.2 Power Processing Unit 20
2.3 Inverter System used in this study 27
2.4 Conclusion 30
CHAPTER 3 : THERMOELECTRIC SYSTEM MODELING 32

3.1. Non-uniform Temperature Distribution 32
3.2. Brief Thermodynamics Review of a Thermoelectric Device 33
3.3. Modeling of a Thermoelectric Generator involving Material Properties 35
3.4. Modeling of Thermoelectric Generators for High-Power Applications 39
3.5. The Proposed Model 42
3.6. The Prototype Building, Testing, and Modeling 47

3.4.1 Prototype Building 48
3.4.2 Prototype Testing 56
3.4.3 Prototype Modeling 61
3.7. Modeling of a Thermoelectric Panel 64
3.8. Modeling of a Thermoelectric String and a Thermoelectric Array 68
3.9. Conclusion 69
CHAPTER 4 : THERMOELECTRIC SYSTEM PERFORMANCEUNDER NON-UNIFORM TEMPERATURE DISTRIBUTION 71
4.1. Results V-I Characteristics of Thermoelectric Module 71
4.2. Performance of a Thermoelectric Panel under a Non-Uniform Heat Distribution 74
4.3. Conclusion 80
CHAPTER 5 : MAXIMIZING METHOD OF A THERMOELECTRIC GENERATOR 81
5.1. Improvement using a Diode 81
5.2. Improvement using MPPT 83
5.3. Conclusion 92
CHAPTER 6 : CONCLUSION 96
6.1. Recommendations for future research 96
Publications arising from this thesis 108
APPENDIX 109

LIST OF FIGURES

Fig. 1.1 Scope of study..... 5

Fig. 2.1. Zone diagram of human temperature 9

Fig. 2.2. Model of thermal generator and thermal load 10

Fig. 2.3. Change in temperature difference as function of time after hand movement 11

Fig. 2.4. TEG is integrated in textile 12

Fig. 2.5. Micro-converter for power processing unit of thermoelectric 13

Fig. 2.6. wireless EEG powered by thermoelectric micro-converter 13

Fig. 2.7. wireless EEG powered by thermoelectric micro-converter…….……14

Fig. 2.8 Model of harnessing energy from the ground and ambient temperature …..14

Fig. 2.9. Solar concentrator as heat source of thermoelectric generator……..….....16

Fig. 2.10. TEGs with the electric power processing unit on car exhaust system 17

Fig. 2.11. Gradient temperature on a household chimney [41]..... 18

Fig. 2.12. The test results of the power generated as function of temperature difference [42] 19

Fig. 2.13. Design of gas combustion power plant for thermoelectric 19

Fig. 2.14. Power processing unit for thermoelectric generator 20

Fig. 2.15. Open loop Boost dc-to-dc converter 20

Fig. 2.16 Open loop flyback converter 21

Fig. 2.17 DC to DC converter and controller for MPPT..... 24

Fig. 2.18 Principles of MPPT pre-setting algorithm..... 25

Fig. 2.19 Flow chart of perturbed and observed MPPT 26

Fig. 2.20 Sinusoidal PWM inverter with volatge-controlled method 29

Fig. 2.21 Sinusoidal PWM inverter with current-controller method 29

Fig. 2.22 The proposed system of thermoelectric generator application 31

Fig. 3.1 Temperature distribution in solid waste incinerator 33

Fig. 3.2 Basic concept and modelling of thermoelectric energy conversion 34

Fig. 3.3 Figure of merit *ZT* as function of temperature of various materials [8]……37

Fig. 3.4 Thermoelectric efficiency in generating and cooling types [12] 38

Fig. 3.5 Heat conversion to electric parameter with Seeback coefficient 40

Fig. 3.6 Models of thermoelectric generator utilize electric equivalent circuit [28].. 41

Fig. 3.7 The diagram of thermoelectric model in electrical equivalent circuit 43

Fig. 3.8 Flowchart diagram of the proposed modelling technique 46

Fig. 3.9 Thermoelectric generator and water block configuration..... 48

Fig. 3.10 Placement of the thermal tape between the TEG and water block 49

Fig. 3.11 Thermoelectric cells placed on both sides of the water block 50

Fig. 3.12 Thermoelectric modules arrangement 51

Fig. 3.13 Temperature probe placement 51

Fig. 3.14 Thermoelectric generator (A-D) multiple angle view (E1, E5) hot side(E2, E4) thermoelectric cells (E3) water cooling blocks (E6) inlet and outlet water pipes 52

Fig. 3.15 Heating element for a controllable heat source 53

Fig. 3.16 Complete set of the heating system and control 54

Fig. 3.17. Prototype of thermoelectric generator module and the control system 54

Fig. 3.18. Prototype and equipment setup 55

Fig. 3.19. Experimental results of open circuit voltage (V_{oc}) vs. temperature difference (ΔT) 57

Fig. 3.20. Comparison of experimental tests and linearized model 58

Fig. 3.21. Experimental results and linearized model of short circuit current (I_{sc}) as function of temperature difference (ΔT) 59

Fig. 3.22. The model of internal resistance (R_s) as function of temperature difference (ΔT) 60

Fig. 3.23 The model of the prototype representing 24 thermoelectric in series 62

Fig. 3.24 The PSIM circuit of 24 TEGs in series with variable resistor load 63

Fig. 3.25. PSIM model of 2 x 3 thermoelectric prototype units in series and parallel 64

Fig. 3.26. Model of thermoelectric panel under uniform heat, 96 Watts, 120 Volts .66

Fig. 3.27. Structure of thermoelectric array, 3600 Watts/ 720 Volts 67

Fig. 4.1 The terminal voltage of the prototype at ΔT=65°C and various load resistances 72

Fig. 4.2 The load current of the prototype at ΔT=65°C and various load resistances 73

Fig. 4.3 Output power of the prototype at ΔT=65°C and various load resistances ... 73

Fig. 4.4 Equivalent circuit of TEG panel when exposed to non-uniform heat distribution 75

Fig. 4.5 Simplified circuit of TEG panel with non-unifrom heat distribution 75

Fig. 4.6 Thermoelectric output power with uniform heat and various ΔT 77

Fig. 4.7 Power of thermoelectric panel during load tests under non-uniform heat.... 77

Fig. 4.8 Volatge of thermoelectric panel during load tests under non-uniform heat . 78

Fig. 4.9 Current of thermoelectric panel during load tests under non-uniform heat.. 78

Fig. 4.10 The current of each line inside TEG panel under non-uniform heat distributtion 79

Fig. 4.11 The output power under dynamical heat distribution 80

Fig. 5.1 Blocking diodes to prevent reverse current flowing to the thermoelectric ... 82

Fig. 5.2 The improved output power when diode is attached 82

Fig. 5.3 The negative current of thermoelectric was blocked by diode 83

Fig. 5.4 MPPT with Buck DC-to-DC converter and the controller 84

Fig. 5.5 Constant increment of duty cycle to catch the maximum power 85

Fig. 5.6 The MPPT controller using modified perturbed & observed method 86

Fig. 5.7 Principles of modified perturbed & observed method 87

Fig. 5.8 The output power of a thermoelectric string under load change with MPPT. 88

Fig. 5.9 The output voltage of MPPT attached to a thermoelectric string under load change 89

Fig. 5.10 The output power of thermoelectric string under non-uniform temperature with MPPT 89

Fig. 5.11 Complete diagram of the proposed system 90

Fig. 5.12 Inverter and the control system 91

Fig. 5.13 Thermoelectric grid-connected system when meeting deep & rapid temperature changes 91

Fig. 5.14 The voltage and current waveform during deep and rapid changes of temperature..... 92

LIST OF TABLES

Table 3.1. Experimental results of TEC1-12706 for generating electricity [13]..... 56

Table 3.2. Results from experimental tests of the prototype 58

Table 3.3. Operating point of thermoelectric systems at ΔT=70^{o}C 65

Table. 4.1. Experimental tests of the prototype at ΔT = 65^{o}C under various loads... 72

Table 4.2. Peak power and the voltage under various gradient temperature 76

List of Abbreviations

DG	Distributed generation
MPP	Maximum power point
MPPT	Maximum power point tracker
MUX	Multiplexer
P&O	Perturb & Observe
PV	Photovoltaic
PWM	Pulse width modulation
SPWM	Sinusoidal pulse width modulation
TEC	Thermoelectric cooler
TEG	Thermoelectric generator

CHAPTER 1
INTRODUCTION

Thermoelectric generation (TEG), originating from the abundant thermal energy in the environment, has become a promising alternative energy source. Various sources of thermal energy, such as body temperature, exhaust pipes of vehicles, chimneys, and solar concentrators, can be converted to electric power via a thermoelectric generator. The TE conversion method is environmentally friendly because it is based on a physical process that directly converts thermal energy to electricity. Other advantages of a TEG system include silent operation, no moving parts, long lifetime, and environmental friendliness. A wide variety of applications have demonstrated the promise of TEG technology, such as micro-power applications (e.g., wearable devices, medical devices, and Internet of Things sensors) and high-power applications (e.g., power generators in space (RTEG), automotive industry, geothermal power harnessing, and distributed power plants).

Despite its advantages, important challenges of TEG technology that must be assessed in the near future include improving semiconductor materials to improve its efficiency, which is currently around 5%. Real-world application of TEG technology requires further improvement in the efficiency of the conversion of thermal energy into electrical energy.

Most TEG researchers in the world are focused on three fields of research: the development of a high efficiency material, thermoelectric generator modeling, and applications of TEG systems [1-12]. Two types of thermoelectric devices based on

established research have been industrially produced: TEG devices for power generator applications and thermoelectric cooling (TEC) devices for cooling system applications. Both types of devices involve similar materials, device constructions, and characteristics; however, TEG and TEC devices are slightly different in terms of efficiency and operating temperature. A typical TEG device has a soldering temperature that exceeds 200^{o}C, whereas a TEC devices has a maximum soldering temperature of 138^{o}C. In terms of market price, a TEG device is approximately 15 times more expensive than a TEC device [13].

Because a thermoelectric device involves the conversion of one form of energy onto another, it can be modeled under the scope of thermal and electrical material properties. The modeling of thermoelectric generators in the literature primarily involves the thermal material property for energy conversion process in the device. Thus, material selection, architecture of design, and manufacturing process must be considered in the model. As a result, the models vary greatly in the literature [14-23]. In contrast to the majority of models, modeling of a TEG in terms of an electrical equivalent circuit has rarely been conducted, with any equivalent circuit work being typically a small part of the entire material analysis.

In applications, researchers have primarily studied thermoelectric generators for use as a micro-power supply for wearable devices, medical devices, Internet of Things sensors, etc. Because such studies involve small-size devices, the modeling of such a small TEG device exposed to a source of a non-uniform distribution of heat has not been considered [14-23]. In contrast to the large amount of research on TEG devices for low-power applications, few research works have considered high-power

applications [24-30]. A TEG system for high-power applications requires a large surface of high temperature as the source of energy. In this case, the distribution of heat temperature may not be uniform. High-power applications also require other models involving larger systems that allow for the use of a pure electrical equivalent circuit.

In this thesis, applications of a thermoelectric generator for a high-power system are discussed. A model of a large system that is extended from individual TEG devices is considered. The modeled system performances involve the use of a thermal source with a non-uniform temperature distribution.

1.1 Research Goal

The research goals are as follows:

- Modeling and analysis of a large TEG system under the presence of a thermal source with a non-uniform heat distribution based on an electrical equivalent circuit and basic laboratory tests, e.g., open circuit and short circuit tests;
- Develop a method to maximize the electrical power output of thermoelectric generators.

A literature review was conducted prior to performing the state-of-the art modeling of applications of thermoelectric generators. To enhance the accuracy of the model, a prototype of a TEG system with a capacity of 80 Volts/ 2 Amperes maximum was built. Data sets from laboratory tests were used to develop further models of large thermoelectric systems and analyze the system performances. Based on the analysis,

a method of maximizing the output power was proposed. Applications of TEGs for grid-connected system with MPPT were also demonstrated. The scope of this study is shown in Fig. 1.1.

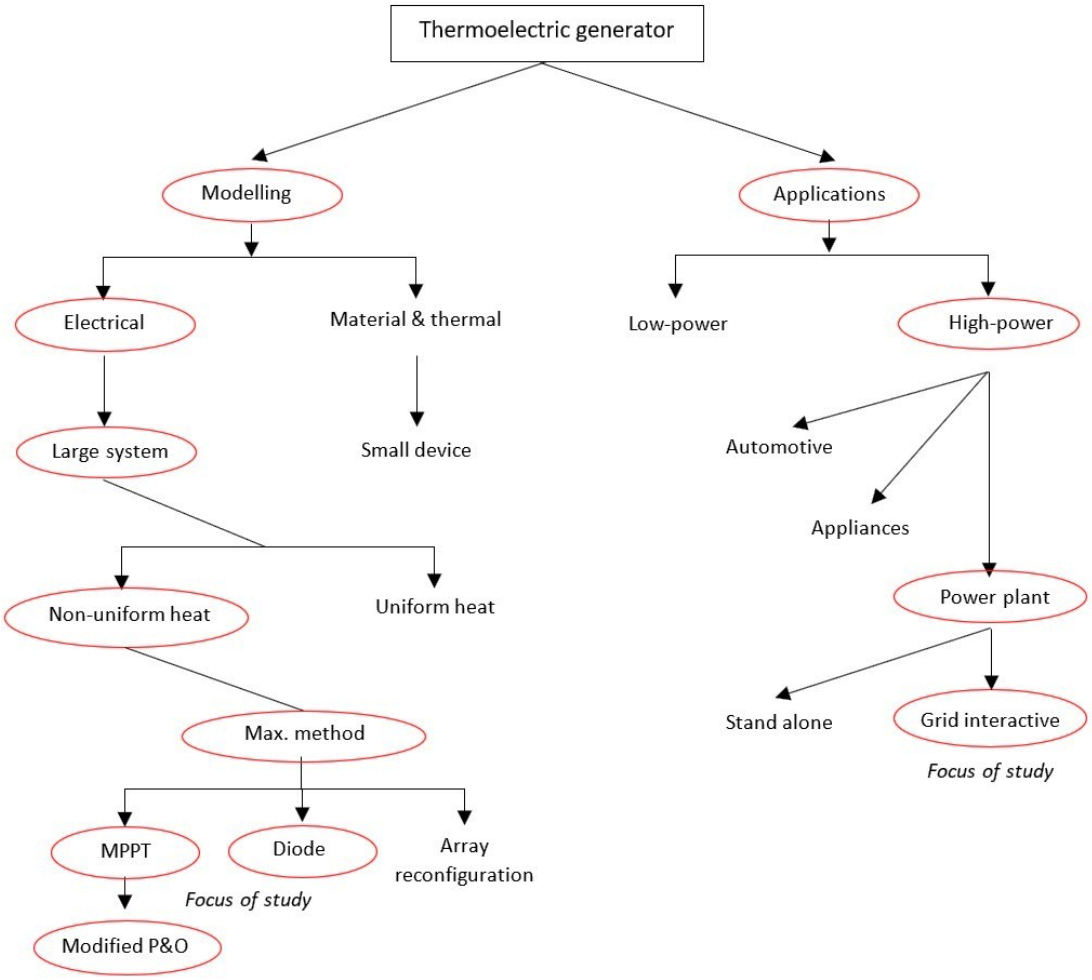

Fig. 1.1. Scope of the study

1.2 Contribution of the Thesis

The Thesis presents three contributions to the knowledge in the field of study, especially in related to the modelling and maximizing power in the large-scale thermoelectric under non-uniform heat distribution. The contributions are as follows:

1. The proposed and development methodology to model the TEG for high power applications. A novel scheme to build a model of single cell and array of TEG is presented.

2. The performance characteristics of TEG under non uniform heat distribution. Results from laboratory test of the prototype built prior to detail simulations support the findings. It is also shown that the proposed TEG model is an effective one to represent the appropriate electrical characteristics of the TEG.

3. The method of achieving maximum power under normal and non-uniform heat distribution. It presents the proposed modified perturbed and observed scheme of Maximum Power Point Tracker for the TEG array.

1.3 Thesis Organization

This thesis is organized as described in the following. The first part introduces the basic concept of a thermoelectric generator, types of TEG models, TEG applications, and the scope of the study. Chapter 2 presents a literature review covering thermoelectric applications, TEG heat sources, TEG models, and maximization methods of a TEG system.

Chapter 3 discusses the modeling of a thermoelectric system. The proposed model is also described. The modeling steps to go from a single device to a larger system (such as a thermoelectric module consisting of several devices, a panel, a string, and an array) are explained. The relevant equations for the model were developed, and the model was used to simulate a TEG device. A prototype of a thermoelectric generator was built and used to collect test data. Finally, the chapter presents the details of the

construction of the prototype, the concept of the prototype, and the measured parameters.

Chapter 4 focuses on the system performances of thermoelectric generators. A TEG panel, a string of TEG panels, and an array of TEG panels are operated under uniform and non-uniform temperature distributions. The highlights of the system performances are noted in this chapter.

Chapter 5 deals with the proposed maximization methods. The methods are based on the findings of Chapter 4. Two methods are proposed to maximize the power output of thermoelectric systems: using a blocking diode and using MPPT.

The conclusion is presented in Chapter 6.

CHAPTER 2
LITERATURE REVIEW

2.1 Introduction

This chapter presents a literature review of thermoelectric generator applications. There are two main applications of TEG systems: low-power and high-power applications. A wearable device (such as a watch, a sensor for medical devices, and an internet of things device) requires a low power electrical supply. High-power applications involve the use of thermoelectric generators to power air conditioning systems, lighting systems, house-hold appliances, etc. This thesis considers a TEG system for high-power applications in which a large system of thermoelectric generators is designed to inject power into the grid. A comprehensive review of the application of thermoelectric generators is presented that covers both low-power and high-power applications as well as the relevant power processing unit.

2.1.1 Wearable TEG

The human body is one of the favorable heat sources for thermoelectric generator applications. Heat from a human body can be used to supply power to a wearable device (such as a watch, a sensor for medical equipment, or a communication device); however, different parts of the body are at different temperatures. For example, the chest area is the warmest part of the human body. A zone diagram of human body temperature presented in reference [31] is shown in Fig. 2.1.

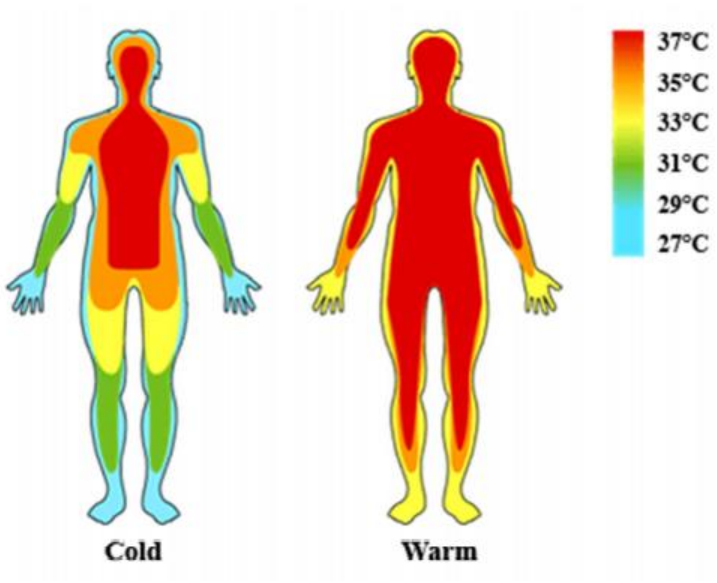

Fig. 2.1. Zone diagram of human temperature [31]

A person emits 100–120 W of heat under the resting condition. During a period of average load, such as walking at 5 km/ hour, the heat emitted is 300 W. During a period of heavy work or sport, the body emits 500 W. The temperature on the skin depends on the human thermal resistance. A model of the human body heat source, as illustrated in Fig. 2.2, was developed in reference [31].

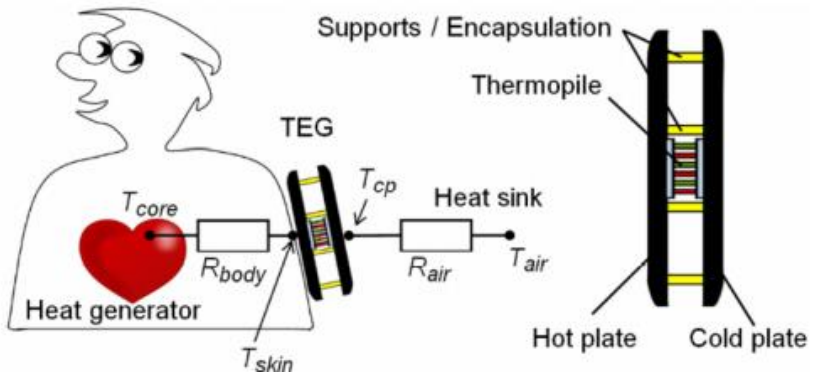

(a)

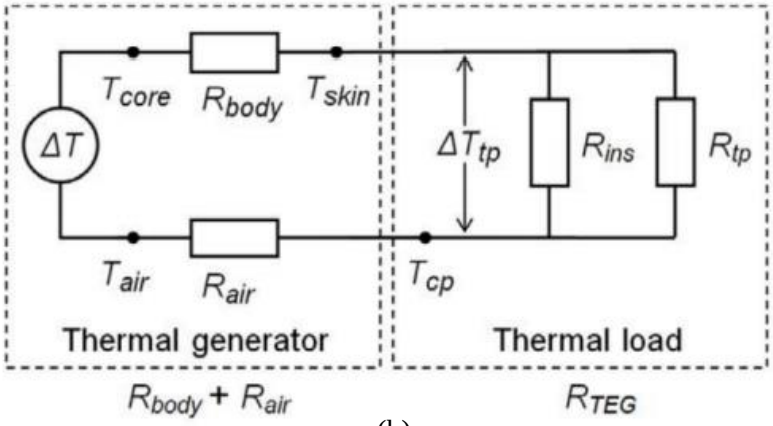

(b)

Fig. 2.2. Developed model of (a) the thermal generator and (b) the thermal load [31]

The model shown in Fig. 2.2 employs a TEG to convert the gradient (ΔT) between the heat generated (T_{core} = 37°C) and room air temperature (T_{air}). The skin temperature (T_{skin}) depends on the body resistance (R_{body}). The gradient of thermopile temperature (ΔT_{tp}) represents the difference between the cold plate temperature (T_{cp}) and the hot plate temperature. The total TEG resistance (R_{TEG}) involves the combination of the parameters in the thermopile, including the internal resistances (R_{ist}) and (R_{tp}). The specific resistance value is R_{body} = 200–500 cm^2 K/W, the air resistance value is R_{air} = 500–1000 cm^2 K/W, and the optimum total TEG resistance value is R_{TEG} = 300–800 cm^2 K/W. Using this model, the heat flow W is given as follows:

$$W = \frac{\Delta T}{R_{body}+R_{air}+R_{TEG}} \quad (2.1)$$

A system based on the model was designed to supply an electronic watch [31]. When the hand of the wrist bearing the watch was immobile, the temperature was found to change dynamically as a function of time, as shown in Fig.2.3. The skin area for the thermoelectric generator is 9 cm^2, with ΔT reaching 0.9°C–5.2°C, thereby generating a voltage of 20 mV–200 mV. This condition is sufficient to activate the electronic circuit and maintain the output voltage at a constant value.

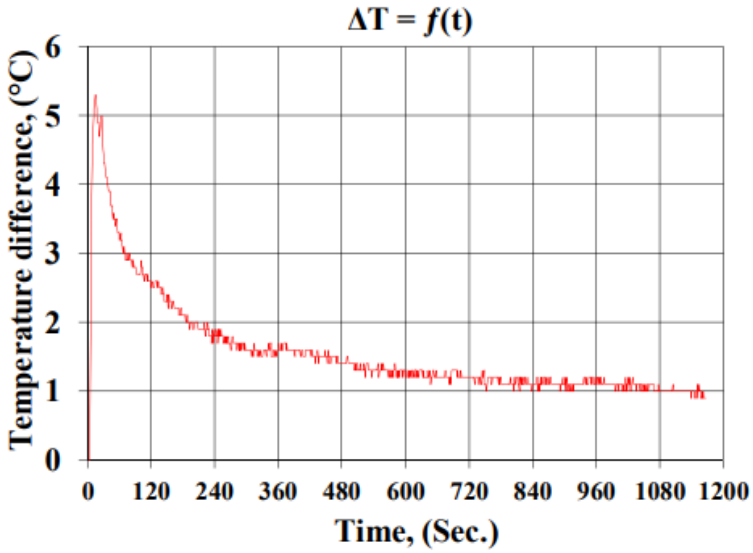

Fig. 2.3. Temperature difference as a function of time after hand movement [31]

Using the same model, a TEG placed in the human body for supplying other wearable devices, such as an electroencephalogram (EEG) and an accelerometer, was studied [14-16], [32-34]. A thermoelectric generator as an energy harvester was seamlessly integrated into a textile or office shirt [35]. This integrated TEG was tested under

actual daily activity conditions. The thermoelectric generator was found to provide 0.5 mW–5 mW of power over a range of ambient temperatures of 27°C–15°C. The hotplate area was 5 cm^2, and the radiator area was 9 cm^2. Fig. 2.4 shows the architecture of the TEG embedded into a textile.

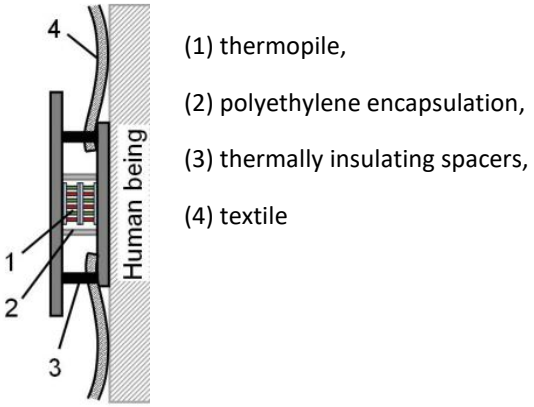

Fig. 2.4 TEG is integrated into a textile [35]

Amin Nozariasbmarz et al. presented research involving the placement of a thermoelectric generator in a wrist, chest, and arm [32]. A power processing unit is required to boost the voltage up to the standard voltage supply for an electronic device. The power processing unit includes a rectification unit, a dc-to-dc or dc-to-ac converter, and a voltage regulator. The embedded system may use a rechargeable battery or be directly connected to the regulator. Joao Paolo Carmo et al. used a micro-converter or a step-up dc-to-dc converter to boost the voltage. Fig. 2.5 shows the circuit of the boost converter.

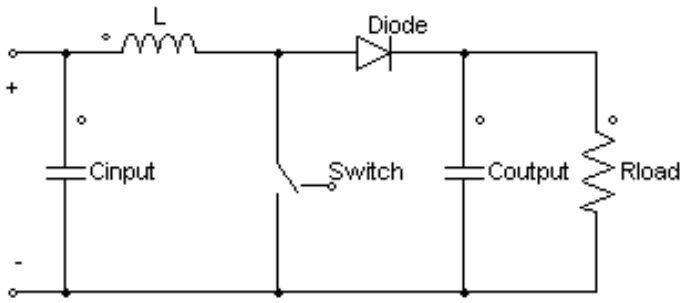

Fig. 2.5 Micro-converter for the power processing unit of a thermoelectric generator [22]

The micro-converter was proposed as a means to supply ultra-low power to electroencephalogram (EEG) amplifiers. An integrated system of human temperature power and wireless electroencephalograms, as illustrated in Fig. 2.6, was demonstrated.

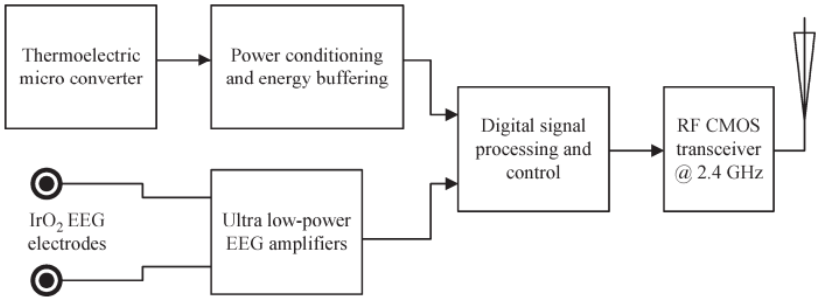

Fig. 2.6 A wireless EEG powered by a thermoelectric micro-converter [22]

A study of an accelerometer attached to the wrist and powered by a thermoelectric generator was presented in reference [34]. The accelerometer detected three-axis accelerations during the period of wrist movements. The TEG dimensions were 22 mm in width and 24 mm in length. At $\Delta T = 18$ K, the generated output power of the thermoelectric was 45 μW. The minimum voltage and power consumption of the

accelerometer were 1.6 V and 2.4 μW, respectively. A step-up dc-to-dc converter was used to amplify the thermoelectric output voltage. The converter involved a transformer to achieve high gain voltage amplification and an integrated circuit to regulate the voltage, as shown in Fig. 2.7.

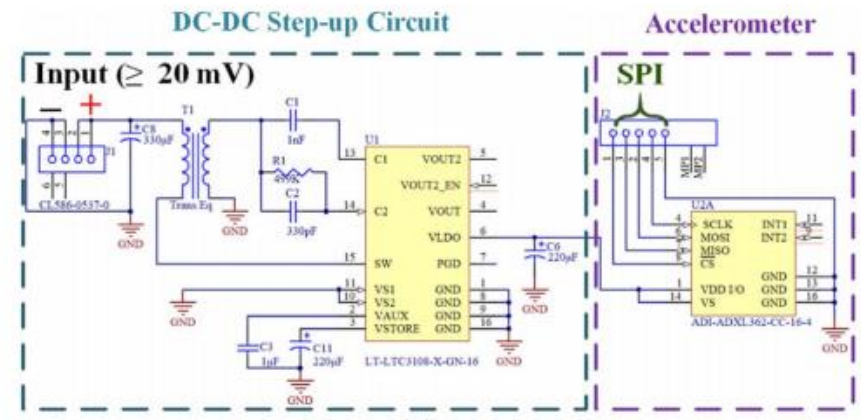

Fig. 2.7. Power conditioning unit for an accelerometer [34]

2.1.2 Ground and Ambient Temperature TEG

Harnessing power from the temperature difference between the earth and the ambient atmosphere was proposed in reference [36]. In that study, a TEG is placed between a black body radiator to absorb heat in ambient and a thermal guide connected to the ground at depth.

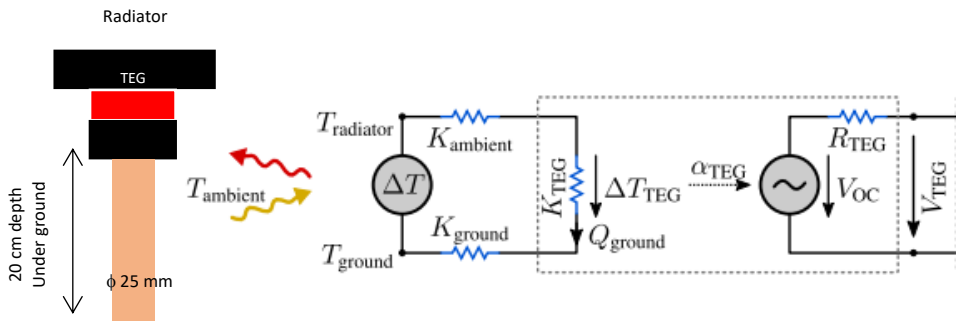

Fig. 2.8 Model of harnessing energy from the temperature difference between the ground and the ambient atmosphere [36]

Fig. 2.8 shows the basic diagram of the model. The gradient temperature ΔT transfers heat through the thermoelectric to the ground via a thermal guide of 25 mm in diameter. The ambient resistance ($K_{ambinent}$) and the ground resistance (K_{ground}) attenuate the heat transferred. The heat generates a voltage (V_{oc}) due to Seeback effect α_{TEG}. The voltage generated powers the load through the equivalent internal resistance R_{TEG}. The system generated the peak power of 27.2 mW during a sunny day and 6.3 mW during night-time.

2.1.3 Solar Dish Concentrator TEG

A solar dish concentrator is another promising heat source for thermoelectric generators [37]. Highly concentrated thermal energy can be collected in an area as small as 5x5 cm^2. The concentrator uses 2 reflective dishes to allow the thermoelectric generator, Stirling engine, or other thermal harvester to be placed on the ground beneath the main dish, as shown in Fig. 2.9. This architecture allows for a lighter mounting structure compared to the mounting structure involving a single disk that requires the thermal receiver to be mounted above the disk. With a thermoelectric generator placed on the concentrator, at the temperature difference of 59^oC, the voltage generated was 2.3 V.

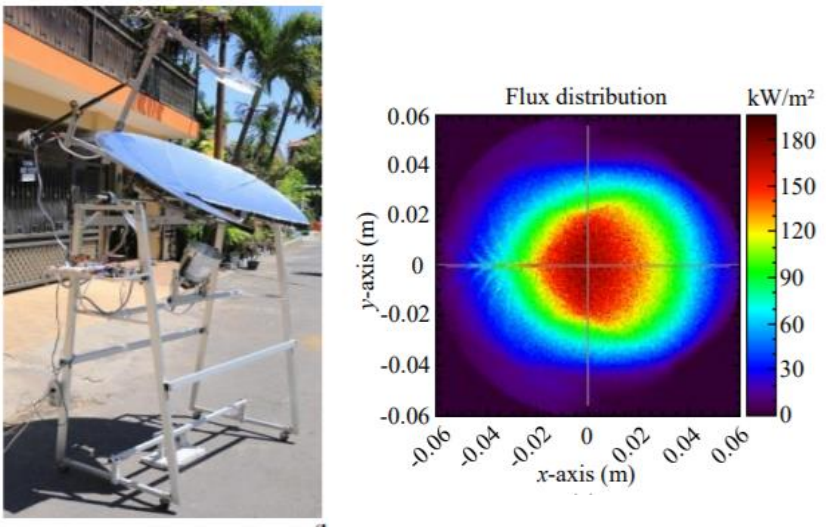

Fig. 2.9 Solar concentrator as a heat source for a thermoelectric generator [37]

The use of car exhaust, chimney exhaust, or other combustion systems as a heat source was introduced in references [38-39]. Because this system employs a larger area of heat source, several series and parallel connections of thermoelectric generators were used, instead of a single thermoelectric generator device. The system is capable of providing power to interior automotive equipment, household appliances, and power plants. An economic analysis found that a TEG system has the favorable characteristics of low operation and maintenance costs, no moving parts, and ability to use of abundant thermal energy [24].

2.1.4 Waste Heat Recovery TEG

Applications for waste heat recovery in a commercial vehicle were introduced [25] by Arash [38]. The thermoelectric system was placed into two sub-systems of car exhaust: the ATS (after treatment system) sub-system with 224 TEGs and the EGR (exhaust gas recycling) sub-system with 240 TEGs. The experiment showed that when the

engine speed was 1000 rpm at 25% load, the ATS temperature was in 248^{o}C and the EGR temperature was 318^{o}C. When the engine speed was 1300 rpm at full load, the ATS temperature was 396^{o}C and the EGR temperature was 560^{o}C.

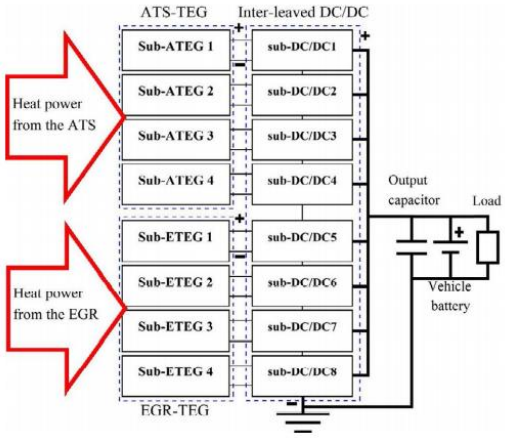

Fig. 2.10. TEGs with an electric power processing unit on a car exhaust system [38]

Fig. 2.10 shows the TEG structure diagram in the ATS and EGR system. The TEGs are separated into 4 sub-systems, for which ΔT is similar to each other. Each TEG sub-system is attached to an electric power processing unit. The system was capable of harnessing 1 kW of electricity from a total of 170 kW of waste heat in combustion vehicles.

Harnessing energy and analysis of heat from a chimney was presented in references [38, 40]. Experimental application of TEGs on a residential incinerator chimney was presented in reference [38]. The temperature was varied up to 300^{o}C. A prototype of 24 series TEGs was found to successfully generate power up to 20 W at the voltage of 46.5 V and the current of 0.43 A.

The temperature gradient in a household chimney was analyzed by Daniel Rudisser (41). The chimney was formed by a precast brick of 20 cm in diameter. The inner chimney temperature was around 90°C, and the outside temperature in the room surrounding the air fresh channel was 25.9°C.

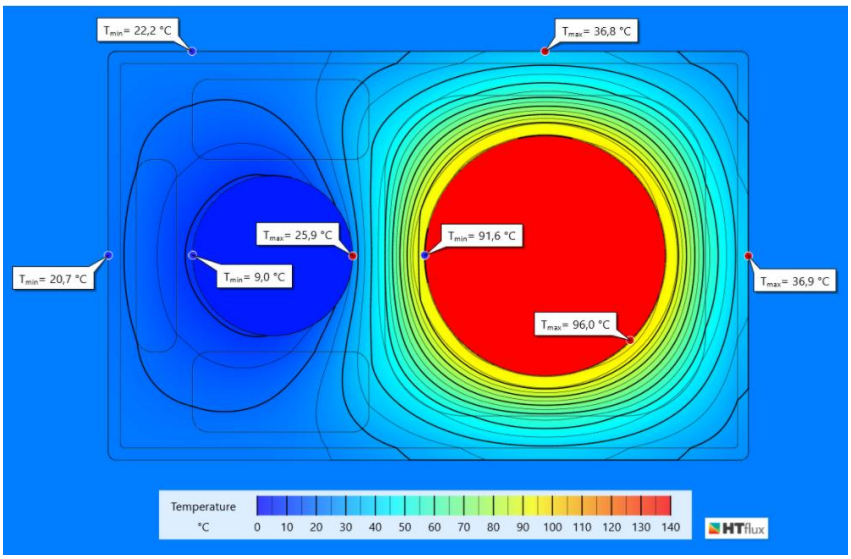

Fig. 2.11. Temperature gradient in a household chimney [41]

Other high-power thermoelectric applications, namely, heating and refrigeration systems, were proposed by researchers in reference [26]. One of them was TEGs for low temperature geothermal sources presented by Liu et al. [27]. The geothermal source studied produced a 120°C heat difference to drive a 1 kW thermoelectric power generator. The experiment proved that power was generated in direct proportion to the temperature gradient. A system containing 96 TEG modules of Bi_2Te_3 type, 16 cm^2 area, and 127 couples with the cost of US$ 3.4 each was proposed in reference [42]. During the test period, the system was operated using 100°C hot water and 20°C tap

water. The output power remained constant at 160 W. The relationship between the temperature difference and the power generated is shown in Fig. 2.12

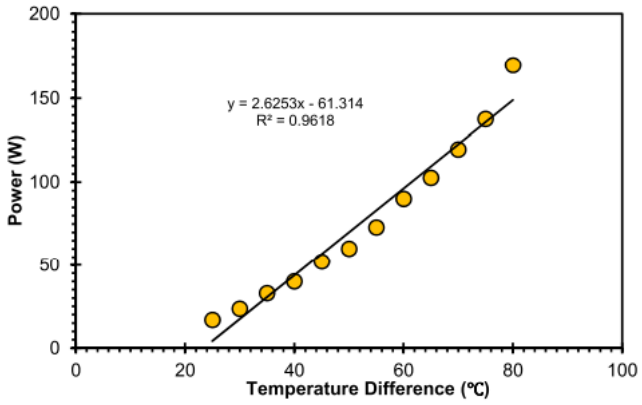

Fig. 2.12. The test results of the power generated as a function of the temperature difference [42]

A design of a gas combustion source with a thermoelectric generator, as shown in Fig. 2.13, was presented in reference [43]. That study found that an open loop 500 MW gas turbine can generate 5.9 MW electricity via a thermoelectric generator.

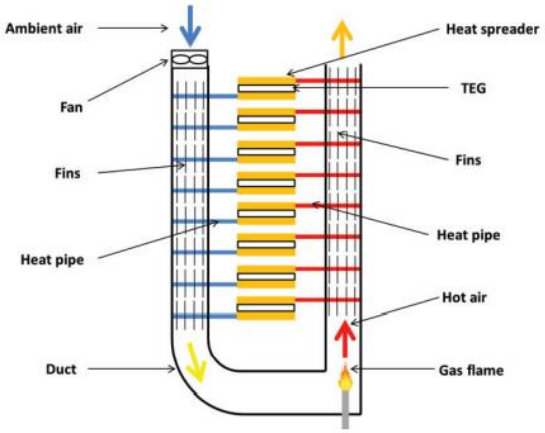

Fig. 2.13. Design of a gas combustion power plant for thermoelectric generation [43]

2.2 Power Processing Unit

A thermoelectric generator produces power at an output voltage that depends on the temperature difference. In low power applications, the area used is small, and the temperature difference is several degrees; thus, the voltage generated is in the millivolt range. As a result, a power processing unit is required to boost the voltage up to a useable standard voltage. Fig. 2.14 shows a closed loop diagram of a power processing unit to increase the output voltage of a thermoelectric generator. The closed loop control is used to stabilize the output at a certain standard voltage

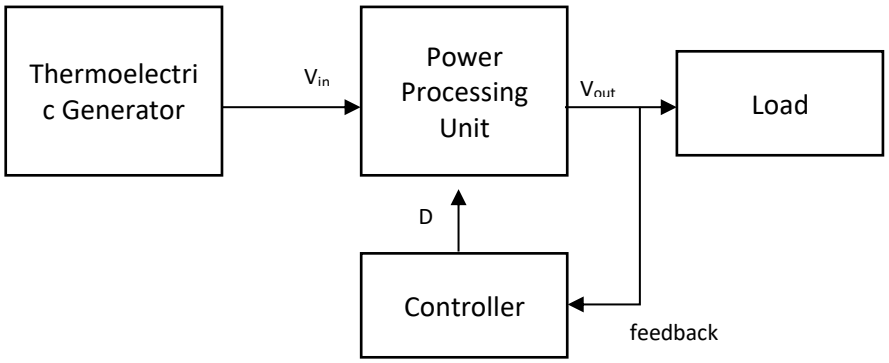

Fig. 2.14. Power processing unit for a thermoelectric generator

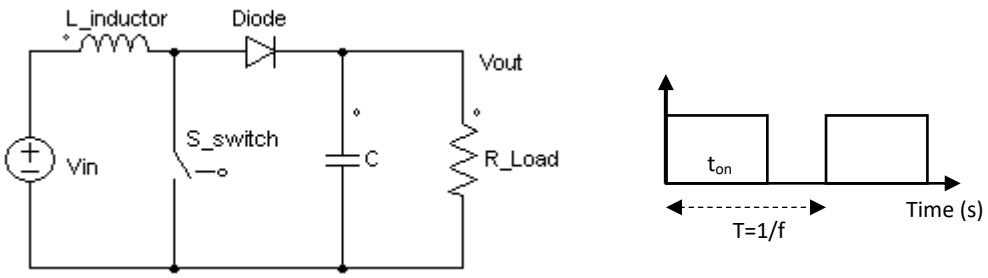

(a) (b)

Fig. 2.15. Open loop Boost dc-to-dc converter (a) power circuit of a Boost converter (b) timing diagram of the switch

Because the function of a power processing unit is mainly to increase the voltage, it may use an open loop boost converter, as shown in Fig. 2.15. A boost converter increases the voltage by using the high pulse current during the transient condition of the inductor caused by operation of the switch. The duty cycle (D) is defined as the ratio of the conduction time (t_{on}) and the period (T) of the switching; thus, the output voltage (V_{out}) is $V_{out} = \frac{V_{in}}{1-D}$

For example, when the switch of a boost converter is operated at 1 kHz, the duty cycle D = 75%, as shown in Fig. 2.15 b). It can be shown that V_{out} = 4 V_{in}. To achieve a high gain ratio of voltage boosting, a flyback dc-to-dc converter may be used. The converter employs a transformer designed with the required turn ratio. The operation of a flyback converter is based on similar principles to the operation of the Boost converter, except for the use of a transformer.

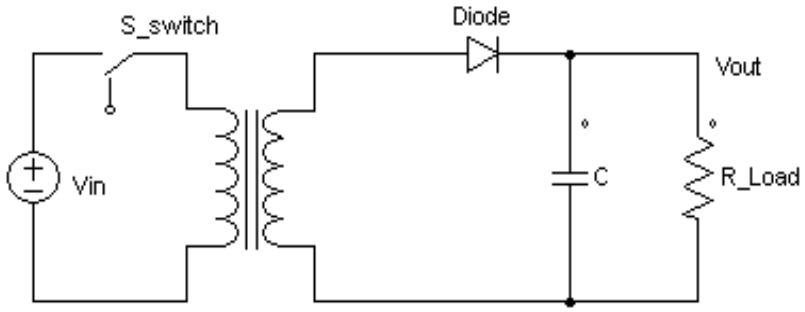

Fig. 2.16. Open loop flyback converter

When the requirement is to not only increase the voltage but also improve the system efficiency, a maximum power point tracker (MPPT) is involved. An MPPT is an electronic circuit whose function is to maximize the available power in a renewable energy source. An MPPT is commonly employed in a solar photovoltaic system; however, with the necessary adjustments, it can be used for other sources, such as wind energy systems and thermoelectric generators. All the TEGs in the model receive uniform irradiance, but the magnitude may change dynamically. The use of maximum power point tracking for a thermoelectric system was proposed by researchers in references [49-56]. The use of TEGs with an MPPT to charge a battery was introduced by Hayati Mamur et al. [58]. Another method to expand the peak power using an array reconfiguration was presented by Qiping et al. [60]. The method employs a number of switches to reconfigure the array. Qiping et al. claimed that the system could remain at high efficiency under various temperature gradients.

Electronically maximizing methods, especially utilizing an MPPT has been widely implemented in PV applications. The basic working mechanism is by adding a converter and adjusting the voltage to yield the highest power possible. There are several main problems in MPPT methods,

1. Maximum Power Point Precision

   Precision has a very important role in MPPT, the slightest shift from the true maximum power point will result a significant difference. An MPPT with a "pre-setting' type is prone to imprecision if the presetting parameter is not set correctly. [55]

2. The time needed to reach MPP

Searching type MPPT works by gradually increasing the duty cycle until the MPP is achieved. By setting the incremental steps wide, MPP will be achieved quickly, but less precise. On the other hand, it will be more precise if the increments are set narrow, but then it will take a long time to achieve MPP. [49]

3. Local Maximum Power Point

   On a large scale application in PV or TEG, it is very common to have differences in irradiance or heat distribution. This will result in several different maximum power points on different areas, causing the MPPT to pick the wrong MPP. This problem can be eliminated by utilizing a smart MPPT that is based on a searching algorithm combined with AI. [52][53]

4. Maximum Power Point Shifting

   Irradiance from the sun is relatively constant, except when it is cloudy that causes partial shading. This does not apply to heat, a wide surface in an incinerator is prone to temperature changes that depends on many factors. [52][53]

An MPPT comprises two major components (as shown in Fig. 2.17): the DC-to-DC converter and the controller.

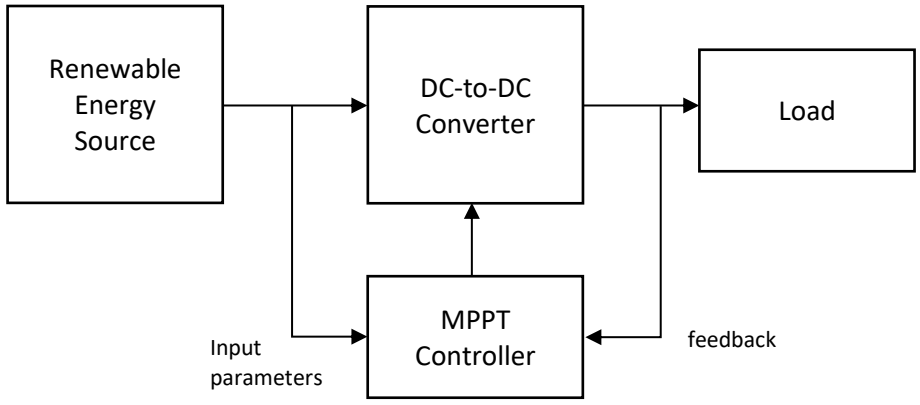

Fig. 2.17. DC-to-DC converter and controller for an MPPT

The MPPT concept is basically to change the terminal voltage of a renewable energy source when supplying power to the load to allow the output power to reach the maximum point. The DC-to-DC converter provides the interface between the renewable source and the load terminals, i.e., the load voltage is fully regulated by the converter. The converter is controlled by pulse width modulation, i.e., adjustment of the duty cycle. The input parameters from the renewable source are used to determine the suitable duty cycle for obtaining the maximum power point. The feedback parameters are used to sacrifice some of the input of the controller to meet the target of the converter output.

Many types of MPPT have been proposed by researchers [49-56]. Podder, A.K, et al. divided their MPPT's algorithm into 8 categories: conventional, mathematical based, measurement & comparison based, constant parameter based, trial & error, numerical,

intelligent prediction, and iterative [49]. According to its tracking process for obtaining the peak power, we can divide MPPT algorithms into 3 categories:

- Pre-setting: lookup table, curve fitting, fractional Open Circuit Voltage, etc.
- Predicting: Fuzzy logic, artificial neural network, ANFIS, genetic algorithm, etc.
- Searching: perturbed & observed, incremental conductance, hill climbing, etc.

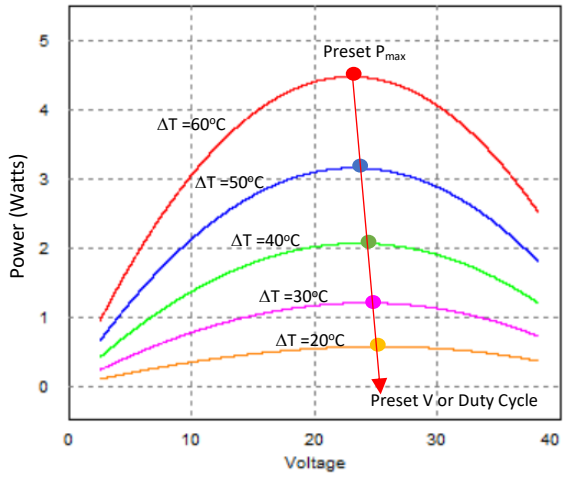

Fig. 2.18. Principles of MPPT pre-setting algorithm

In MPPT operation, a predetermined pre-setting algorithm introducing a typical data set–such as peak powers and duty cycles under several conditions–is utilized. By considering the input parameters, an appropriate duty cycle is then selected for controlling the DC converter. Fig. 2.18 shows the principles of this pre-setting algorithm. Lookup table, curve fitting, fractional of open circuit voltage, fractional of short circuit current, etc. are included as pre-setting MPPT types.

The predicting algorithm uses artificial intelligent methods to identify such conditions based on the input parameters. Next, a duty cycle is selected based upon consideration of those parameters and the internal data base. This technique commonly requires training procedures to generate the internal data base. Fuzzy logic, neural network, ANFIS, genetic algorithm, etc. are the artificial intelligence schemes used by researchers for an MPPT control system [52-54].

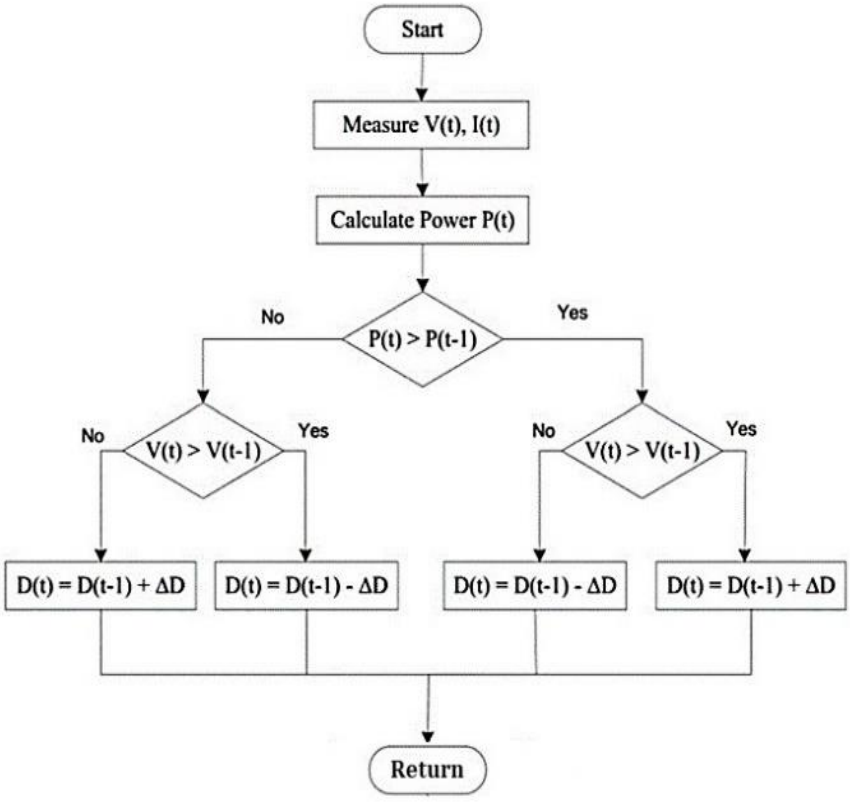

Fig. 2.19. Flow-chart of perturbed and observed MPPT [52]

A searching algorithm utilizes step-by-step increments to increase the voltage of the DC converter until the peak power is achieved. The algorithm compares the previous step of calculation or measured data with the recent one. When the recent power is

higher than the previous result, it means that the peak power remains to be achieved. Thus, searching is continued. When the recent power value is lower than the previous power value, it means that the peak power was previously achieved. Thus, the voltage of the DC-to-DC converter must be reduced. Oscillation may occur at the point of peak power. Famous names for this type of MPPT are perturbed and observed (P&O), incremental conductance (INC), hill climbing, etc. [49-51], [55-56]. Fig. 2.19 shows a flow-chart diagram of the perturbed and observed method. The P&O method uses a constant increment step to increase the DC converter voltage; it also utilizes a constant decrement to reduce the voltage when the peak power went through. Another P&O type involves an adaptive increment instead of a constant one.

In this thesis, the P&O method is utilized to investigate the thermoelectric generator performance. The method is a simple but effective approach to obtain the maximum power point without pre-setting any values or training the system. Modification to the control system was implemented to allow the MPPT to cover rapid and deep changes of local temperature.

2.3 Inverter System used in this study

An inverter system is a piece of power electronic equipment used to convert from dc voltage to ac voltage. An inverter system is applied when the source is a dc voltage source, whereas the load is an ac voltage load. There are 2 types of inverters: stand alone and grid-interactive inverter. The stand-alone inverter supplies load only, without connection to other sources.

An inverter grid-interactive circuit is an electronic circuit used as an interface between a renewable energy source and an electricity grid system. The inverter injects power generated by the renewable source to the grid. This system is commonly-known as Distributed Generation (DG). The renewable energy sources include solar photovoltaic (PV) house rooftop, small wind turbine, and thermoelectric generators. Larger renewable energy systems are called farms, e.g., PV farms and wind farms, whose capacity reaches tens to hundreds of megawatts.

Many types of inverters for distributed generation have been proposed by researchers [57-65]. Inverters can be categorized by their number of phases, waveform patterns, parameter-controlled types, etc. A single-phase inverter is employed for low-power applications, whereas a three-phase inverter is for high-power applications. Both types of inverters are commonly used for uninterruptible power supply systems and distributed generation interfaces. The first inverters utilized a square wave pattern of output voltage. Subsequently, better inverter technology was released that utilized pulse width modulation patterns. A very famous pattern that is widely used in industries is the sinusoidal pulse width modulation (SPWM) [58].

In terms of the parameter controlled, an inverter is grouped into 2 types: voltage controlled and current controlled. A block diagram of an inverter involving a voltage-controlled SPWM is shown in Fig. 2.20.

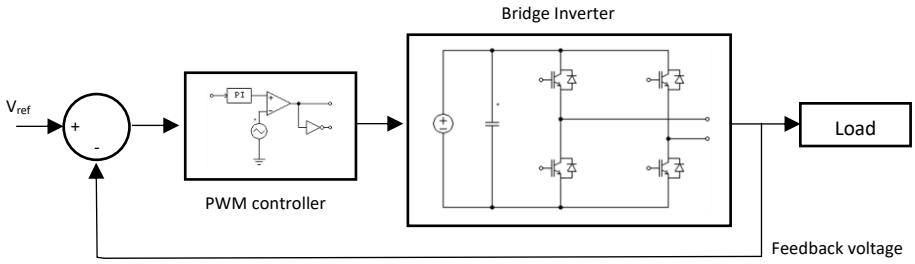

Fig. 2.20. Sinusoidal PWM inverter based on the voltage-controlled method

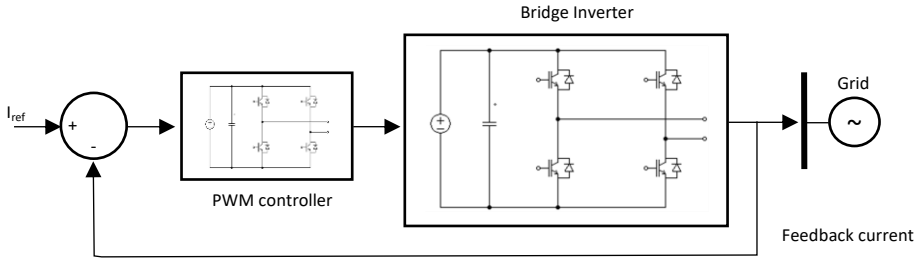

Fig. 2.21. Sinusoidal PWM inverter based on the current-controlled method

Fig. 2.21 illustrates a Sinusoidal PWM inverter based on the voltage-controlled method. The inverter is used for stand-alone power supplies, uninterruptible power supplies, or distributed generation systems [60-62]. For supplying stand-alone loads, the voltage is maintained at a constant value according to certain standards and quality. When connected to the grid, the inverter is coupled with an inductor. The power allowed to the grid is controlled through the phase angle and the voltage magnitude. Detection of the grid voltage availability, namely, the islanding method, determines whether the inverter is isolated or connected to the grid. When the grid fails, the inverter must be isolated to the grid; however, it can supply the load to replace the grid voltage immediately. Hence, it functions as an uninterruptible power supply system.

Fig. 2.21. shows the current-controlled inverter connected to an electricity grid system. The amount of power injected is adjusted from the current while the voltage follows the grid voltage. The current phase angle can be set at any value, such as in phase, leading, or lagging relative to the grid voltage. This type of inverter is mostly used for distributed generation applications because of its simple control method [63-65]. The disadvantage of the system is that the inverter shuts down when the grid fails. The loads that may connect to the inverter will also black out. Other advanced controls include dual inner and outer loops, triple loops, and cascade [62].

In this thesis, the current-controlled method is used in a thermoelectric inverter grid-tied system. The system is a favorable technology for DG applications. A proposed additional control that considers the thermoelectric available power is embedded into the system.

2.4 Conclusion

Based on the application reviews stated above, it is concluded that thermoelectric generators have widely been analyzed, tested, and implemented. Most applications employ small area of thermoelectric generators, especially for low power implementations. Some applications use an array of thermoelectric generators for high-power applications. In addition, none of the applications reported in the literature consider a non-uniform temperature distribution in the analysis. However, a non-uniform heat distribution typically occurs over the large area of a hot surface because of the ambient and heat source conditions. This thesis focuses on high-power

thermoelectric generator applications, especially for powering a distributed generating unit. The block diagram of the entire system is shown in Fig. 2.22.

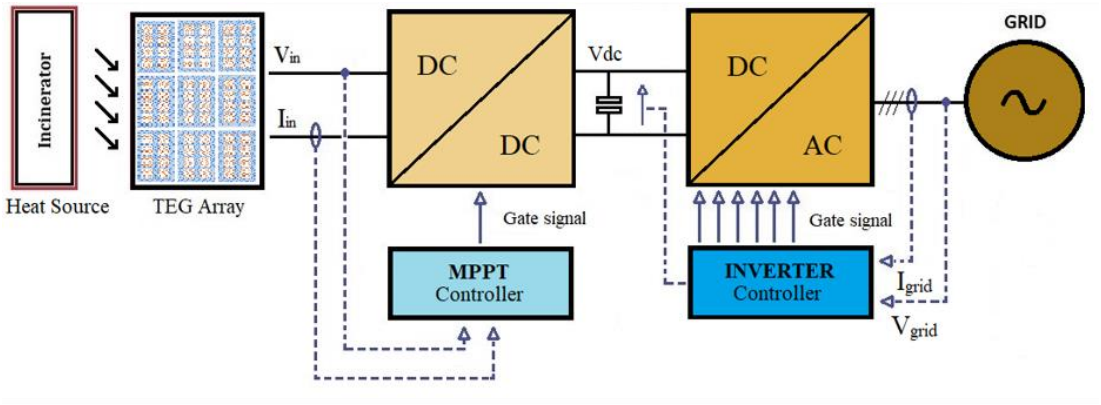

Fig. 2.22. The proposed system of a thermoelectric generator application

The system is designed in small- to medium- scale with a peak capacity of around 3000 Watt. The system is connected to the grid through a low-voltage distribution system of 220 V/ 380 V.

CHAPTER 3
THERMOELECTRIC SYSTEM MODELING

This chapter presents a model of a thermoelectric system. A proposed model is introduced based on an electric circuit for large-power applications. The model includes features to simulate the thermoelectric system under a non-uniform temperature distribution.

3.1. Non-uniform Temperature Distribution

Non-uniform temperature distribution can also be translated as different temperature gradients that occur on a large surface. This phenomenon is mostly present on equipments that uses combustion in its process. A waste incinerator is a good sample of an equipment that produces heat as a byproduct and prone to non-uniform temperature distribution. This heat byproduct can be utilized as the heat source for the thermoelectric generator. Sagi Samlas and Anilkumar S.H, did a reaserch about Comparative evaluation of different design configurations for a Solid Waste Incinerator which includes the analysis of heat non-uniformity inside a working incinerator [67]. Fig. 3.1 shows the temperature gradients present on the incinerator. It is clear that the part closest to the core has the highest temperature, while the part furthest from the core will have the lowest temperature. Applying thermoelectric generators to the walls of this incinerator whithout any ancillary equipment (e.g., MPPT controller) will result to a power generation with very poor efficiency.

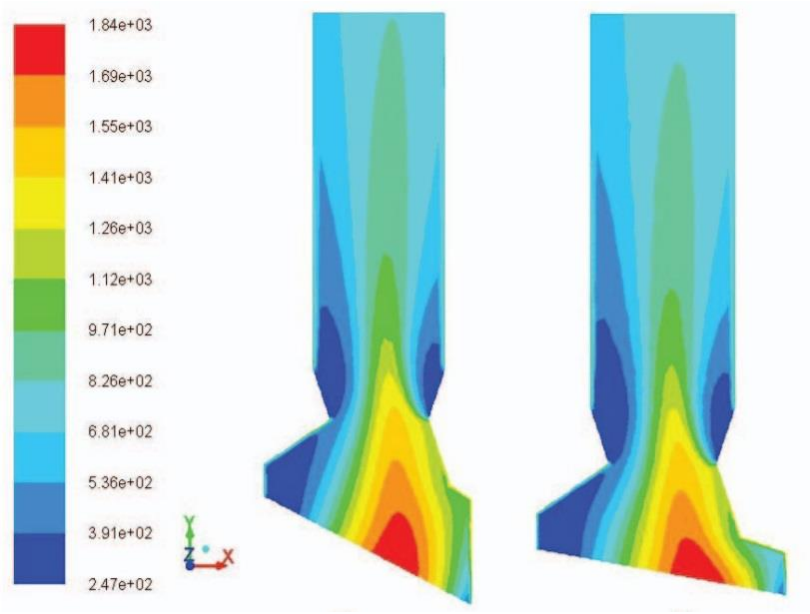

Fig. 3.1. Temperature distribution in solid waste incinerator [67]

3.2. Brief Thermodynamics Review of a Thermoelectric Device

According the first law of thermodynamics, *The change in a system's internal energy is equal to the difference between heat added to the system from its surroundings and work done by the system on its surroundings*. This means that that energy can neither be created nor destroyed, only altered in form. In the matter of thermoelectric devices, the correlation is between heat flow and electromotive force. Thermoelectric devices works in both ways, it will generate a temperature gradient when electromotive force is applied and vice versa. These effects was discovered by Thomas J. Seebeck and Jean C. Peltier. Thomas J. Seebeck founded that when a piece of copper wire and a piece of bismuth wire is connected in series, it will generate electric current when one of the junctions is heated. This effect is called *Seebeck's Thermoelectric Effect*. While the reverse mechanism is found by Jean C. Peltier and later known as the *Peltier's Thermoelectric Effect*.

In the thermodynamics study, a thermoecouple composed of metals A and B with junctions at different temperature, there are four different heat flows. First there is Peltier heat, which is proportional to the current. Second, the rate of absorpsion of Thomson heat is proportional to the temperature gradient and to the current. Third, Fourier's heat flow is proportional to the temperature gradient. And the last is Joule's heat generation rate according to Ohm's law.

In recap, the thermoelectric generator is a heat engine that directly converts heat taken from the environment into electricity. The active medium subject in thermoelectric devices is a stream of electrons that are present in the semiconductors (metal A and B). The semiconductors are connected at one end by another metal (e.g., copper), identified as a grey colored strip in Fig. 3.2a. The presence of the connecting strip does not affect the thermoelectric effect, since the connections are isothermal [33]. The temperature gradient is defined as the difference between the hot temperature T_h and cold temperature T_c of a semiconductor junction. When a TEG is run in reverse, electricity will cause a temperature gradient between two different metals that conduct electricity. The basic concept and modeling of thermoelectric energy conversion are shown in Fig. 3.2.

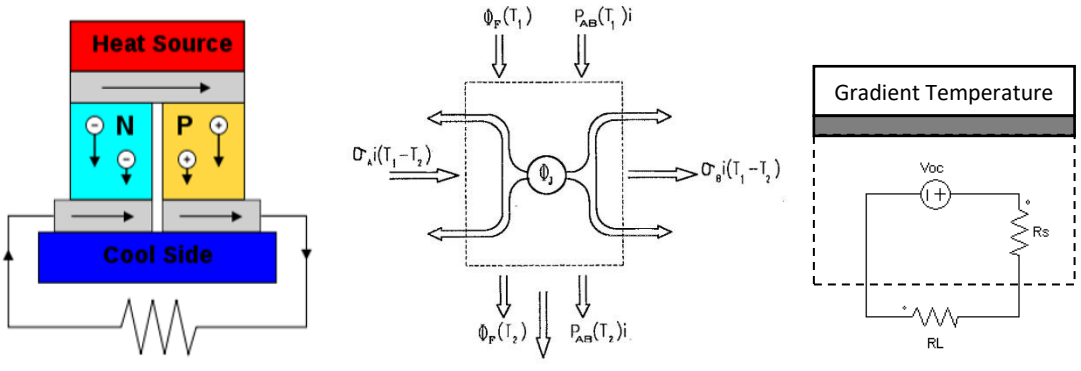

(a) (b) (c)

Fig. 3.2. Basic thermoelectric energy conversion (a) conceptual diagram (b) thermoelectric energy flows [33] (c) electrical diagram

Fig. 3.2 shows the basic concept of thermoelectric conversion; it consists of two conversion stages. The first stage is the use of a temperature gradient to generate the internal voltage source (V_{oc}), and the second stage is the flow of electric energy to the load through the internal equivalent resistance (R_s). In this case, both V_{oc} and R_s are dependent on the thermoelectric material properties.

To analyze the conversions and performances, researchers use models. Many types of models of thermoelectric generators have been presented [1- 12]. Each of the models was developed according to the application of the TEGs. The model that is based on the material properties is intended for low-power applications [14-23], whereas the model that is based on an electric equivalent circuit is primarily for high-power applications [24-30].

3.3. Modeling of a Thermoelectric Generator involving Material Properties

Modeling of a thermoelectric generator starts with understanding the Seebeck effect, the Peltier effect, and the Figure of Merit. Thomas Johann Seebeck found that when semi-conductors are connected to an electric circuit in series, they can convert heat into electricity; the Seebeck coefficient α that characterizes this phenomenon is defined as follows [8]:

$$\alpha = -\Delta V / \Delta T \quad (2.1)$$

where V is the voltage, and T is the temperature. The Seebeck process drives charge carriers to diffuse from the hot side, where they have higher thermal energy, to the cold side in the thermoelectric material.

The Peltier effect represents the reverse process of the Seebeck effect. When two different semiconductors are driven by an electric current, a heating at a rate of q occurs at one side of the junction and cooling occurs on the other side. The Peltier coefficient Π is defined as follows [8]:

$$\Pi = I / q \quad (2.2)$$

where I is the electric current and q is the rate of cooling.

The thermoelectric figure of merit is useful to estimate the performance of the material. The non-dimensional thermoelectric figure of merit, ZT, is given as follows [8]:

$$ZT = \alpha^2 \sigma T / \kappa \quad (2.3)$$

where α is Seebeck coefficient, σ is electrical conductivity, and κ is thermal conductivity of the thermoelectric materials. ZT presents the symbol of performance on thermoelectric. To obtain high ZT, both the Seebeck coefficient and the electrical conductivity must be high, whereas the thermal conductivity must be minimized. The temperature T is thus maintained.

Characteristics of thermoelectric materials are classified into three categories based on the operating temperature. In low-temperature operation, up to 450^{o}K is applied to Bismuth-based alloys containing elements of Antimony, Tellurium, and Selenium. In

medium-temperature operation, up to 850°K, Chalcogenides, Skutterudites, and Half-Heuslers are used. Application for high temperatures up to 1300°K involves Silicon Germanium alloys [8]. Fig. 3.3. illustrates the relationship between ZT and operation temperatures of various materials.

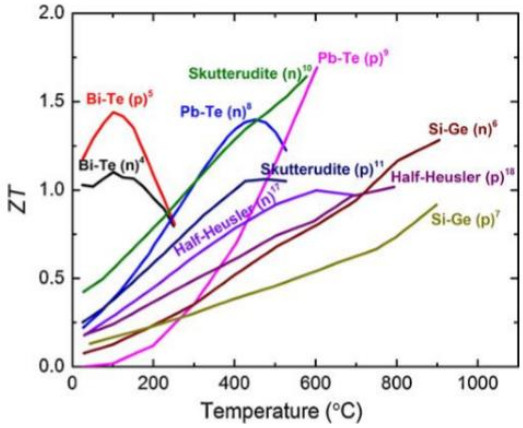

Fig. 3.3. Figure of merit *ZT* as a function of temperature of various materials [8]

Thermoelectric performances can be demonstrated in terms of either efficiency or output power. TEG efficiency for power generation and cooling modes is given as follows [12]:

Power-generating efficiency η_p:

$$\eta_p = \frac{T_h - T_c}{T_h}\left[\frac{\sqrt{1+ZT}-1}{\sqrt{1+ZT}+\frac{T_c}{T_h}}\right] \quad (2.4)$$

Cooling efficiency η_c:

$$\eta_c = \frac{T_h}{T_h - T_c}\left[\frac{\sqrt{1+ZT}-\frac{T_h}{T_c}}{\sqrt{1+ZT}+1}\right] \quad (2.5)$$

As an example, curves in generating and cooling modes of a typical thermoelectric generator are given by Xiao Zhang as shown in Fig. 3.3 [12].

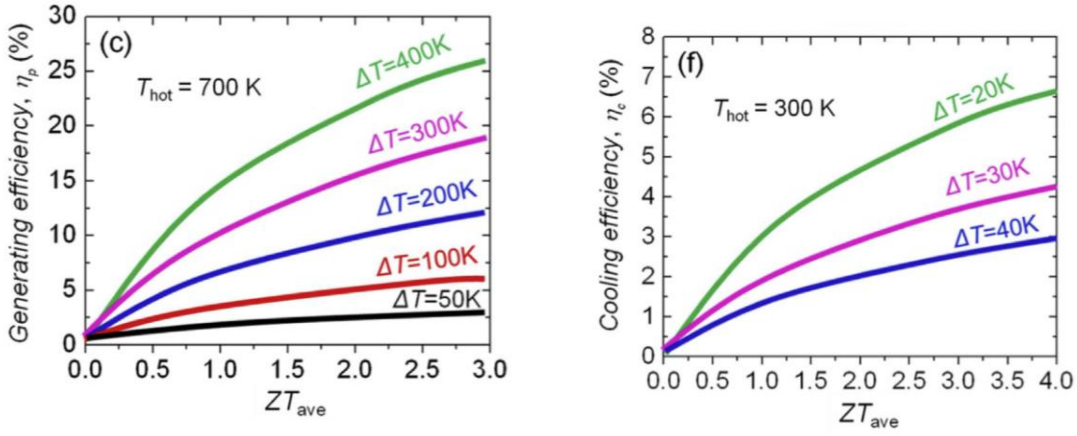

Fig. 3.4. Thermoelectric efficiency in generating and cooling types [12]

Both curves show similarities and differences in terms of efficiency and operating temperature. The power-generating type utilizes higher temperature –(almost 2.5 times) and has a higher efficiency compared to the cooling type. The TEG generating type obviously is more complicated and is more expensive to manufacture. From Fig. 3.4, both generating and cooling types have similar characteristics when operating at low temperatures (around 300^{o}K) with low temperature gradients. Marco Nesajah et al. [13] conducted experiments to compare thermoelectric products for generating power. A cooling type (or TEC) was utilized for generating power. In terms of market price, the TEC types are 15 times cheaper compared to TEG generating types. The results showed that both demonstrated very similar characteristics if the operating

temperature were below 100°C. For a low temperature difference, a TEC presented slightly better performances compared to a TEG [13].

TEG efficiency is also defined as the ratio of electrical power delivered to the load (P_L) and the thermal power absorbed by the hot surface (Q_h). Assuming the heat flow absorbed by the hot side equals that of the cold side (Q_c) and the electrical power to the load, the efficiency is given as follows [9]:

$$\eta_p = \frac{P_L}{Q_h} = \frac{P_L}{Q_c + P_L} \tag{2.6}$$

Once the *ZT* is determined from the material properties, the efficiency can be calculated. When the heat flow is calculated or measured, the electrical power of thermoelectric can be found. This type of modeling is commonly used for research involved in obtaining higher efficiency or supplying low-power equipment.

3.4. Modeling of Thermoelectric Generators for High-Power Applications

A model involving both the material properties and an electrical circuit of a thermoelectric system for high-power applications was proposed [24-27].

High-power application systems require wide areas of hot surface as the source of energy. Most systems presented operated using a uniform heat distribution. Gunay et al. proposed models and applications using a heat source from an industrial chimney [10]. The temperature difference could reach 100°C. The model concentrates on heat

conversion. Another model consists of a 3-stage thermoelectric system [44]. A dynamic model of energy conservation, unsteady heat conduction, and fluid dynamics is involved in the 3-stage model.

Another model of a thermoelectric generator that utilizes an electric equivalent circuit was proposed by researchers [28-30]. The model primarily considers the electric power side. The components of the model consist of an equivalent voltage source V_o and an equivalent internal resistance R_s as shown in Fig. 3.4. Gunay et al. presented the relationship between the electric parameters of the load and thermoelectric properties as follows [10]:

$$I = \frac{\alpha(T_h - T_c)}{R_s + R_L} \tag{2.7}$$

$$V = \frac{2N\alpha(T_h - T_c)}{R_s + R_L} R_L \tag{2.8}$$

$$P = \frac{2N\alpha^2(T_h - T_c)^2}{R_s + R_L} \tag{2.9}$$

where I is the load current, V is the terminal voltage of the thermoelectric device, and P is the power absorbed by the load. N is the number of cells, and R_s represents the internal electric resistance and thermal resistance.

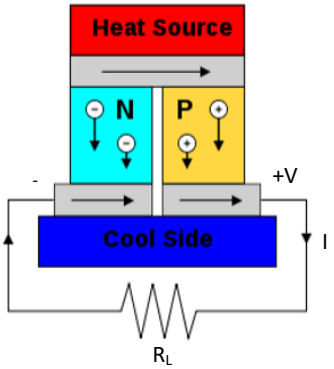

$$V = 2N\alpha \frac{(T_h - T_c)}{R_s + R_L} R_L$$

$$I = \frac{\alpha(T_h - T_c)}{R_s + R_L}$$

Fig. 3.5. Heat conversion to electric parameters with the Seeback coefficient

Two types of electric equivalent models were introduced, namely [28-30]:

- Constant temperature gradient condition,
- Constant heat flow condition.

Fig. 3.6 (a) shows the electric equivalent circuit used in the constant gradient condition model. At a gradient temperature ΔT, for the given TEG's parameters, the equivalent voltage source and the internal equivalent resistance are constant. Fig 3.5 (b) depicts the electric equivalent circuit for the constant heat flow condition. In this case, the internal equivalent resistance is load current-dependent. This model neglects the thermal resistance.

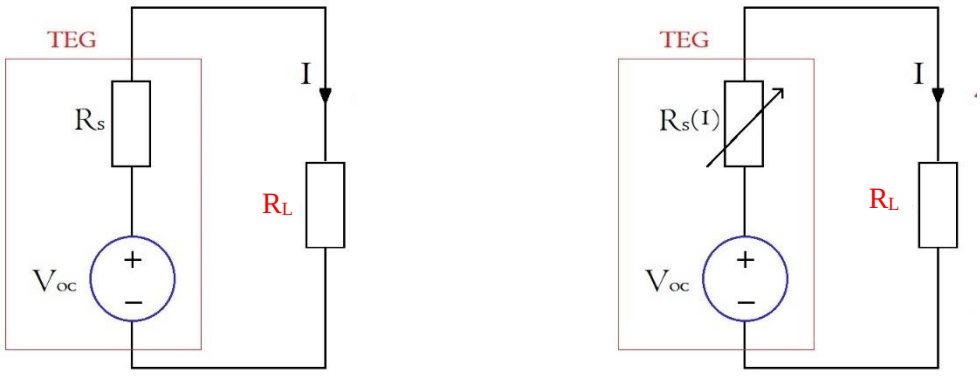

(a) (b)

Fig. 3.6. Models of a thermoelectric generator utilizing an electric equivalent circuit (a) constant temperature gradient model (b) constant heat flow model [28]

All models presented in the past used material properties for determining the electric

parameters. The thermoelectric properties are dependent on the material selection, design layout, manufacturing process, etc.; therefore, they involve complicated equations, parameters, and constants.

3.5. The Proposed Model

The proposed model is developed using an electrical engineering approach, as it is more practical rather than based on the development of material property technology. The model has the following important features:

- The model uses an electric equivalent circuit;
- The model is based on electrical test procedures to determine the electric parameters, avoiding the figure of merits and other constants commonly embedded in a thermoelectric model;
- The model is suitable for large systems designed to operate under non-uniform temperature distributions.

The steps consider laboratory tests of open and short circuits of a typical module that is studied in the research project. This method is similar to analysis and determination of the parameters of an electric machine or an induction motor. This method works in a fully electrical equivalent circuit. Thus, this method becomes favorable for engineers in the field, as it avoids complicated numbers and constants, including figure of merits for the thermoelectric properties. The flowchart can be used to characterize a single device as well as a set of devices or an array of thermoelectric devices. A single device

under typical conditions generates a very small output power and a current in the milli- or micro-ampere range, which requires high accuracy measurement equipment to monitor. Scaling up the output power can be achieved by connecting a set of thermoelectric devices in series and parallel.

As stated, modeling of a thermoelectric generator considers the following 3 main parameters:

- Seeback coefficient α, which is dependent on the materials used, the construction, and the process of manufacture;
- The internal electrical resistance R_E, which is the resistance in the junctions that is in contact with the load;
- The internal thermal resistance θ_m and the contact thermal resistance θ_c, which is the thermal resistance contact between the TEG and the thermal source.

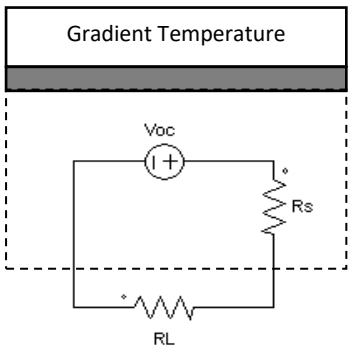

Fig. 3.7 The diagram of a thermoelectric model based on an electrical equivalent circuit

From Fig. 3.7, the model of a thermoelectric generator is based on an electrical equivalent circuit consisting of a voltage source, V_{oc}, and an internal resistance, R_s. According to Siouane et al., both V_{oc} and R_s can be assumed as constants if we used a constant temperature gradient in the conversion process [28]. At the given ΔT, the equivalent voltage source V_{oc}, and the equivalent internal resistance R_s are determined as follows:

$$V_{oc}(at\ \Delta T) = \alpha \Delta T \frac{\theta_m}{\theta_m + \theta_c} \tag{3.1}$$

$$R_s\ (at\ \Delta T) \approx R_E + \frac{\alpha^2 \theta_c \theta_m (T_H + T_C)}{\theta_m + 2\theta_c} \tag{3.2}$$

As mentioned, parameters of a thermoelectric device, such as the Seeback coefficient α, the internal electrical resistance R_E, the internal thermal resistance θ_m, and the contact thermal resistance θ_c, are dependent on the materials used, the structure designed, and the process of manufacture. If those parameters can be assumed as constants at the given ΔT, then equation (3.1) and (3.2) can be rewritten as follows:

$$V_{oc}(at\ \Delta T) = c_1 \Delta T \tag{3.3}$$

$$R_s\ (at\ \Delta T) \approx R_E + c_2 (T_h + T_c) \tag{3.4}$$

where the constants are $c_1 = \alpha \frac{\theta_m}{\theta_m + \theta_c}$ and $c_2 = \frac{\alpha^2 \theta_c \theta_m}{\theta_m + 2\theta_c}$. Expression (3.3) proves that the equivalent voltage source V_{oc} depends on the temperature gradient ΔT directly. The

temperature gradient is defined as follows:

$$T_h = T_c + \Delta T \tag{3.5}$$

Substituting Equation (3.5) into (3.4), equation (3.4) can be rewritten as follows:

$$R_s\ (at\ \Delta T) \approx R_E + c_2(T_c + \Delta T) \tag{3.6}$$

The cold surface of the thermoelectric device T_c is maintained constant; hence, $c_3 = R_E + c_2 T_c$. Equation (3.6) thus becomes:

$$R_s\ (at\ \Delta T) \approx c_3\ + c_2\ \Delta T \tag{3.7}$$

Equation (3.7) shows that the equivalent internal resistance is a function of the gradient temperature ΔT. Hence, it is proven that V_{oc} and R_s can be determined directly from the temperature gradient.

The proposed modeling technique is based on the following procedures, which begin with open and short circuit tests of a typical thermoelectric device, as illustrated in the flowchart diagram in Fig. 3.8.

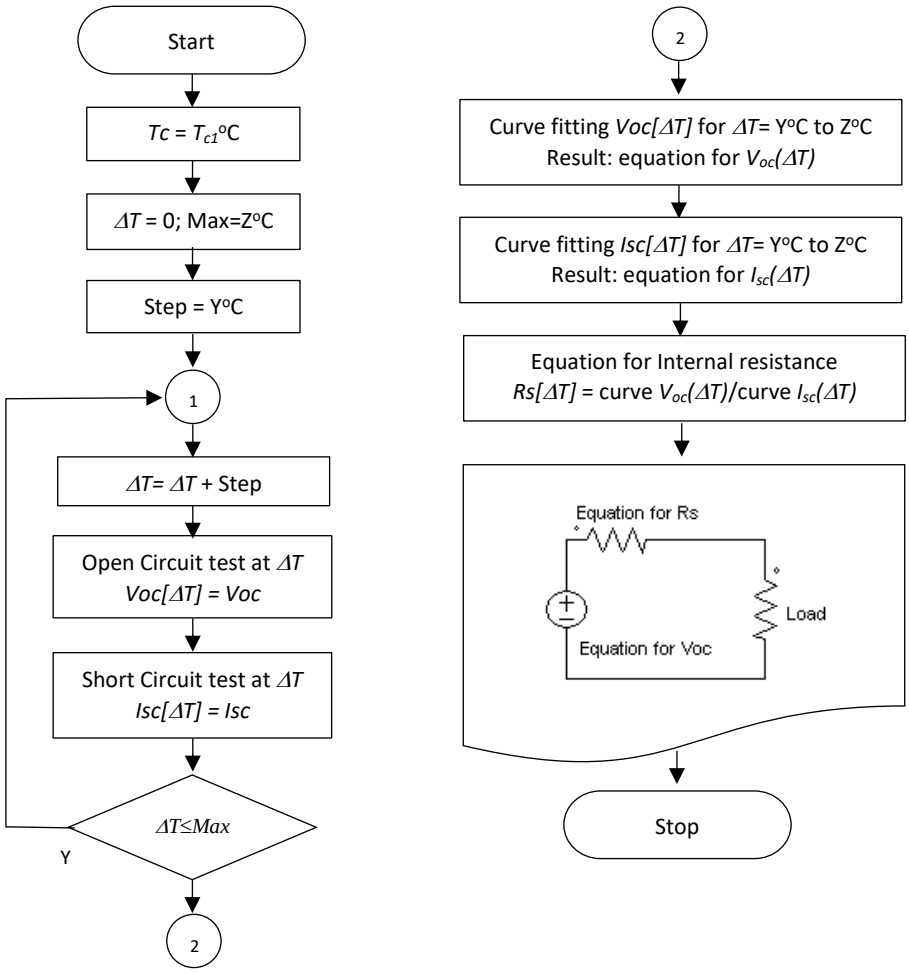

Fig. 3.8. Flowchart diagram of the proposed modeling technique

The temperature of the cold surface is maintained at a constant value, whereas the temperature gradient is varied. During the open circuit test, the current is zero while the terminal voltage of the thermoelectric device is V_t. Because there is no current flow, the terminal voltage is equal to the equivalent voltage source V_{oc}. Thus, at the given ΔT, V_{oc} is determined as follows:

$$V_{oc}\ (\Delta T) = V_t \tag{3.8}$$

During the short circuit test, at a given ΔT, when the thermoelectric terminals are shorted, the current flowing at the terminal I_t is equal to I_{sc}.

$$I_{sc}(\Delta T) = I_t \tag{3.9}$$

The data set of V_{oc} and I_{sc} for various ΔT is obtained. To achieve a general condition, both V_{oc} and I_{sc} can be determined by fitting the curve. Next, equations of both curves are found for the defined range of temperature gradient.

$$V_{oc} = f\,(\Delta T) \tag{3.10}$$

$$I_{sc} = f\,(\Delta T) \tag{3.11}$$

Finally, the equivalent internal resistance is calculated as follows:

$$R_s = \frac{V_{oc}=f(\Delta T)}{I_{sc}=f(\Delta T)} \text{ for the defined range of } \Delta T \tag{3.12}$$

3.6. The Prototype Building, Testing, and Modeling

3.4.1 Prototype Building

Practically, a thermoelectric device is quite similar to a photovoltaic device, which consists of a set of small cells that are connected in series and parallel in order to output a usable voltage and current. In a photovoltaic device, the smallest scale unit is called a cell, which normally generates less than a volt. Correspondingly, the smallest part in a thermoelectric device application is called a junction. Much weaker compared to a single photovoltaic cell, a single junction is only able to generate a very small voltage of around 20mV. As a result, thermoelectric generators are commonly manufactured in a package with a dimension of 40 × 40mm; this package consists of 127 junctions that are connected in series, with a voltage generated of around 3V (depending on the applied temperature difference). In this matter, the thermoelectric we are using is TEC1-12706, which can handle temperatures from -50^{o}C to 138^{o}C.

To further increase the voltage to be usable while still utilizing common components sold in the market, those 40 x 40mm thermoelectric modules are stacked side by side to each other 3 in a row. This 3 in a row configuration is to conform to the water block, which is commonly sold in dimensions of 120 x40mm. The setup is Fig. 3.9.

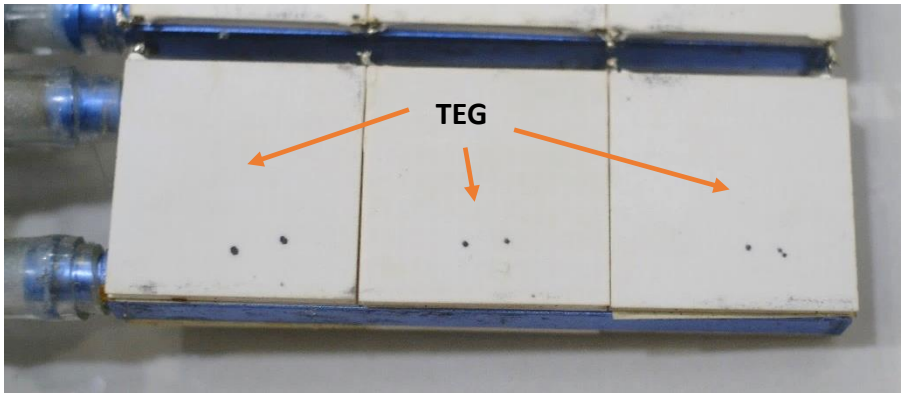

Fig. 3.9 Thermoelectric generator and water block configuration

To maintain a good thermal connection between the thermoelectric generator and the water block, thermal conducting tape is used. A thermal conducting material is characterized by a unit that is called W/mK. The larger the W/mK number, the better the thermal conductivity. Thermal tape with a thermal conductivity of 3.2W/mK was the best we found in the market. The thermal tape placement and configuration is shown on Fig. 3.10.

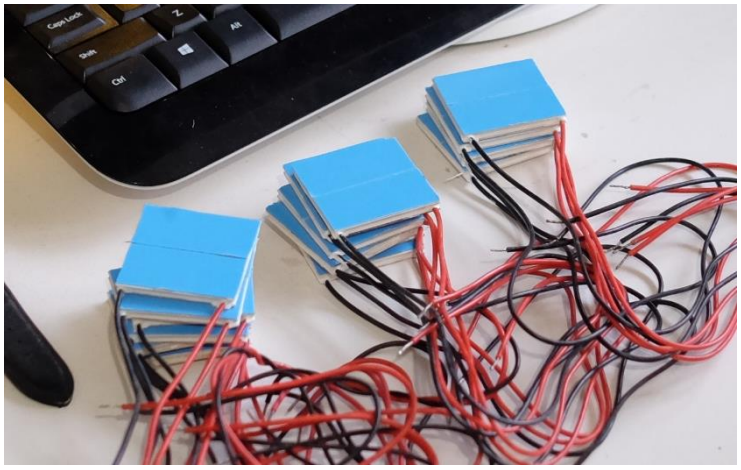

Fig. 3.10 Placement of the thermal tape between the TEG and the water block

To maximize the output power while maintaining a small dimension of the thermoelectric panel, thermoelectric module is also placed on the other side of the water block. A single 120 x 40mm water block will have 6 thermoelectric modules attached to both sides of it, as shown in Fig 3.11.

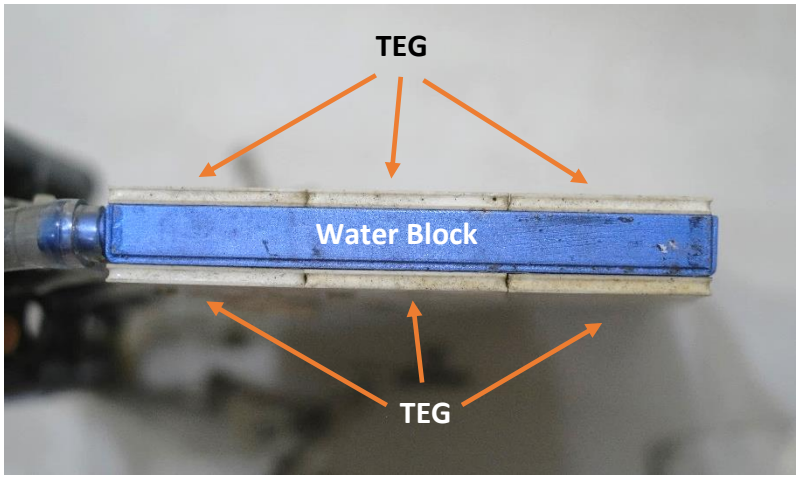

Fig. 3.11. Thermoelectric cells placed on both sides of the water block

Next, all of the steps are repeated 3 more times to obtain 24 thermoelectric generator modules attached to 4 water blocks. The water blocks are then stacked, aligning the inlet and outlet ports to one side. Fig. 3.12 shows the arrangement of the thermoelectric modules in a 3 x 4 configuration on both sides of the water block, corresponding to a total quantity of 24 cells. All of the thermoelectric modules are then connected in series. In order to keep all of the components in place and reduce the non-uniform heat distribution, the thermoelectric generator modules and the water blocks are sandwiched in place by 2 plates of aluminum and then bolted together. A small temperature probe is placed on each side of the thermoelectric panel for monitoring and as a reference for the heater closed loop system, as shown in Fig. 3.12.

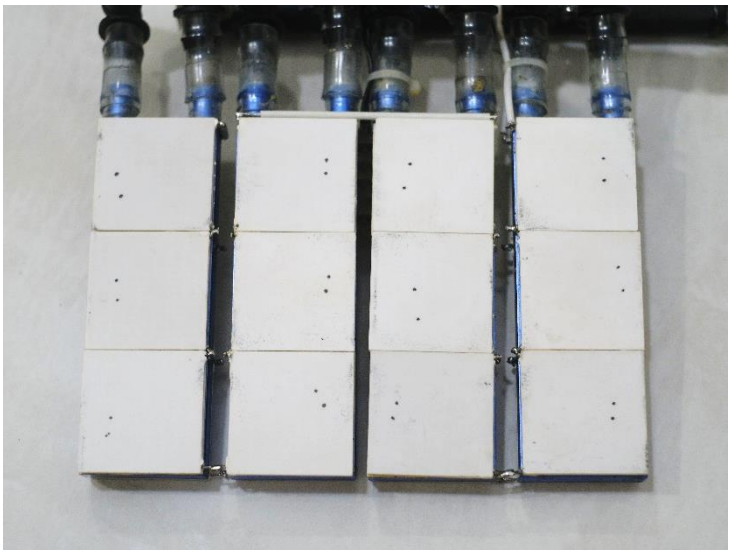

Fig. 3.12 Thermoelectric modules arrangement

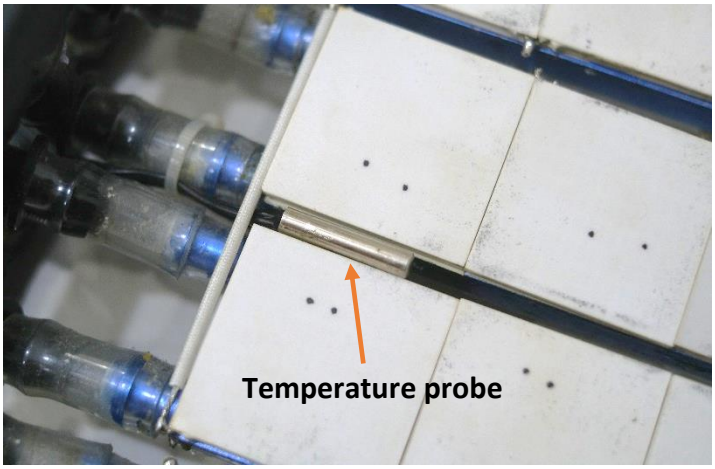

Fig. 3.13 Temperature probe placement

Fig. 3.14 displays the completed thermoelectric generator prototype. Fig. 3.14 are 3D model renderings of the completed thermoelectric generator. The thermoelectric generator is illustrated from multiple angles in 3.14A–3.14D. An exploded view of the generator is illustrated in 3.14E. An actual picture of the completed prototype is displayed in 3.14F. As seen in the illustration, especially on the exploded view, all of the individual components of the thermoelectric generator module are visible. The water blocks responsible for heat exchange are located in the center and are color

coded in blue. Thermoelectric cells are marked as number 2 and 4; there are 24 of them arranged in a 3 x 4 configuration on both sides of the water blocks. The outermost parts number coded as 1 and 5 are the aluminum plates that hold everything together and maintain a good thermal connection between all of the thermoelectric cells, thereby reducing the effect of non-uniform heat distribution. On the back side of the prototype are the inlet and outlet pipes of the water-cooling system. All four of the water blocks are connected in parallel to ensure that all of them receive cool water at an equal temperature. If the water blocks are connected in series, then the last water block will receive preheated water that was heated by the previous water block.

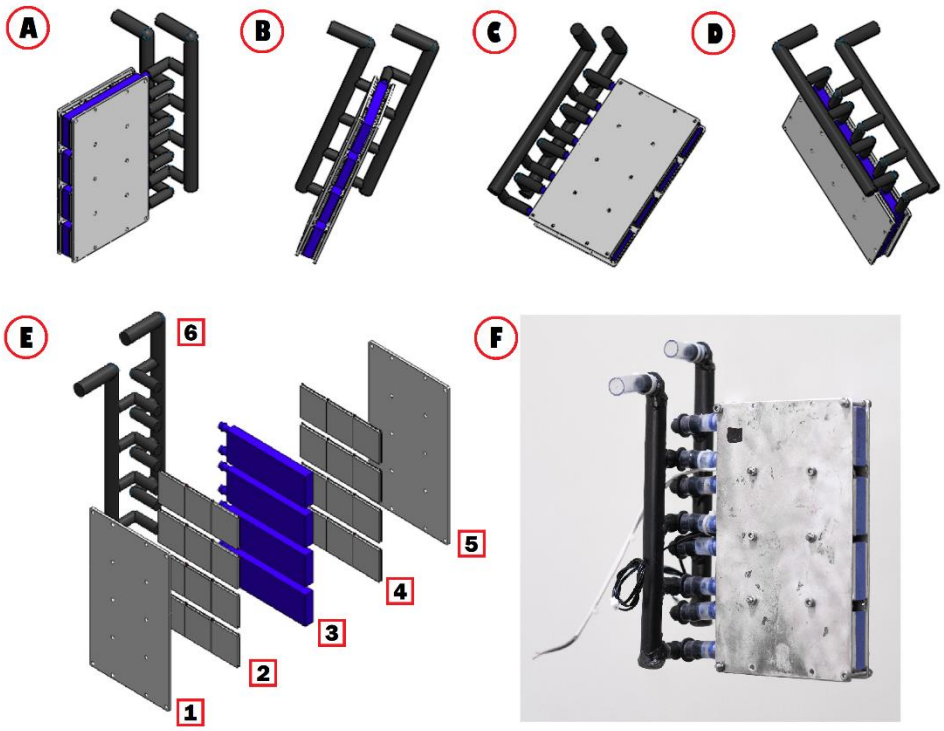

Fig. 3.14 Thermoelectric generator prototype (A-D) multiple angle view (E1, E5) hot side (E2, E4) thermoelectric cells (E3) water cooling blocks (E6) inlet and outlet water pipes (F) actual photo of the thermoelectric panel prototype

This prototype of a thermoelectric generator module containing 24 thermoelectric cells connected in series can generate a peak voltage of 80V and a peak current of 2A. For verification purposes, the thermoelectric generator cannot stand alone; a heat source is required to generate heat on the two sides of the generator, and a cooling system is required to remove heat from the water-cooling system. To yield a good and accurate set of data for verification purposes, the heating and cooling systems must be monitored and controlled accurately. Controlling these systems manually by a human operator is not feasible because human response is not consistent. Thus, an Arduino controller is utilized to handle the monitoring and controlling of the heating and cooling systems.

To determine the efficiency of a thermoelectric generator, a heating element with a minimal of 1000W of heating capability is needed. A stove heating element is used to keep the experiment affordable but reliable. Two stove heating elements are presented in Fig. 3.15; these elements are used to heat the two sides of the thermoelectric generator. These two heating elements are 1000W each.

Fig. 3.15 Heating elements used as controllable heat sources

The heating elements are fixed on a frame that is designed to fit the thermoelectric generator perfectly. The frame also houses all of the electronic components for the monitoring and controlling systems.

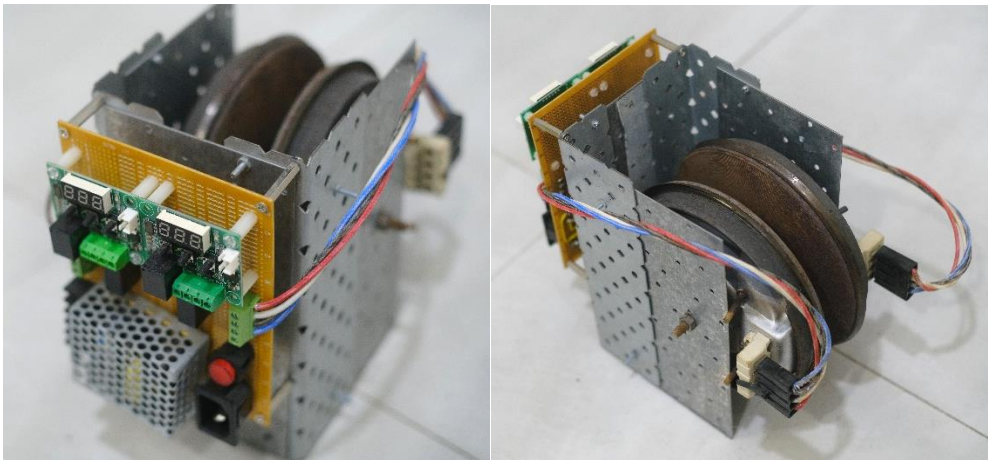

Fig. 3.16 Complete set of the heating system and control

To remove heat that is close to 1000W, a heat exchanger is required. In this matter, a PC water cooling radiator was chosen for its good cooling capability, a relatively small size, and large selection of sizes. Fig. 3.16 shows the heating element and the control sytem. Fig. 3.17 illustrates the complete prototype system in a block diagram.

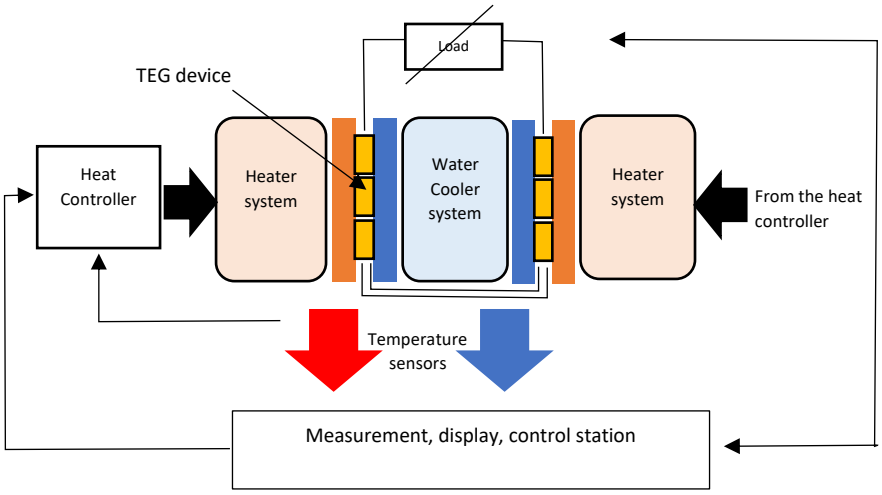

Fig. 3.17. Prototype of a thermoelectric generator module and the control system

The parameters to be measured include voltage, current, short circuit current (I_{sc}), and open circuit voltage (V_{oc}) at various load resistances (R_L) and temperature differences (ΔT). The temperature difference is defined as the difference between the hot side (T_h) and cold side (T_c) of the thermoelectric generator. Fig. 3.18 shows the prototype and the measurement set up.

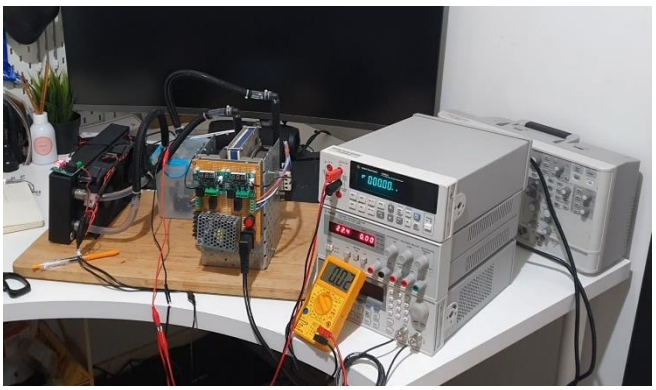

Fig. 3.18. Prototype and equipment setup

The prototype employs a thermoelectric cooling type device, instead of a generator type device. A typical device of TEC1-12706 comprised of 127 cells of thermocouples connected in series is used. The device is widely available in markets for the purpose of cooling electronic equipment, such as computer processors, dehumidifiers, and mobile refrigerators. To increase the simplicity and accuracy of the investigation, the 24 devices of TECs were connected in series. The output voltage is thus presented at a suitable accuracy for the measurement equipment.

3.4.2 Prototype Testing

After the prototype was built, it was tested to obtain the relevant parameters, as presented in the flowchart of Fig. 3.1. Before conducting the open circuit and short circuit test of the prototype, this sub-chapter presents parameters from similar testing presented by other researchers. Marco Nesajah et al. introduced the operation and testing of a cooling thermoelectric device for generating electric power [13]. As previously mentioned, TEGs and TECs have the same materials, design layouts, and structures, but are different in terms of the process of manufacture and the operating temperature. For example, the soldering temperature for a TEC is at 138^{o}C maximum, whereas it exceeds 200^{o}Cfor a TEG. TEGs and TECs are found to have very similar characteristics when applied for the purpose of generating electric power, especially for a hot temperature not higher than 100^{o}C. Experimental results conducted are presented in Table 3.1 [13].

Table 3.1. Experimental results of TEC1-12706 for generating electricity [13]

	ΔT = 20^{o}C	ΔT = 30^{o}C	ΔT = 40^{o}C
V_{oc} (Volt)	0.63	0.9	1.2
P (Watt)	0.05	0.10	0.15

The following presents steps to determine the parameters of the thermoelectric prototype. As stated, the prototype employs 24 devices of cooling type, TEC1-12706, connected in series. The maintained parameters, T_c and ΔT, are also controlled as

suggested in the flowchart. The cold side is kept at 30°C, and the gradient temperature is adjusted from 10°C to 65°C in 10°C temperature incremental steps. The maximum hot-surface temperature was 100°C to prevent damage of the thermoelectric because the soldering temperature of TEC1-12706 is 138°C.

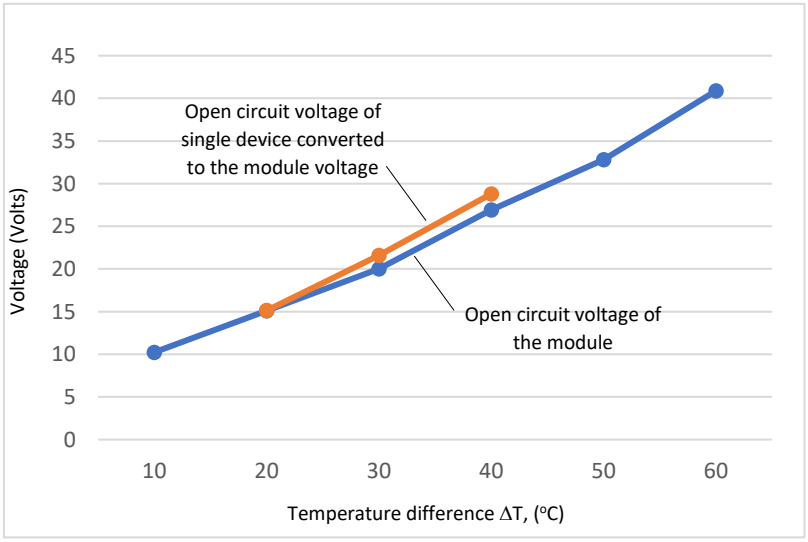

Fig. 3.19. Experimental results of open circuit voltage (V_{oc}) vs. temperature difference (ΔT)

Experimental results of the prototype V_{oc} as function of the gradient temperature ΔT are shown in Fig. 3.19, as a continued line of the curve. The results are also given in Table 3.2. The curve is compared with the results of other experiments that are tabulated in Table 3.1. The results presented in table were obtained for a single TEC1-12706. Therefore, for comparison purposes, the results are multiplied by 24, which is the number of devices in series of the prototype. The average of the errors between results in Table 3.1 and the prototype experiments is found to be 4.7%.

The curve of the prototype V_{oc} shown in Fig. 3.19 was plotted from data obtained in the experiments. By fitting the curve, a linear expression can be written as follows:

$$V_{oc} = 0.60925\,\Delta T + 3 \qquad for\ 10^{o}C \leq \Delta T \leq 60^{o}C \qquad (3.13)$$

Next, comparison of 3 curves is presented in Fig. 3.20.

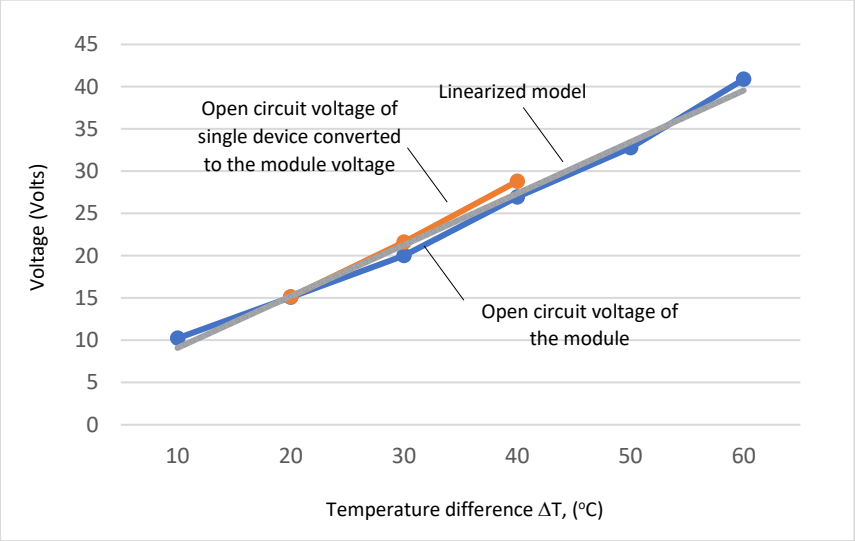

Fig. 3.20. Comparison of experimental tests and a linearized model

Table 3.2. Results from experimental tests of the prototype

Gradient Temperature, ΔT (°C)	10	20	30	40	50	60
Open Circuit Voltage (Volts)	10.232	15.085	20.029	26.933	32.793	40.874
Short Circuit Current (Amps.)	0.08	0.125	0.187	0.253	0.316	0.387

Another experiment was also conducted to measure the output current (at short circuit condition) as a function of the temperature difference. The short circuit current from laboratory tests is also given in Table 3.2. After the data is plotted and linearized, the mathematical model is found, as shown in Fig 3.21.

$$I_{sc} = 0.0066\,\Delta T - 0.0058 \qquad \text{for } 10^{o}C \le \Delta T \le 70^{o}C \tag{3.14}$$

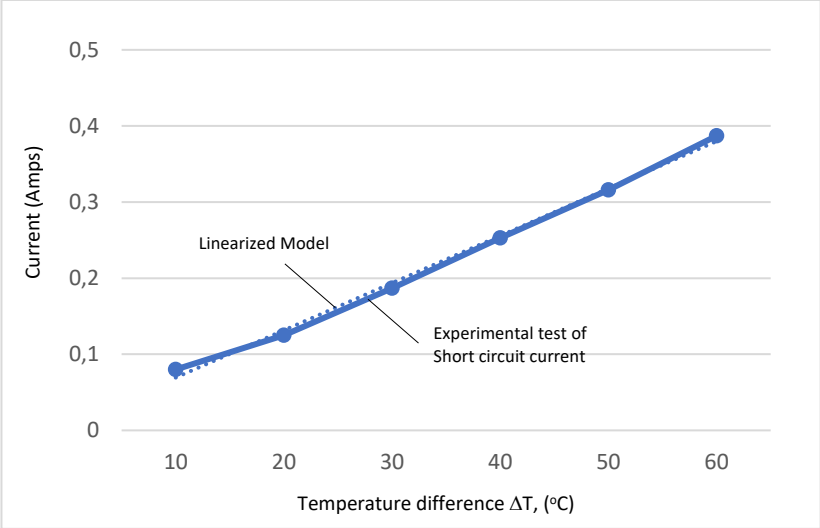

Fig. 3.21. Experimental results and linearized model of the short circuit current (I_{sc}) as a function of the temperature difference (ΔT)

Both model parameters, the open circuit voltage and the short circuit current, are obtained. The next step is to determine the internal resistance of the thermoelectric generator. Referring to equation (3.12), the expression of the internal resistance R_s for $10^{o}C \le \Delta T \le 70^{o}C$ is given as follows:

$$R_s = V_{oc} / I_{sc} = (0.60925\,\Delta T + 3) / (0.0066\,\Delta T - 0.0058) \tag{3.15}$$

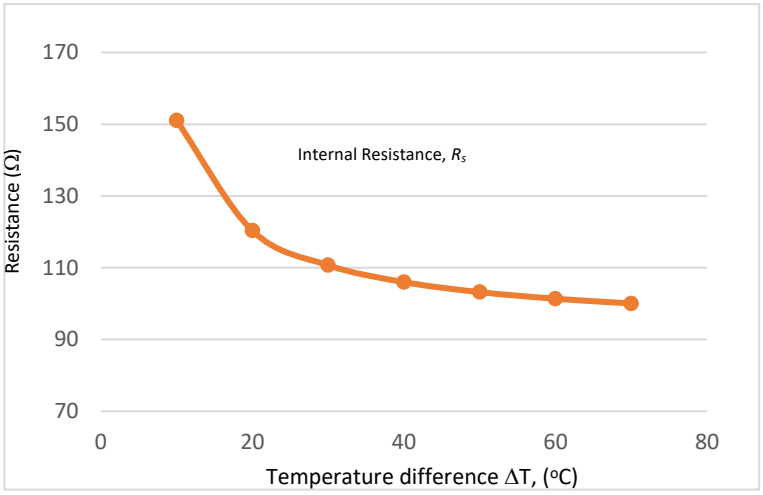

Fig. 3.22. Model of the internal resistance (R_s) as function of the temperature difference (ΔT)

An essential model for the system is given in terms of the voltage-current characteristics loaded with a resistance. From Fig. 3.22 (a), when the thermoelectric terminals are connected to a load resistance R_t, the current flowing I_t and the terminal voltage V_t are written as follows:

$$V_t = V_{oc} - I_t \, x \, R_s \tag{3.16}$$

$$I_t \; R_t = V_{oc} - I_t \, x \, R_s \tag{3.17}$$

In equations (3.16) and (3.17), when the open-circuit voltage V_{oc} is substituted with equation (3.13), and the internal resistance R_s is replaced by equation (3.15), the final V-I expression of thermoelectric is as follows:

$$V_t = (0.60925 \, \Delta T + 3) - I_t \, (0.6982 \, \Delta T + 3)/(0.0066 \; \Delta T - 0.0058) \tag{3.18}$$

The output power P_t of the thermoelectric becomes

$$P_t = V_t \ I_t \tag{3.19}$$

3.4.3 Prototype Modeling

A model of the prototype for PSIM circuit simulation was developed. PSIM is an Electronic circuit simulation software package developed by Powersim. The software package is designed specifically for the purpose of simulations in power electronics, motor drive, or other any electronic circuits.

Modeling of the prototype starts with the given specifications, which are presented as follows:

- Device : TEC 12706
- Number of devices : 24 in series
- Designed output voltage : 80 V
- Designed output current : 2 A peak

Results from open circuit and short circuit tests conducted are as follows, rewriting (3.13–3.15):

- $V_{oc} = 0.60925\ \Delta T + 3$ *for* $10^oC \leq \Delta T \leq 60^oC$ (3.13)
- $I_{sc} = 0.0066\ \Delta T – 0.0058$ *for* $10^oC \leq \Delta T \leq 70^oC$ (3.14)
- $R_s = V_{oc} / I_{sc} = (0.60925\ \Delta T + 3) / (0.0066\ \Delta T – 0.0058)$ (3.15)

As previously mentioned, the model consists of a voltage source V_{oc} and an internal

resistance R_s. The Simplified C Block is called using a menu in PSIM with the following path: Element\ Other\ Function Blocks\ Simplified C Block; it has a default of one input and 1 output. The Simplified C Block represents 24 thermoelectric generators in series; it has one input, which is the temperature difference dT. The output is set in 2 ports, which represent the voltage source V_{oc} and the internal resistance R_s. V_{oc} is given by equation (3.13), and R_s is given by equation (3.15). These equations are filled in the dialog box. Because the outputs of V_{oc} and R_s are numerical values, conversion into electric circuit is required via connecting it to a Voltage Control Voltage Source and a Variable Resistor R, as shown in Fig. 3.23.

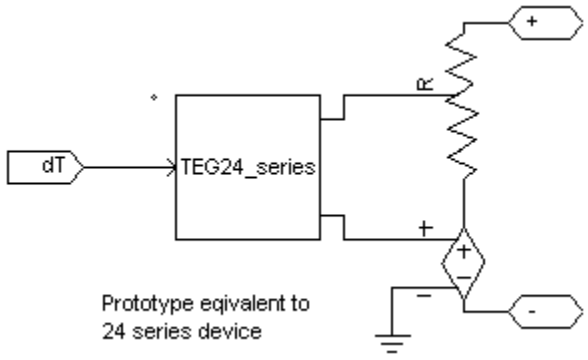

Fig.3.23 The model of the prototype representing 24 thermoelectric devices in series

To test the performance, a resistor variable R as a load is connected to the TEG 24 series of Simplified C Block, as given in Fig. 3.24. By applying the temperature difference dT1 and adjusting the resistor R from 0 Ω to the desired values, the terminal voltage (V_t), the load current (I_t), and the output power (P_t) can be obtained.

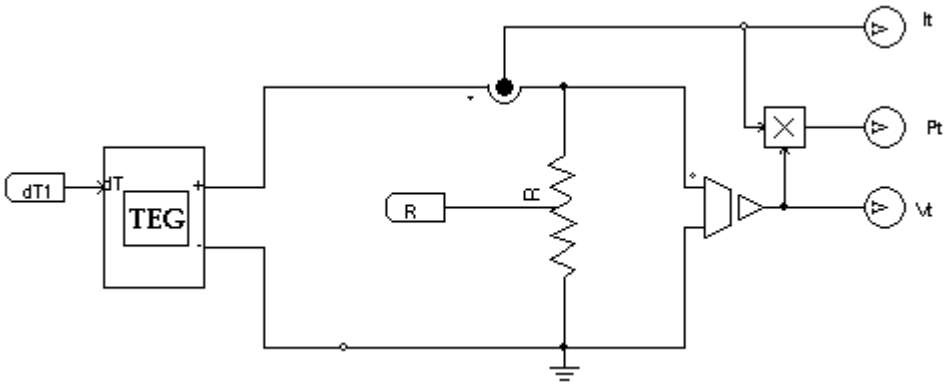

Fig. 3.24 The PSIM circuit of 24 TEGs in series with a variable resistor load

A model for strings or arrays of thermoelectric generators can also be developed in a PSIM circuit for simulation. The number of series and parallel of the prototype units can be set as desired. Fig. 3.25 shows an example of 2 x 3 units of the thermoelectric prototypes connected in series and parallel.

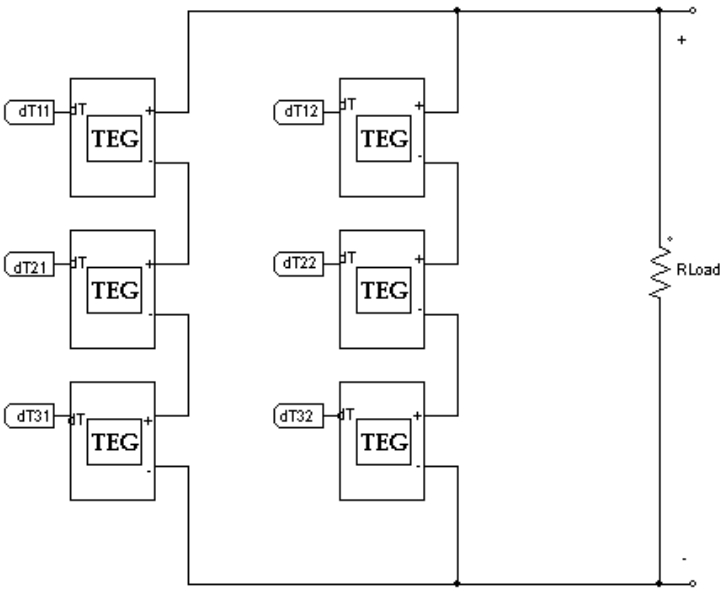

Fig. 3.25. PSIM model of 2 x 3 thermoelectric prototype units in series and parallel

By using the simulation circuit shown in Fig. 3.24, the temperature difference on each TEG can be set independently. The model simulates the condition of non-uniform temperature distribution, which is one of the focuses of discussion in this thesis.

3.7. Modeling of a Thermoelectric Panel

Similar to a photovoltaic system, a large thermoelectric system also contains arrays that consist of strings. The strings are constructed from panels and modules. Modeling of large thermoelectric systems is commenced from the basic model, which follows the V-I characteristics described in equation (3.18).

From equation (3.18), we can calculate the maximum power or other designed rated operations. For example, if a 70^{o}C temperature difference is applied to the

thermoelectric generator, the power can reach 5.2 Watts, with the terminal voltage of 24 Volts and the current of 0.22 Amperes. This model is used as the basic component to scale up into a model of a panel, string, or array. The operating point and basic construction of the thermoelectric system are determined as shown in Table 3.3.

Table 3.3. Operating point of thermoelectric systems at ΔT=70°C

	MODULE (Prototype)	PANEL	STRING	ARRAY
Power (Watts)	5.2	96	600	m x n x 600
Voltage (Volts)	24	120	720	m x 720
Current (Amps)	0.22	0.8	0.8	n x 0.8
Number of series circuit	24	5	6	m
Number of parallel circuits	1	4	1	n

The panel configuration of a thermoelectric generator given in Table 3.3 is comprised of 4 parallel lines, with each line containing 5 modules connected in series. Thus, a panel has 20 modules of thermoelectric generators, as shown in Fig. 3.26 (a). The panel supplies a load resistance R_p. When a line in the thermoelectric panel receives uniform irradiance, the response of each module will be the same. Therefore, each line containing 5 modules in series can be simplified by a single equivalent circuit of a thermoelectric generator. Because the panel has 4 parallel lines, the panel has 4 equivalent circuits that are connected in parallel, as depicted in Fig. 3.26 (b). The symbols V_{oc_L1}, V_{oc_L2}, V_{oc_L3}, and V_{oc_L4} represent the equivalent voltage sources at Line 1, Line 2, Line 3, and, Line 4, respectively. The same subscripts are applied for the equivalent internal resistances R_{s_L1} to R_{s_L4}.

If the temperature is distributed uniformly to the 4 parallel equivalent circuits, then the panel can be modeled with a single equivalent circuit, as illustrated in Fig. 3.26 (c). The subscript *P* in the symbols V_{oc_P}, R_{s_P}, and R_P denote Panel.

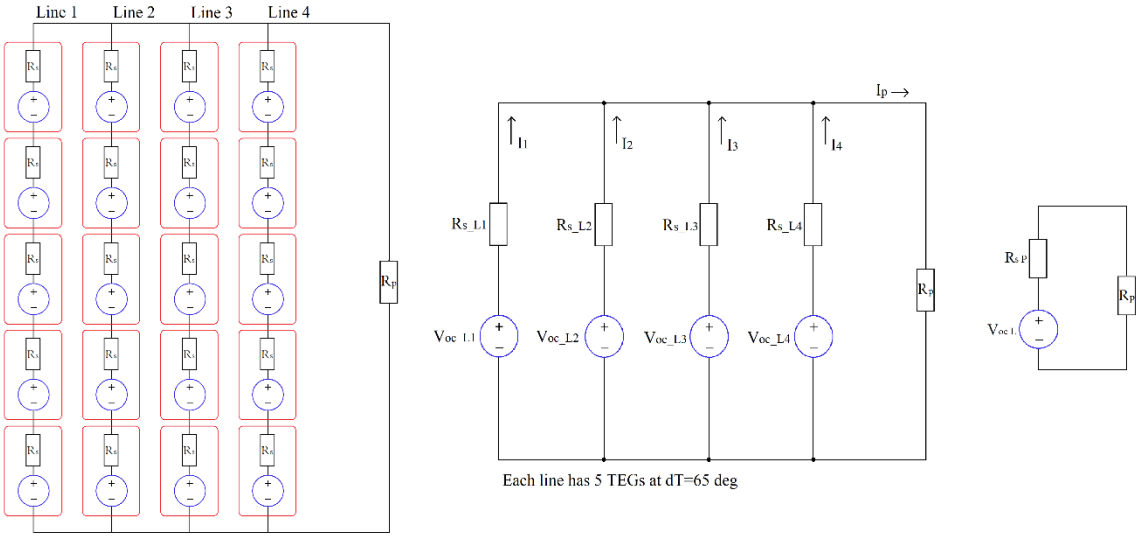

(a) (b) (c)

Fig. 3.26. Model of a thermoelectric panel under uniform heat: 96 Watts and 120 Volts (a) TEG configuration in a panel (b) a simplified circuit of a line (c) a simplified panel

The mathematical model of equivalent voltage source Line 1, V_{oc_L1} in Fig. 3.26 (b) is the multiplication of the single module open circuit voltage (V_{oc}) and the number of series connections (m). Similarly, the module resistance R_s is multiplied by the number of series connection ($m=5$), resulting in the equivalent resistance in the line. When the temperature is uniformly-distributed, the voltage sources V_{oc_L1} to V_{oc_L4} will have the same value of v_{oc_L}, and the internal resistance values of R_{S_L1} to R_{S_L4} are equal to R_{S_L}.

From equations (3.13) and (3.15), the components in Fig. 3.26 (b) can be written as follows:

$$V_{oc\_L} = V_{oc\_L1} = V_{oc} * m \quad (3.20)$$

$$V_{oc\_L} = (0.60925\ \Delta T + 3)\ 5 \quad (3.21)$$

$$R_{s\_L} = R_{s\_L1} = R_s * m \quad (3.22)$$

$$R_{s\_L} = (0.60925\ \Delta T + 3) / (0.0066\ \Delta T – 0.0058)\ 5 \quad (3.23)$$

In Fig. 3.26 (c), the panel equivalent voltage source V_{oc_P} has the same value as that of the single voltage source of the line V_{oc_L}. The equivalent internal resistance R_{s_P} of the entire panel is obtained from the line resistance R_{s_L} divided by the number of parallel lines, $n = 4$, as shown in Fig. 3.25 (b). The components in Fig. 3.26 (c) can be written as follows:

$$V_{oc\_P} = V_{oc\_L} = V_{oc} * m \quad (3.24)$$

$$V_{oc\_P} = (0.60925\ \Delta T + 3)\ 5 \quad (3.25)$$

$$R_{s\_P} = R_{s\_L} / n = R_s\ (m/n) \quad (3.26)$$

$$R_{s\_P} = (0.60925\ \Delta T + 3) / (0.0066\ \Delta T – 0.0058)\ (5/4) \quad (3.27)$$

The complete mathematical model of the thermoelectric panel to supply a resistive load with current I_p is expressed in equation (3.28). The terminal voltage of the panel is V_p, and the temperature difference is ΔT. The thermoelectric modules inside the panel are configured in n parallel lines, with each line containing m modules in series.

$$V_p = (0.60925\ \Delta T + 3)\ m - \{I_p\ (0.60925\ \Delta T + 3)/(0.0066\ \Delta T - 0.0058)\}\ (m/n) \qquad (3.28)$$

Each panel can generate approximately 100 Watts, 120 Volts, and 0.8 Amperes.

3.8. Modeling of a Thermoelectric String and a Thermoelectric Array

The structure of a string is similar to a thermoelectric panel. A string is comprised of n number of parallel lines, with each line having m number of series connected thermoelectric panels. According to Table 3.1, the string is designed to have 6 series panels and only one line, $m = 6$ and $n = 1$. The thermoelectric string is depicted in Fig. 3.27 as a single line containing 6 series panels. The string supplies current I_{s1} from the string of line 1, I_{s2} from the string of line 2, and I_{sn} from the last-end string. Each string generates a power of 600 Watts at 720 Volts. In this design, the array uses 6 strings; thus, the output power of the array is 3600 Watts. The string and array configuration is shown in Fig. 3.27.

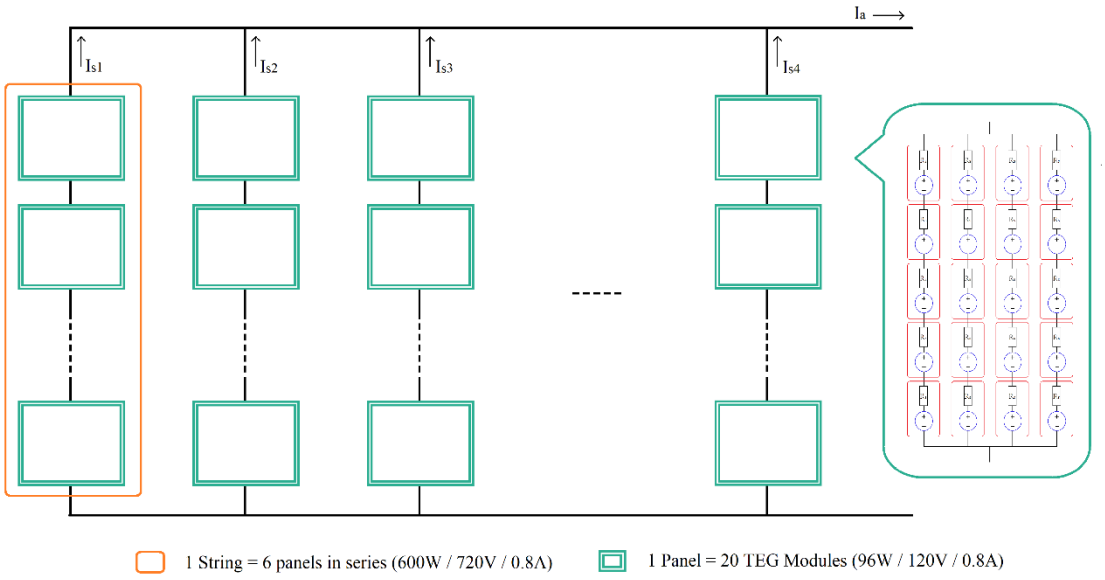

Fig. 3.27. Structure of the thermoelectric array, 3600 Watts/ 720 Volts

3.9. Conclusion

The proposed and developed methodology to model a single cell, module, and an array of TEG is presented in this chapter. The model uses an electric equivalent circuit and is based on electrical test procedures to determine the electric parameters. The steps consider laboratory tests of open and short circuits of a typical module under various gradient temperature. This results in a mathematical model for the output voltage, output current, and nonlinear curve of internal resistance as function of gradient temperature.

A prototype of thermoelectric generator containing 24 TEG modules connected in series with a peak voltage of 80V and a peak current of 2A was built for verification purposes. The prototype is attached with an electronic control system for arranging the heat source and temperature.

Comparison results from simulations and laboratory tests of the model are found very similar with error less than 5%. It indicates that the proposed TEG model is an effective one to represent the appropriate electrical characteristics of the TEG.

A simulation circuit model of TEG using software PSIM is also built. The model represents the prototype, the string, and the array of TEG systems.

CHAPTER 4
THERMOELECTRIC SYSTEM PERFORMANCE UNDER NON-UNIFORM TEMPERATURE DISTRIBUTION

The modeling of various thermoelectric systems was presented in Chapter 3. Chapter 4 deals with simulation results of the models under certain conditions. The panel and string of a thermoelectric system are treated under various load resistances and irradiances. The configurations are also pre-designed to receive a non-uniform heat distribution ranging from $\Delta T=15^{o}C$, $\Delta T=25^{o}C$, and $\Delta T=65^{o}C$.

4.1.Results V-I Characteristics of Thermoelectric Module

The performances of the thermoelectric prototype were investigated using the proposed model. The gradient temperature ΔT is set as $65^{o}C$, and the cold side temperature is maintained at $30^{o}C$. When we calculate each parameter, we find that V_{oc} is 42.6 Volts, and R_s = 99.7 Ohms, which are recalled from equations (3.13), (3.15), (3.18), and (3.19) as follows:

$$V_{oc} = 0.60925\ \Delta T + 3 \tag{3.13}$$

$$R_s = (0.60925\ \Delta T + 3) / (0.0066\ \Delta T - 0.0058) \tag{3.15}$$

$$V_t = (0.60925\ \Delta T + 3) - I_t\ (0.6982\ \Delta T + 3)/(0.0066\ \Delta T - 0.0058) \tag{3.18}$$

$$P_t = V_t\ I_t \tag{3.19}$$

The results of laboratory tests showed that the load resistance varies from 10Ω to 120Ω. The terminal voltage, current, and output power were measured. The measurement results are presented in Table 4.1. The simulated output can be calculated using equations (3.18) and (3.19).

Table. 4.1. Experimental tests of the prototype at ΔT = 65ºC under various loads

R (Ohm)	V_t (Volts)	I_t (Amps)	P_t (Watts)
20	9.3	0.343	3.216
30	11.2	0.324	3.629
40	13.5	0.310	4.185
50	14.7	0.300	4.410
60	15.5	0.289	4.480
70	17.0	0.274	4.658
80	18.0	0.260	4.680

R (Ohm)	V_t (Volts)	I_t (Amps)	P_t (Watts)
90	19.2	0.250	4.800
100	21.1	0.230	4.853
110	22.5	0.215	4.838
120	23.0	0.209	4.807
Open circuit	45.1	0.000	-
Short circuit	0.0	0.417	-

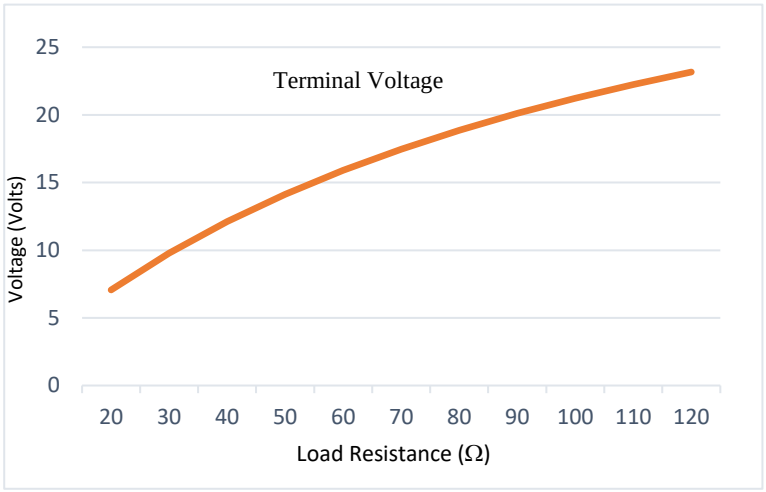

Fig. 4.1. The terminal voltage of the prototype at ΔT=65ºC for various load resistances

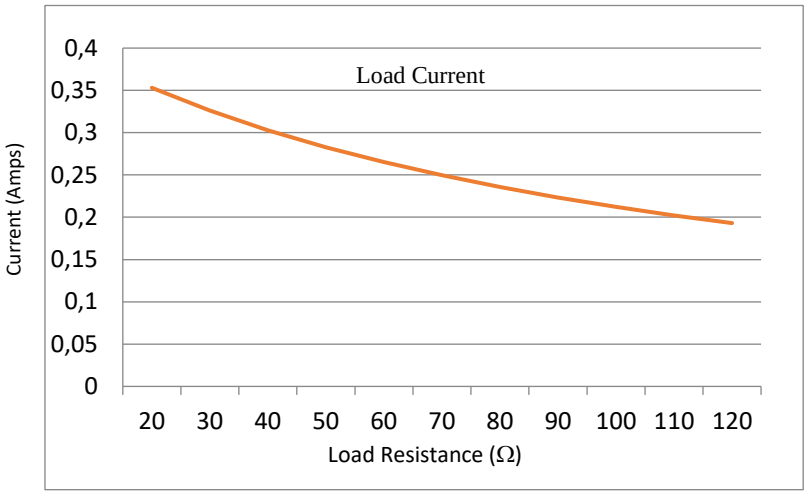

Fig. 4.2. The load current of the prototype at ΔT=65°C for various load resistances

Plots of the terminal voltage and load current are depicted in Fig. 4.1 and 4.2, respectively. The results from the prototype tests and those from the simulations prove to be very similar. The average error between the test and the simulation for the thermoelectric voltage is 7.1%, and the error for the load current is 6.9%. The output power as a function of the terminal voltage is illustrated in Fig. 4.3.

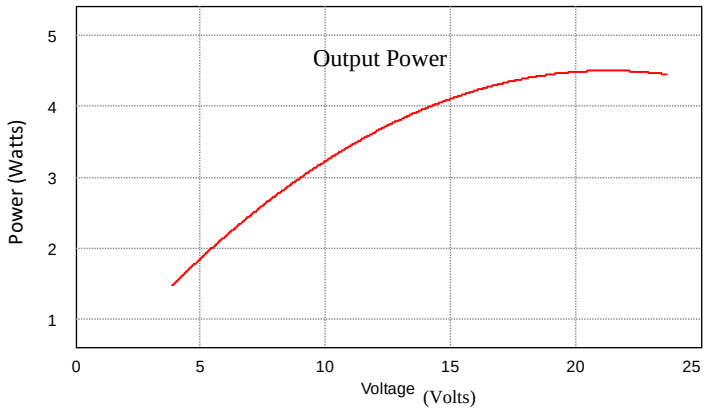

Fig. 4.3. Output power of the prototype at ΔT=65°C for various load resistances

4.2.Performance of a Thermoelectric Panel under a Non-Uniform Heat Distribution

A simulation of the thermoelectric panel was conducted, measuring its performance parameters when treated under non-uniform heat distribution. Heat changes received by the thermoelectric may occur in 3 conditions:

- Change of irradiance or the temperature magnitude;
- Change of the distribution;
- Both of the above concurrently.

The thermoelectric panel with the rated power of 96 Watts/120 Volts supplies a load resistance. The load varied from nearly short circuit to open circuit, from 10Ω to 2000Ω. The first condition is applied for a uniform heat distribution at constant ΔT = 65^{o}C. Next, a non-uniform temperature distribution was employed. The arrangement of 20 modules inside the panel that received different irradiances is clustered, as shown in Fig. 4.4. Line 1 consists of 5 modules in series, $TEG_{1.1}$ to $TEG_{1.5}$. Two of them, $TEG_{1.1}$ and $TEG_{1.2}$, are set to receive full irradiance ΔT = 65^{o}C, whereas the others in Line 1 receive the lowest irradiance, ΔT = 15^{o}C. In Line 2, there are 2 modules, $TEG_{2.4}$ and $TEG_{2.5}$, with lower gradient temperature at ΔT = 25^{o}C. Other modules are under full irradiances. This represents a non-uniform temperature distribution, which may occur frequently over a wide area of a hot surface, compared to solar insolation. The layout of arrangement is shown in Fig. 4.4. The groups of irradiances are given as follows:

Group 1: $\Delta T = 15^{o}C$ for $TEG_{1.3}$, $TEG_{1.4}$, $TEG_{1.5}$

Group 2: $\Delta T = 25^{o}C$ for $TEG_{2.4}$, $TEG_{2.5}$

Group 3: $\Delta T = 65^{o}C$ for the rest

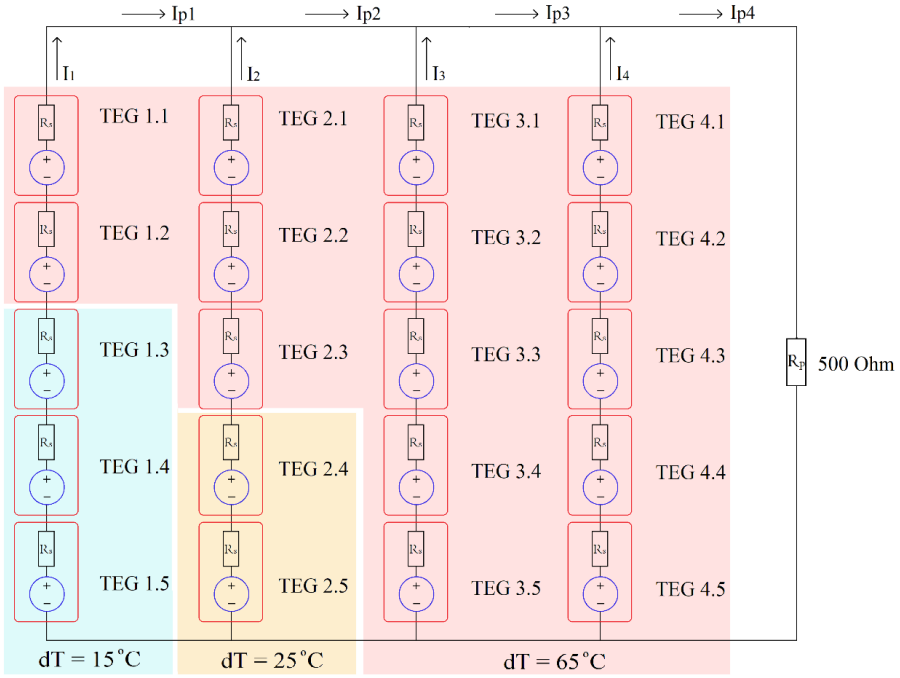

Fig. 4.4. Equivalent circuit of a TEG panel receiving energy from a non-uniform heat distribution

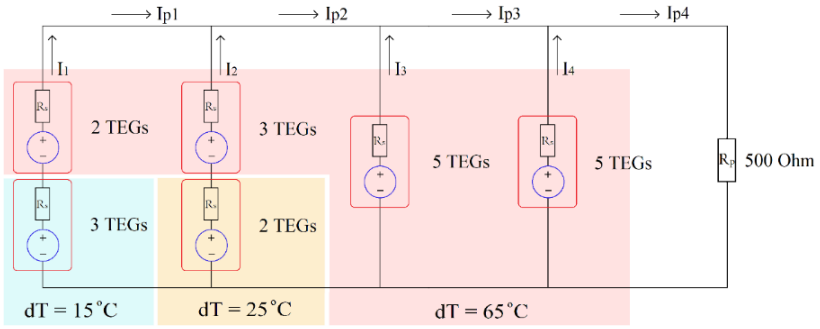

Fig. 4.5. Simplified circuit of a TEG panel under a non-uniform heat distribution

Fig. 4.5 shows the simplified version of Fig. 4.4. A thermoelectric device under uniform irradiance can be represented by a single equivalent circuit. This case makes the model simpler. This is also the solution when there is a limitation of the amount of memory, the number of nodes, and the number of sub-circuits used for a typical software package.

The model in Fig. 4.5 was run under the first condition, i.e., a uniform heat distribution for all the thermoelectric devices. However, the temperature difference varied at ΔT = 65°C, 50°C, 40°C, and 30°C. The output power produced when utilizing the temperature difference variation and various load resistances from 10Ω to 1500Ω is depicted in Fig. 4.6. As can be seen, the peak power when ΔT = 65°C is 90.1 Watts, and the voltage at the peak power is 106.8 Volts. The complete results are written in Table 4.2.

Table 4.2. Peak power and voltage under various temperature gradients

UNIFORM DISTRIBUTION	ΔT = 65°C	ΔT = 50°C	ΔT = 40°C	ΔT = 30°C
Peak Power, P_{peak} (Watts)	90.1	54.2	35.3	20.4
Voltage at P_{peak} (Volts)	106.8	108.0	109.2	111.6

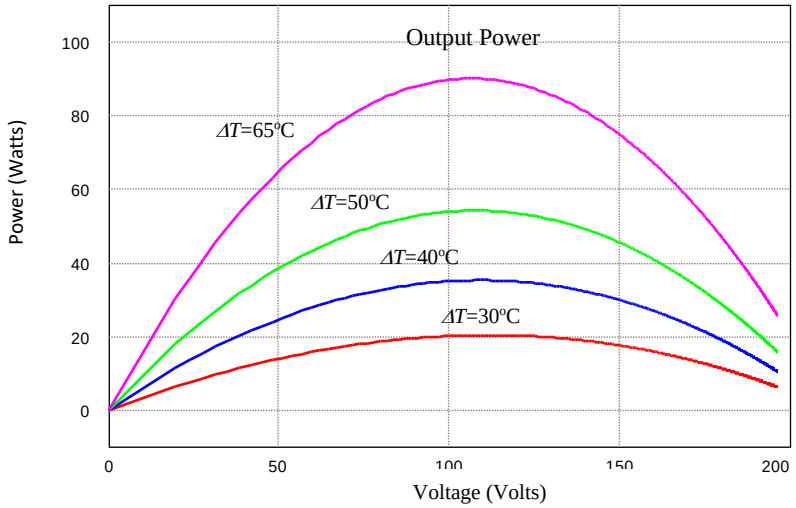

Fig. 4.6. Thermoelectric output power with uniform heat and various ΔT

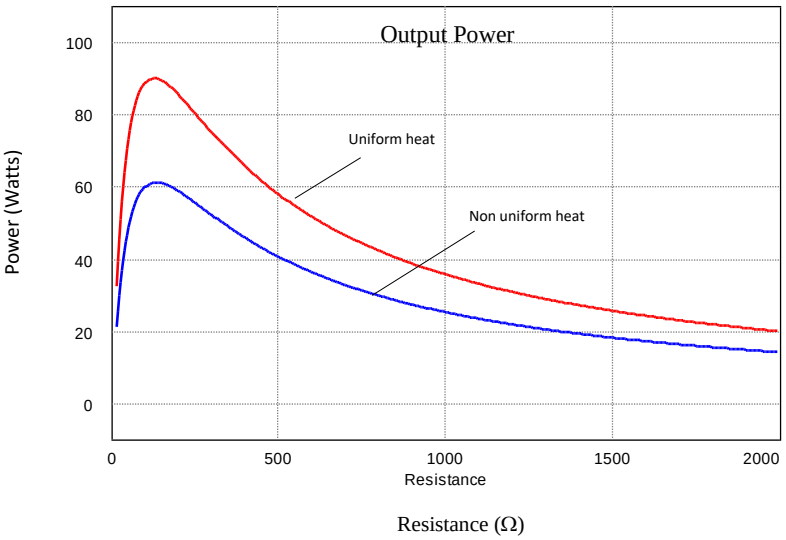

Fig. 4.7. Power of thermoelectric panel during load tests under a non-uniform heat distribution

For the second condition, the model was run under a non-uniform temperature distribution. Based on the model shown in Fig. 4.5, part of thermoelectric device is under a temperature gradient of ΔT = 15°C, with other parts being at ΔT = 25°C, and the remainder being at ΔT = 65°C. The output power of a non-uniform curve is shown below the uniform temperature, as depicted in Fig. 4.7. The peak power is reduced by

30%. The terminal voltage of the thermoelectric is shown in Fig. 4.8, and the load current is illustrated in Fig. 4.9.

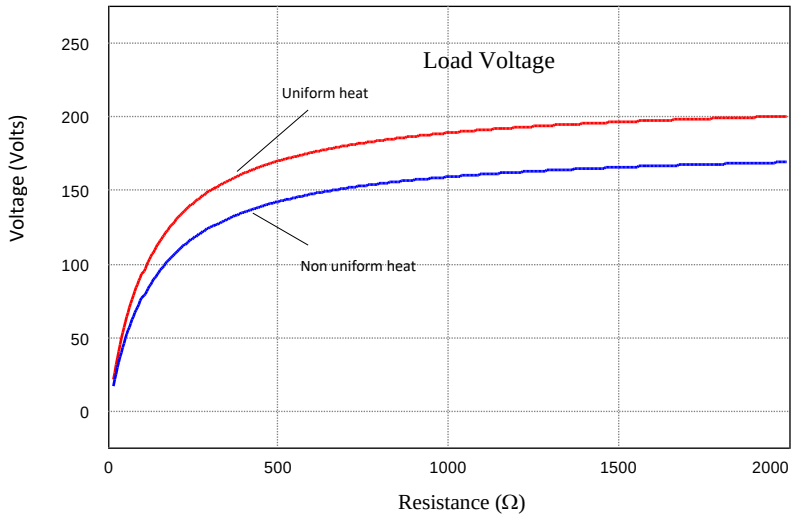

Fig. 4.8. Voltage of the thermoelectric panel during load tests under a non-uniform heat distribution

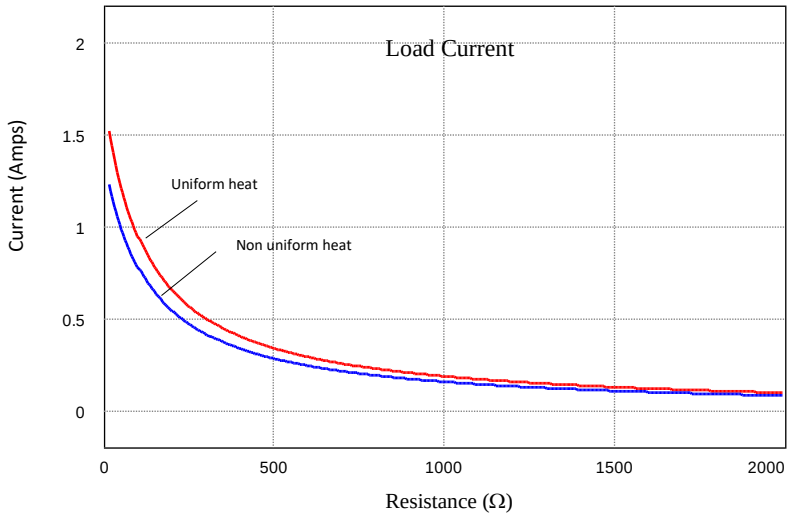

Fig. 4.9. Current of the thermoelectric panel during load tests under a non-uniform heat distribution

Running under a non-uniform heat distribution, the current in each line (as illustrated in Fig. 4.10) is investigated. Lines 3 & 4, which share an irradiance at ΔT = 65°C, contribute the largest current; they produce 0.4 Amps when the load resistance is 10Ω, and 0.09 Amps when the resistance is high. The curve of the current I_2 at Line 2 is below the currents in Lines 3 (I_3) & 4 (I_4). The curve from Line 1 deserves special attention; it contributes the lowest current because the thermoelectric receives the lowest gradient temperature of ΔT = 15°C. However, in certain conditions, the current changes from positive to negative polarity, i.e., the thermoelectric shifts from generating power into absorbing electric power.

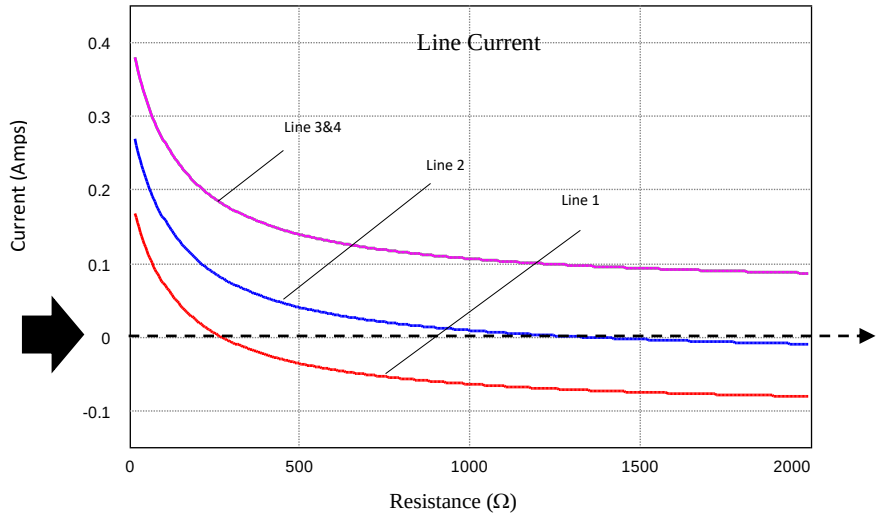

Fig. 4.10. The current of each line inside the TEG panel under non-uniform heat distribution

For the third condition, the model was under a dynamic temperature distribution. In the first stage, the thermoelectric generators were run uniformly under ΔT = 65°C; subsequently, the temperature distribution was changed to non-uniform, as shown in

Fig. 4.11. The output power was suddenly dropped around 30% when the non-uniform temperature was applied.

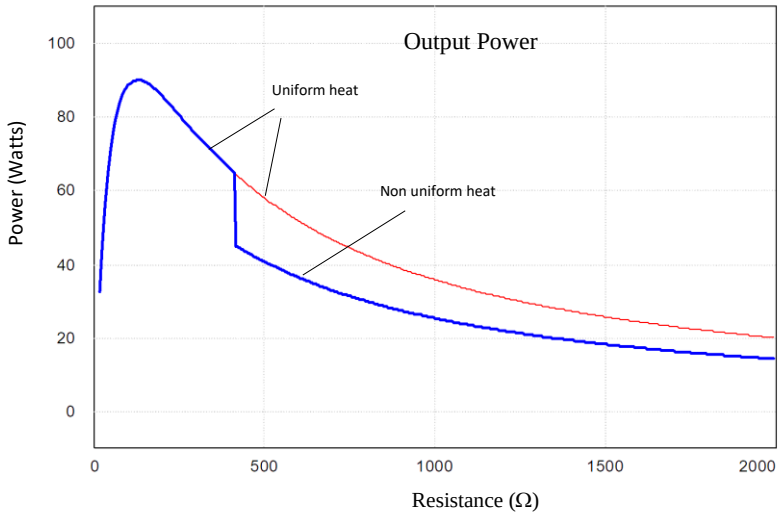

Fig. 4.11. The output power under a dynamical heat distribution

4.3. Conclusion

This chapter presented simulations of TEG system for high power application. The TEGs were arranged to form a panel, string, and array. The system was simulated to obtain the TEG characteristics under uniform and non-uniform heat distribution for various temperature differences, and loads.

Non-uniform heat distribution received by the thermoelectric array was simulated by separating the array into 3 parts. Each part is exposed to different temperatures. Then, the system is operated dynamically by changing the load.

It is found that under non-uniform heat distribution causes the output voltage and current to drop. The peak power of TEG system drops to 30% on a typical condition compared to the uniform heat distribution. In parallel connection of TEG systems, non-uniform heat distribution changes the TEG mode, from generating to consuming electric current when the TEG is receiving less heat compared to others.

CHAPTER 5
MAXIMIZING METHOD OF A THERMOELECTRIC GENERATOR

The previous chapter discussed the performances of a thermoelectric generator under uniform and non-uniform temperature distributions. The following two interesting findings were obtained:

1. In a typical condition, the parallel thermoelectric generator may shift from generating power to absorbing electric power. When the thermoelectric absorbs electricity, it acts as a heat pump.
2. The case of a non-uniform heat distribution results in lower output power of the thermoelectric generator compared to the case of a uniform distribution.

This chapter presents proposed solutions to improve the thermoelectric performances. Based on the findings, two methods for maximizing the output power of thermoelectric systems are introduced here.

5.1.Improvement using a Diode

A parallel operation with various conditions applied on the thermoelectric generators may lead them to supply electric power to each other. For a non-uniform heat distribution, this phenomenon of one thermoelectric generator powering another was demonstrated in the previous chapter. A diode is used to prevent the reverse current flow to the thermoelectric generator. A diode is connected in series in each line of the thermoelectric array, as shown in Fig. 5.1.

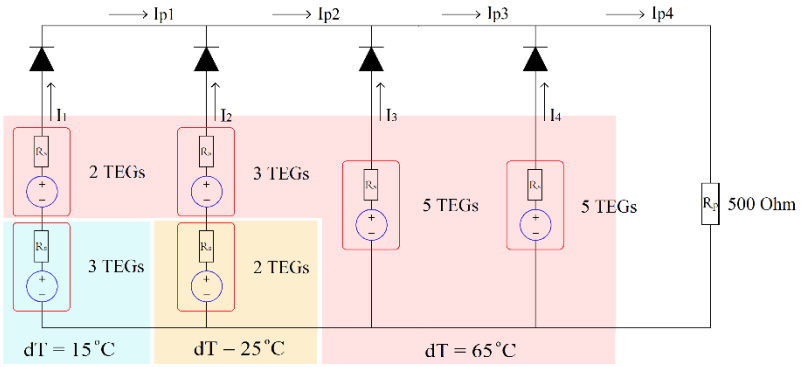

Fig. 5.1. Blocking diodes to prevent reverse current flowing through each thermoelectric generator

A comparison between a thermoelectric generator with a diode and without a diode was simulated. Fig. 5.2 shows that the output power of the model increased when a diode was attached to each thermoelectric generator. The curve tends to increase when the resistance is higher. In Fig. 5.3, the negative current is zero because it is blocked by the diode; this prevents the thermoelectric generator from operating in heating mode.

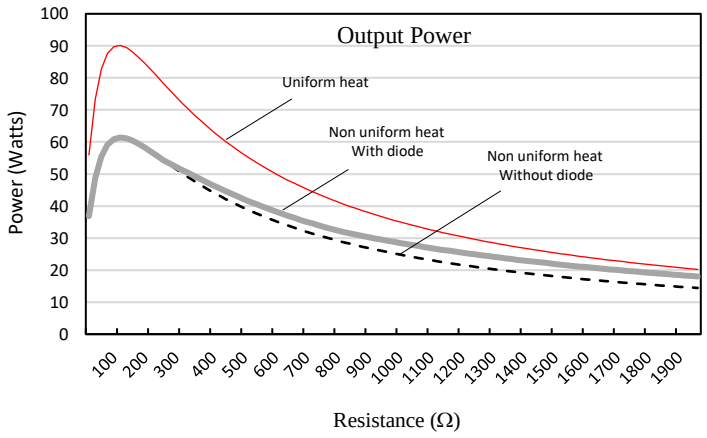

Fig. 5.2. The improved output power when a diode is attached

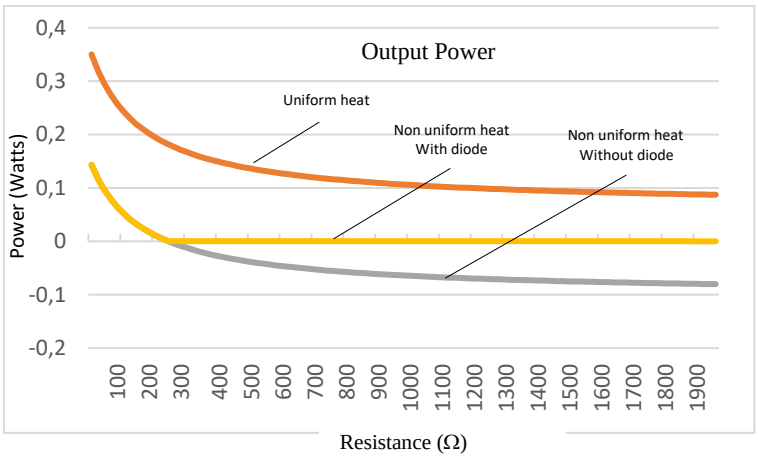

Fig. 5.3. The negative current of a thermoelectric generator was blocked by a diode

5.2.Improvement using MPPT

Harnessing electricity from thermal energy by employing a thermoelectric generator can be achieved at a conversion efficiency in the vicinity of 4% to 20%, depending on the thermoelectric type and the gradient temperature applied. It was demonstrated in the previous chapter that a typical non-uniform temperature distribution will reduce the power generation by 30%. Similar to photovoltaic systems, a maximum power point tracker (MPPT) is also needed for thermoelectric systems. MPPT works to increase or decrease the voltage of a thermoelectric generator so that the maximum power is obtained.

The occurrence of a non-uniform heat distribution over the large surface of a thermoelectric system may be more frequent compared to the occurrence of partially-shaded surfaces in a photovoltaic system. Different temperatures in different areas may occur at any time and may rapidly change because of the dynamic movements of flame, hot air, or other high temperature sources. A maximum power point tracker that

is able to accommodate temperature change and rapid change of irradiance is proposed. A diagram of an MPPT is shown in Fig. 5.4.

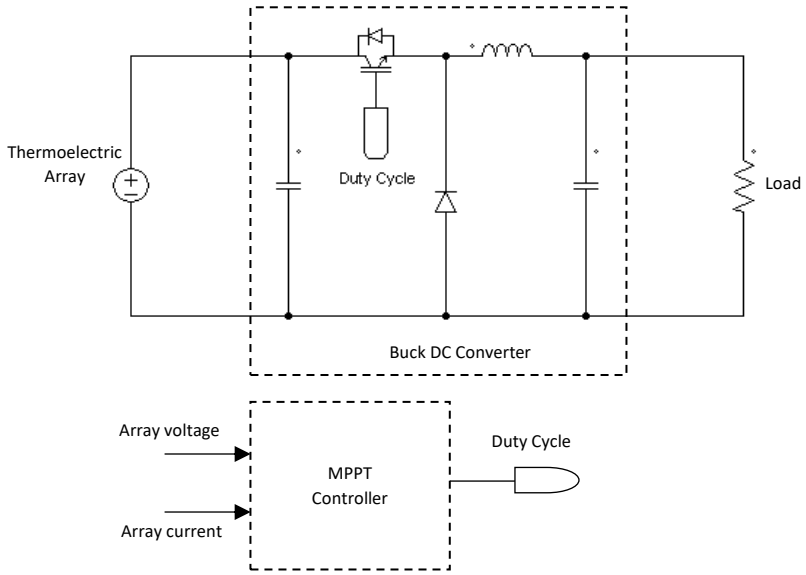

Fig. 5.4. MPPT with Buck DC-to-DC Converter and the controller

The DC-to-DC converter chops the array voltage through a semiconductor switch. The switch is turned on and off at the duty cycle, with pulse width modulation generated by the MPPT controller. Adjusting the duty cycle will adjust the average output voltage of the Buck converter. While chopping the array voltage, the controller also monitors the output power of the array. The duty cycle is regularly changed until the peak power of the array is reached.

The commonly used MPPT controller is a “search type”, which uses a searching method to catch the peak power, instead of a pre-determined power point or other predictive methods. Perturbed and Observed (P&O) is a well-known method that searches the maximum point by adding a constant increment or decrement to the duty

cycle. This method has the ability to effectively achieve the maximum power point. However, this method takes time when the peak position is far away from the latest position of search. When the maximum point has dynamically moved and rapidly shifted, the method may lag behind. Fig. 5.5 shows the principles of MPPT P&O type.

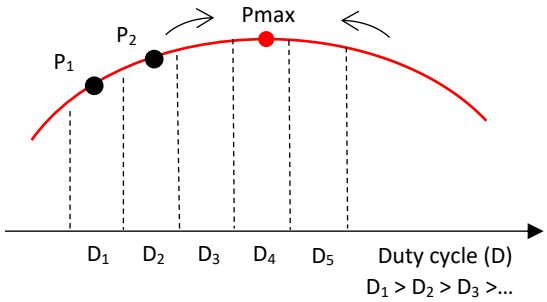

Fig. 5.5 Constant increment of the duty cycle to achieve the maximum power

Fig. 5.5 shows the concept of P&O MPPT when the dc converter is at low duty cycle to reach the peak power point of the thermoelectric generator (P_{max}). Initially, the duty cycle is set at D_1, resulting in the generated thermoelectric output power of P_1. Using a certain increment, for example 0.1 point, added to the duty cycle, D_1 becomes D_2. For this case, the measured output power is P_2. Subtracting the power second power from the first power (P_2–P_1) results in a positive value because $P_2 > P_1$. The duty cycle is continuously increased until the peak power point is achieved or passed through, as indicated by a negative value of the power subtraction. Once the peak power point is obtained, the duty cycle is decreased using a constant decrement. A problem arises when P_{max} dynamically moves or shifts to other positions according to the surface temperature. A wide area of hot surface tends to be a non-uniform distributed temperature. This situation may be different compared to the situation of a

photovoltaic system, for which the maximum power point commonly remains constant due to the relatively constant of sun ray irradiance.

The proposed MPPT offers a modification from the P&O method, namely, it employs an asymmetrical increment to the duty cycle. A constant increment is involved when the peak point is in the forward position, whereas a wide decrement is used after the peak power has been passed through. The MPPT controller of the modified Perturbed and Observed block diagram is shown in Fig. 5.6.

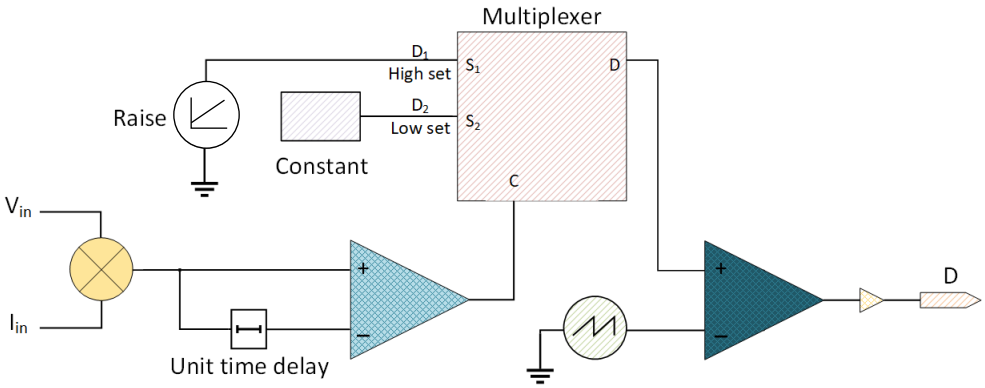

Fig. 5.6. The MPPT controller using the modified perturbed & observed method

Fig. 5.6 shows how the control system uses two inputs, *i.e.*, the voltage and current from the array. The multiplication of both results in the array output power. Prior to feeding the comparator, the output power is registered in the Unit Time Delay. The output powers from the recent and last calculation are compared. The comparator output signals “high” when the recent array power is higher than the last array power. The “high” signal drives the multiplexer (MUX) to connect the output with the “Hi-

set" duty cycle. The "Hi-set" applies a constant increment duty cycle to work for the PWM modulator. In this stage, the voltage of the DC converter is increased with constant increments until the maximum point is obtained.

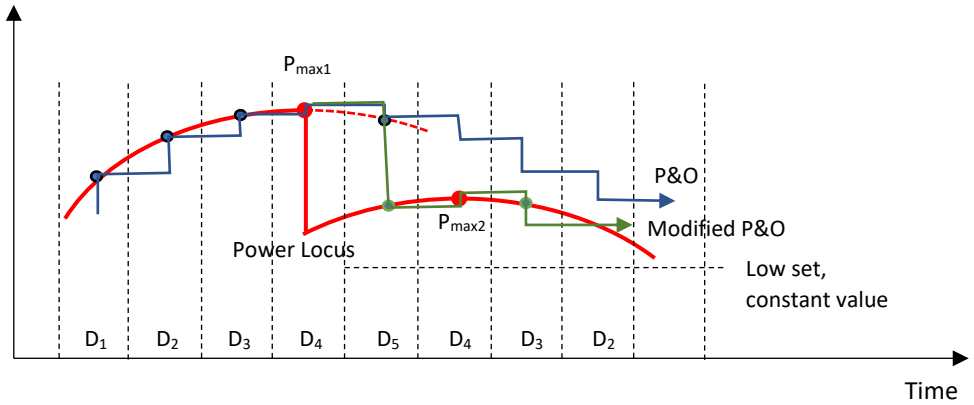

Fig. 5.7. Principles of the modified perturbed & observed method

An opposite condition occurs when the recent array power is lower than the previous data step, i.e., the maximum point has been passed through. The comparator signals "low", and the MUX connects the "Lo-set" to the multiplexer output. The "Lo-set" uses a constant value instead of a constant decrement. The trajectory to search a maximum power point is presented in Fig. 5.7. The power locus changes from P_{max1} to P_{max2}. Both P&O and the Modified P&O have the same trajectory when catching the maximum point from the lower power condition. Using the P&O method, P_{max2} can be reached after decreasing the duty cycle in 5 steps. However, applying the Modified P&O method, P_{max2} can be obtained in a shorter period, within 2 steps. After achieving the peak point, the modified P&O applies the Low set value to reset the duty cycle. It shows one period steps of calculation. The period will be repeated after the

algorithm finishes its cycle. The proposed method has the ability to cover deep changes of temperature variations because of its wide range of duty cycle configurations.

To demonstrate the performance, a thermoelectric array connected to an MPPT (as shown in Fig. 5.4) is simulated. The array uses one string consisting of 6 panels connected in series. Because the rated power of one panel is 100 Watts, 120 volts, the string outputs 600 Watts and 720 Volts. The load is varied dynamically from 200Ω, 600Ω, and 300Ω. The results of power-maximizing are shown in Fig. 5.8. This treatment is under a uniform temperature distribution heat at ΔT=65°C. When the load resistance is 200Ω, the array output power can be increased from 358 Watts without MPPT to 391 Watts with MPPT, i.e., an improvement of 9.2%. Fig. 5.9 depicts the voltage when an MPPT is connected to the thermoelectric string; it is slightly improved compared to the voltage without an MPPT.

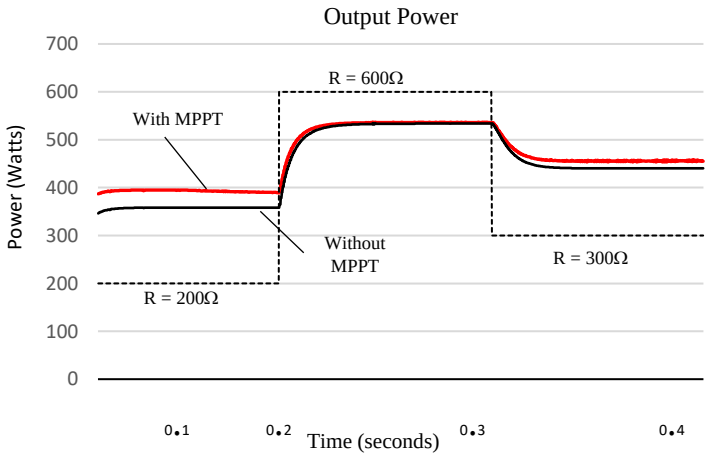

Fig. 5.8. The output power of a thermoelectric string under load change with an MPPT

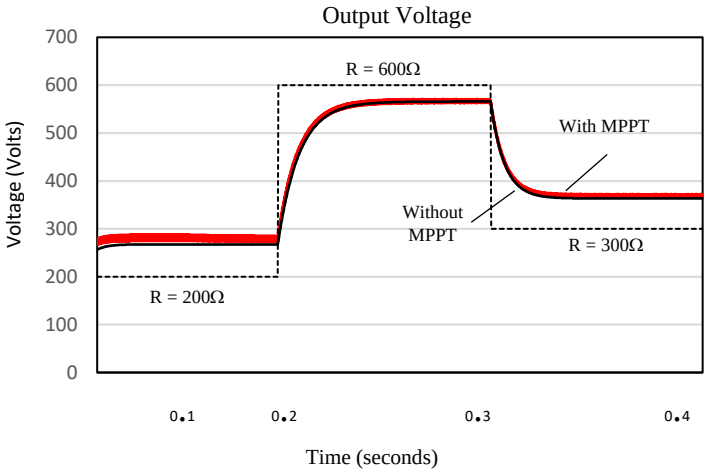

Fig. 5.9. The output voltage of a thermoelectric string attached to an MPPT under load change

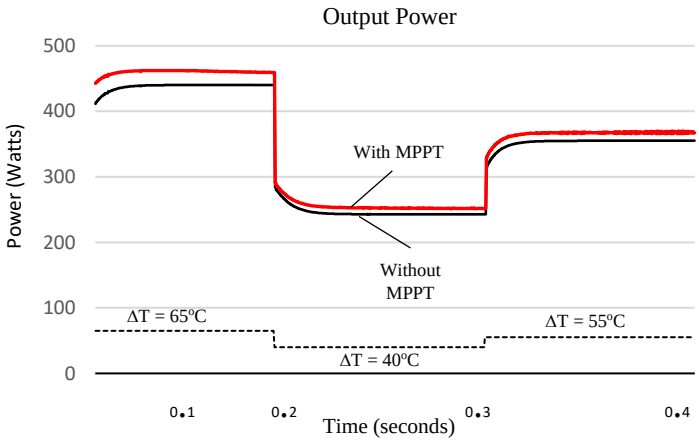

Fig. 5.10. The output power of a thermoelectric string under a non-uniform temperature with an MPPT

The thermoelectric string was also run under a non-uniform temperature distribution. One-third of the thermoelectric received a constant temperature difference at ΔT=65°C, while two-thirds received dynamically-varied gradient temperatures at ΔT=65°C, ΔT=40°C, and ΔT=55°C, as shown in Fig. 5.10. It can be seen that the MPPT

still works properly under this condition. The thermoelectric power is increased from 440 Watts without MPPT to 462 Watts with MPPT, i.e., an increase of 5%.

The complete proposed system is illustrated in Fig. 5.11; it employs a thermoelectric array with 6 strings. The total rated power is 3600 Watts, 720 Volts. An MPPT and an inverter grid-tie are embedded. A three-phase inverter of current-controlled type is used; it injects the power available in the thermoelectric array into the grid system. The bridge inverter and the control system are depicted in Fig. 5.12. The DC source of the inverter is the thermoelectric array, which is maximized by the MPPT. The amount of power injected to the grid must be equal to the output of the MPPT. Thus, the inverter control must coordinate between the grid and the MPPT. The power data available from the array is divided by the peak voltage of the grid, resulting in the amount of current used to regulate the 3-phase oscillator for controlling the current injected to the grid. Any changes in the array power will be automatically followed by the inverter.

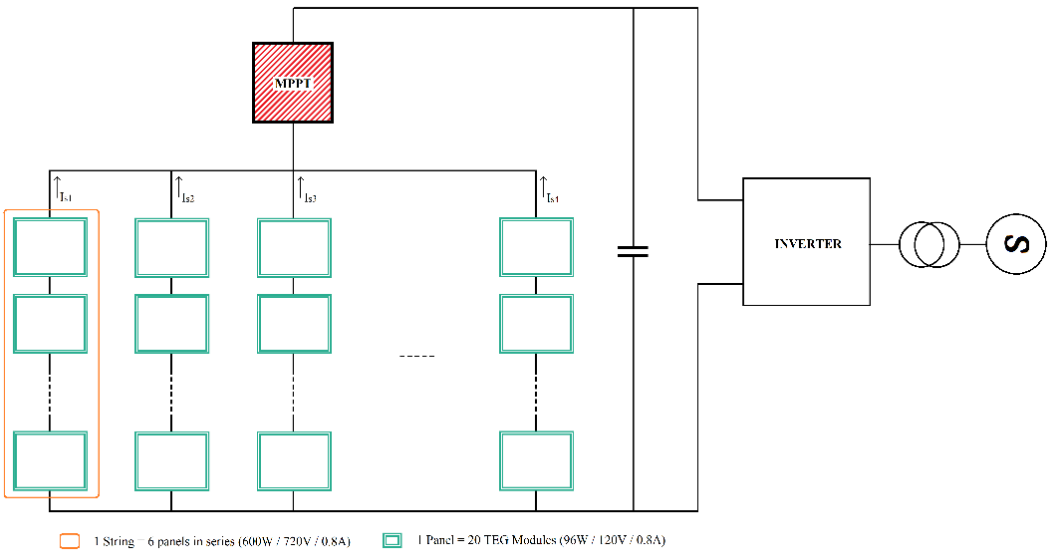

Fig. 5.11. A complete diagram of the proposed system

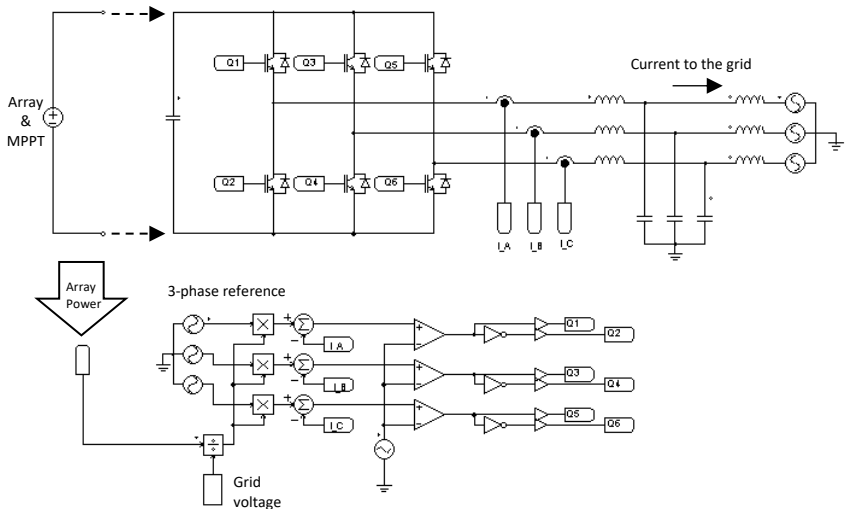

Fig. 5.12. The inverter and the control system

The results of the complete system when injecting power to the grid are shown in Fig. 5.13. The gradient temperature is deeply and rapidly changed. Initially, the gradient temperature is set at $\Delta T = 65^{o}C$; subsequently, it becomes $\Delta T = 40^{o}C$ and then increases again to $\Delta T = 55^{o}C$ for a total of 0.6 seconds.

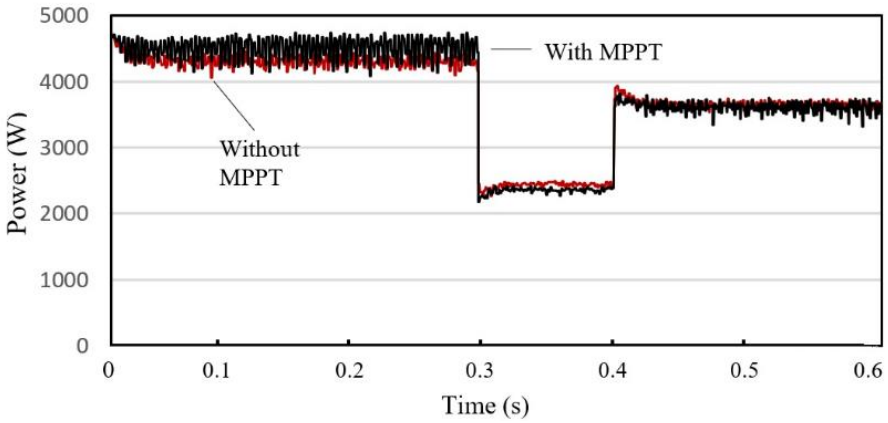

Fig. 5.13. Thermoelectric grid-connected system when encountering deep & rapid temperature changes

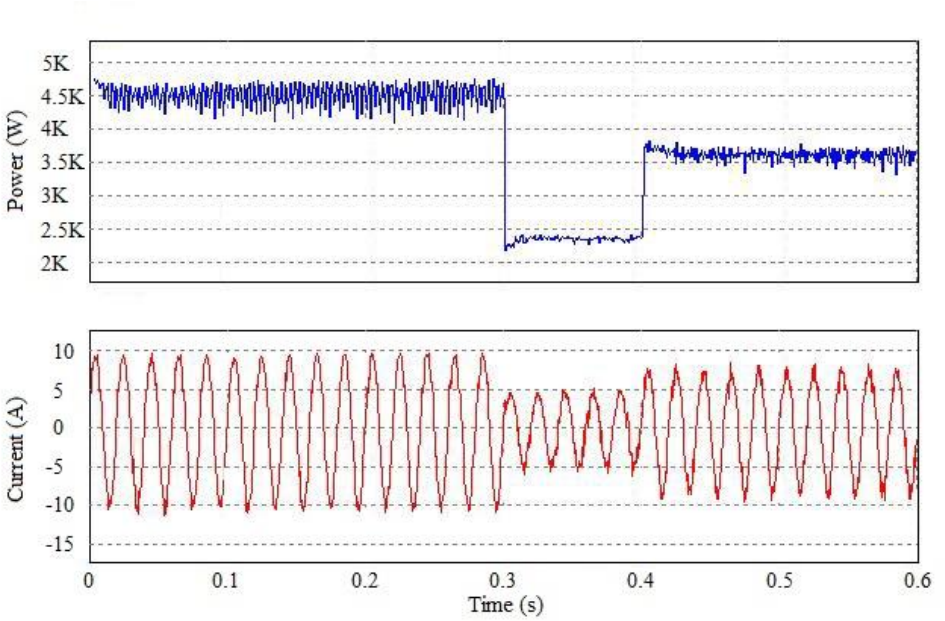

Fig. 5.14. The voltage and current waveform during the period of deep and rapid changes of temperature

Fig. 5.13 depicts the power transferred to the grid when the thermoelectric array received dynamically-changed temperatures. The available power is highlighted by the bold line, whereas the injected power is highlighted by the curve with hysteresis bands. The inverter injects power, adding to the one available from the thermoelectric array. During the sudden drop of gradient temperature, from 65^{o}C to 40^{o}C for only 0.2 seconds, the inverter control system still works properly to follow the array output.

5.3. Conclusion

A maximizing method of TEG system is proposed in this chapter. There are 2 schemes of maximizing method, e.g. employing a blocking diode, and using a maximum power point tracker (MPPT). The blocking diode is attached in every parallel TEG strings. Thus, it blocks the current flowing to the TEGs with mode of absorbing electric power.

The maximizing method using MPPT inserts a dc-to-dc converter between the terminal output of TEG array and the loads. The common perturbed and observed (P&O) MPPT works electronically to adjust the converter voltage in a constant increment or decrement duty cycle until the maximum output power is reached. However, the proposed modified P&O employs a constant low set value of duty cycle, instead of using decremental to catch the power point.

Simulation results show that the modified P&O scheme is effective to improve the output power of TEG system. Under uniform heat, the MPPT improves the output power of TEG up to 9%, while under non-uniform heat distribution, the MPPT still works to increase the power output by 5%. Simulations of the entire system that includes inverter for injecting the TEG power to the grid, demonstrate an effective operation. The injected power follows the available TEG array output under dynamically changing temperature differences.

CHAPTER 6
CONCLUSION

A model, a description of applications, and a maximizing technique of a thermoelectric generator system were presented in this thesis. In particular, the application of thermoelectric generators in a high-power, spatially-distributed generating system connected to the grid was considered. The modeling work involved the development of a thermoelectric model, testing of the model, and consideration of the use of the model in larger systems and applications.

A model of a thermoelectric generator system was proposed based on an equivalent electrical circuit. The elements of the model include an equivalent voltage source connected in series with an equivalent internal resistance. The parameters of the model were determined through open circuit and short circuit electrical tests under various temperature differences between the hot and cold surfaces of the thermoelectric systems. Based on the laboratory test results, formulas for the equivalent circuit were obtained. The model was tested using a prototype system; the results between them proved to be very close, with an average error of around 7%. A larger thermoelectric system was developed based on the proposed model. The design was expanded from the single device model to a module that consisted of 24 devices in series as a string and as an array of thermoelectric generators.

High-power applications require the configuration of a thermoelectric generator system to have each generator connected in series and in parallel to scale up the output power. However, parallel connections of thermoelectric generators may lead to the thermoelectric generators powering each other. Attaching a diode to each parallel line of thermoelectric generators was found to be a potential solution to this problem.

In high-power applications, a large surface area of thermoelectric generators exists to receive heat. Flame or high temperature with the characteristics of dynamic movements may lead to a non-uniform distribution of temperature. Such a non-uniform temperature distribution was considered to analyze the thermoelectric performance of a system. Under typical conditions, the case of a non-uniform heat distribution can reduce the output power by up to 30% compared to the case of a uniform heat distribution.

The use of a maximum power point tracker (MPPT) was proposed to maximize the output power of a thermoelectric system. By applying an asymmetrical incremental duty cycle, the MPPT has the ability to handle deep and rapid changes of temperature. The MPPT properly operates under various loads, various temperature differences, and dynamic operations involving those changes. The power extracted under typical conditions is around 9%, depending on the temperature gradient and load impedances.

6.1. Recommendations for future research

1. Large scale deployment of the TEG technology

   The study can include the challenges and opportunities regarding the utilization of a large system of Thermoelectric Generator for power generation in industrial applications.

2. Power system studies on Grid-tied TEG Syetem

   Detailed and more focused study regarding a TEG generation system that is connected to the grid.

3. More sophisticated MPPT technology connected to the cooling system

   In thermoelectric generator applications, the cooling system is also directly related to the power generation of the TEG. The cooling system considered in this thesis was only programmed to control the cold side of the TEG in order to maintain a certain temperature difference. In future research work, the cooling system can be connected with the MPPT to achieve a higher overall efficiency.

REFERENCES

1. H. J. Goldsmid. Introduction to thermoelectricity. Heidelberg, New York: Springer, 2010.
2. S. Dhoopagunta. Analytical Modeling and Numerical Simulation of a Thermoelectric Generator Including Contact Resistances. Master's Theses, Western Michigan University, December 2016.
3. Y. David. Modeling and Application of a Thermoelectric Generator MASc Thesis. 2011.
4. Xiaodong Jia, Quiuting Guo. Design Study of Bismuth-Telluride-based thermoelectric generators based on thermoelectric and mechanical performance. Energy, 190 (2020)
5. Yazawa, K.; Shakouri, A. Cost-efficiency trade-off and the design of thermoelectric power generators. Environ. Sci. Technol. 2011, 45, 7548–7553.
6. Nemir, D.; Beck, J. On the significance of the thermoelectric figure of merit z. J. Electron. Master.2010, 39, 1897–1901.
7. Austin Lee Jurgensmeyer. High efficiency thermoelectric devices fabricated using quantum well confinement techniques. Master thesis, Colorado State University, 2011
8. Buddhima Pasindu Gamarachchi. Thermoelectric system modelling and design. Master thesis, Boise State University, 2017

9. Tomas Katkus. Design and construction of high temperature thermoelectric power generator module characterization system. PhD thesis, University of Wollongong, 2015.
10. Gunay Omer, Abdullah Hakan Yavuzb, Rasit Ahiska, Kagan Ekrem Calisal. Smart thermoelectric waste heat generator: Design, simulation and cost analysis. Sustainable Energy Technologies and Assessments, Volume 37, February 2020
11. Daniel Champier. Thermoelectric generators: A review of applications. Energy Conversion and Management, Volume 140, 15 May 2017, Pages 167-181
12. Xiao Zhang, Li-Dong Zhao. Thermoelectric materials: energy conversion between heat and electricity. Journal of Materiomics1 (2015), 92-105.
13. Marco Nesarajah, Georg Frey. Thermoelectric power generation: Peltier element versus thermoelectric generator. IECON 2016 - 42nd Annual Conference of the IEEE Industrial Electronics Society.
14. Yancheng Wanga, Yaoguang Shi, Deqing Meia, Zichen Chen. Wearable thermoelectric generator to harvest body heat for powering a miniaturized accelerometer. Applied Energy, Volume 215, 1 April 2018, Pages 690-698
15. Antonino Proto, Daniele Bibbo, Martin Cerny, David Vala, Vladimir Kasik, Lukas Peter, Silvia Conforto, Maurizio Schmid, Marek Penhaker. Thermal Energy Harvesting on the Bodily Surfaces of Arms and Legs through a Wearable Thermo-Electric Generator. Journal Sensors, Volume 18, Issue 6 (June 2018)

16. Choong SunKim, Gyu SoupLee, HyeongdoChoi, Yong JunKim, Hyeong ManYang, Se HwanLim, Sang-GugLee, Byung JinCho. Structural design of a flexible thermoelectric power generator for wearable applications. Applied Energy, Volume 214, 15 March 2018, Pages 131-138
17. Abu Raihan Mohammad Siddique, Shohel Mahmud, Bill VanHeyst. A review of the state of the science on wearable thermoelectric power generators (TEGs) and their existing challenges. Renewable and Sustainable Energy Reviews, Volume 73, June 2017, Pages 730-744
18. Amin Nozariasbmarz, Henry Collins, Kelvin Dsouza, Mobarak Hossain Polash, Mahshid Hosseini, Melissa Hyland, Jie Liu, Abhishek Malhotra, Francisco Matos Ortiz, Farzad Mohaddes, Viswanath Padmanabhan Ramesh, Yasaman Sargolzaeiaval, Nicholas Snouwaert, Mehmet C.Özturk, Daryoosh Vashaee. Review of wearable thermoelectric energy harvesting: From body temperature to electronic systems. Applied Energy, Volume 258, 15 January 2020
19. Nesrine Jaziria, Ayda Boughamoura, Jens Müller, Brahim Mezghania, Fares Tounsia, Mohammed Ismaile. A comprehensive review of Thermoelectric Generators: Technologies and common applications. Energy Report, Elsevier, Dec 2019. https://doi.org/10.1016/j.egyr.2019.12.011
20. Vladimir Leonov. Thermoelectric Energy Harvesting of Human Body Heat for Wearable Sensor. IEEE Sensors Journal, VOL. 13, No. 6, June 2013

21. Vladimir Leonov. Human Machine and Thermoelectric Energy Scavenging for Wearable Devices. International Scholarly Research Network ISRN Renewable Energy Volume 2011, Article ID 785380
22. Mieke Van Bavel, Vladimir Leonov, Refet Firat Yazicioglu, Tom Torfs, Chris Van Hoof, Niels E. Posthuma and Ruud J. M. Vullers. Wearable Battery-free Wireless 2-Channel EEG Systems Powered by Energy Scavengers. Sensors & Transducers Journal, Vol. 94, Issue 7, July 2008, pp. 103-115.
23. Aime Lay-Ekuakille, Giuseppe Vendramin, Giuseppe Vendramin, Amerigo Trotta profile, Amerigo Trotta, Gabriella Mazzotta, Gabriella Mazzotta. Thermoelectric generator design based on power from body heat for biomedical autonomous devices. MEMEA '09: Proceedings of the 2009 IEEE International Workshop on Medical Measurements and Applications, May 2009 Pages 1–4.
24. Mikel Larrañaga Aizpurua, Zbigniew Leonowicz. Advanced Solar Energy Systems with Thermoelectric Generators. IEEE International Conference on Environment and Electrical Engineering and IEEE Industrial and Commercial Power Systems Europe (EEEIC / I&CPS Europe), Italy, 12-15 June 2018
25. Arash Edvin Risseh, Hans-Peter Nee, Christophe Goupil. Electrical Power Conditioning System for Thermoelectric Waste Heat Recovery in Commercial Vehicles. IEEE Transactions on Transportation Electrification, vol 4, issue 2, Jun 2018

26. Saket Kumar, Ashutosh Gupta, Gaurav Yadav, Hemender Pal Singh. Peltier module for refrigeration and heating using embedded system. International Conference on Recent Developments in Control, Automation and Power Engineering (RDCAPE), 12-13 March 2015
27. C. Liu, P. Chen, and K. Li. A 1 kW thermoelectric generator for low-temperature geothermal resources. Transactions - Geothermal Resources Council, 38:749-754, January 2014.
28. Siouane, S.; Jovanovic, S.; Poure, P. Fully electrical modeling of thermoelectric generators with contact thermal resistance under different operating conditions. J. Electron. Mater. 2017,46, 40–50
29. Siouane, S.; Jovanovic, S.; Poure, P. Equivalent electrical circuit of thermoelectric generators under constant heat flow. In Proceedings of the IEEE 16th International Conference in Environment and Electrical Engineering (EEEIC), Florence, Italy, 7–10 June 2016; pp. 1–6.
30. Saima Siouane, Slavisa Jovanovi´c and Philippe Poure, “Equivalent Electrical Circuits of Thermoelectric Generators under Different Operating Conditions”, Energies 10(3):386, March 2017.
31. Kaloyan Ivanov. Design, Realization and Study of Thermoelectric Watch. 2020 21st International Symposium on Electrical Apparatus & Technologies (SIELA). 3-6 Jun 2020.
32. Amin Nozariasbmarsk et all. “Review of Wearable Thermoelectric Energy Harvesting: From Body Temperature to Electronic Systems”, Applied Energy Volume 258, Elsevier, 15 January 2020.

33. João Paulo Carmo, Member, IEEE, Luis Miguel Gonçalves, and José Higino Correia, “Thermoelectric Microconverter for Energy Harvesting Systems”. IEEE Transactions on Industrial Electronics, VOL. 57, NO. 3, March 2010
34. Yancheng Wanga, Yaoguang Shi, Deqing Meia, Zichen Chen. Wearable thermoelectric generator to harvest body heat for powering a miniaturized accelerometer. Applied Energy, Volume 215, 1 April 2018, Pages 690-698
35. Vladimir Leonov, “Thermoelectric Energy Harvesting of Human Body Heat for Wearable Sensor”. IEEE Sensors Journal, VOL. 13, NO. 6, June 2013
36. Lukas Sigrist , Naomi Stricker , Dominic Bernath , Jan Beutel , and Lothar Thiele. Thermoelectric Energy Harvesting from Gradients in the Earth Surface. IEEE Transactions on Industrial Electronics, vol 67 (11), Nov 2020.
37. Asepta Surya Wardhana, Mochamad Ashari, Heri Suryoatmojo. Optimal Control of Robotic Arm System to Improve Flux Distribution on Dual Parabola Dish Concentrator. International Journal of Intelligent Engineering Systems. Vol 13 (1), Feb. 2020.
38. Arash Edvin Risseh, Hans-Peter Nee, Fellow, and ChristopheGoupil . Electrical Power Conditioning System for Thermoelectric Waste Heat Recovery in Commercial Vehicles. January 2018 IEEE Transactions on Transportation Electrification PP (99):1-1.
39. Min He, Enhua Wang, Yuanyin Zhang, Wen Zhang, Fujun Zhang, Changlu Zhao, “Performance analysis of a multilayer thermoelectric generator for exhaust heat recovery of a heavy-duty diesel engine”
40. M. Y. Fauzan, S. M. Muyeen, S. Islam, “Experimental Modelling of Grid-tied Thermoelectric Generator from Incinerator Waste Heat,” International

Journal of Smart Grid and Clean Energy, vol. 9, no. 2, March 2020, pp. 304-313.

41. HTflux, Daniel Rüdisser. Thermal simulation of a chimney flue with integrated combustion air channel. https://www.htflux.com/en/thermal-simulation-of-a-flue-chimney-with-combustion-air-channel/
42. Changwei Liu, Pingyun Chen, Kewen Li. “500 W low-temperature thermoelectric generator: Design and experimental study”. International Energy of Hidrogen Energy, 39, 2014.
43. Bradley Orr*, Aliakbar Akbarzadeh, “Prospects of waste heat recovery and power generation using thermoelectric generators”. Energy Procedia 110 (2017) 250 – 255. 1st International Conference on Energy and Power, ICEP2016, 14-16 December 2016, RMIT, University, Melbourne, Australia
44. Rong Shen, Xiaolong Gou, Haoyu Shu, Kuanrong Qiu. Dynamic performance analysis of a cascaded thermoelectric generator. Applied Energy 203, 1 Oct 2017, pages 808-815.
45. Hayati Mamur, Rasit Ahiska. Application of a DC–DC boost converter with maximum power point tracking for low power thermoelectric generators. Energy Conversion and Management, vol. 97, June 2015, pp 265-272
46. Bond, M.; Park, J.D. Current-sensorless power estimation and MPPT implementation for thermoelectric generators. IEEE Trans. Ind. Electron. 2015, 62, 5539–5548.
47. Qiping Wan ; Ying-Khai Teh ; Yuan Gao ; Philip K. T. Mok “Analysis and Design of a Thermoelectric Energy Harvesting System With Reconfigurable

Array of Thermoelectric Generators for IoT Applications", IEEE Transaction on circuits and systems , vol. 64 (9), 2017.

48. Rémy Rigo-Mariania, Sean Ooi Chea Wae, Stefano Mazzoni, Alessandro Romagnolia. Comparison of optimization frameworks for the design of a multi-energy microgrid. Applied Energy, 257 (2020).
49. Amit Kumer Podder, Naruttam Kumar Roy, Hemanshu Roy Pota. MPPT methods for solar PV systems: a critical review based on tracking nature. IET Renewable Power Generation, vol 13, issue 10, July 2019.
50. S Akbari, P C Thang, and D S Veselov. Maximum power point tracking for optimizing energy harvesting process. IOP Conf. Series: Materials Science and Engineering 151 (2016)
51. Ahteshamul Haque. Maximum Power Point Tracking (MPPT) Scheme for Solar Photovoltaic System. Energy Technology and Policy, I, 115-122, (2014).
52. A Rajagukguk, M Ashari, DC Riawan. Maximum Power Point Tracking control for stand-alone photovoltaic system using fuzzy sliding mode control. International Conference on Information Technology, Computer, and Electrical Engineering, 2014.
53. M Ashari, S Anam, Surojo. A wide range fuzzy based maximum power point tracker for improving the efficiency and sizing of PV systems. Journal of Electrical Engineering 11 (2), 2010.

54. Abdullah M. Noman, Khaled E. Addoweesh, Hussein M. Mashaly. DSPACE Real-Time Implementation of MPPT-Based FLC Method. Journal of Photoenergy. 2013

55. Lijun Zhang, Samson Shenglong Yu, Tat Kei Chau, Tyrone Fernando and Herbert Ho-Ching Iu. An advanced incremental conductance MPPT technique considering time-varying solar irradiances. International Conference on Smart Power & Internet Energy Systems, IOP Conf. Series: Earth and Environmental Science 322 (2019).

56. Guiza Dhaouadi, Djamel Ounnas, Youcef Soufi, Chenikhe Salah. Implementation of Incremental Conductance Based MPPT Algorithm for Photovoltaic System. The 4th International Conference on Power Electronics and their Applications (ICPEA), Turkey, 2019.

57. S. Kaku, S. Hashimoto, K. Yoshida. PWM sinusoidal inverter with modulation switching and carrier frequency modulation. IEEE. International Conference on Power Electronic Drives and Energy Systems for Industrial Growth, 1998. Proceedings. Dec. 1998.

58. Rashid, M. Power Electronics Handbook. Academic Press. 2001.

59. Raju, N.I, Islam, N.S. Sinusoidal pwm signal generation technique for three phase voltage source inverter with analog circuit & simulation of pwm inverter for standalone load & micro-grid system. International Journal of Renewable Energy Research. January 2013.

60. Chemmangot V Nayar, Mochamad Ashari, WWL Keerthipala. A grid-interactive photovoltaic uninterruptible power supply system using battery storage and a backup diesel generator. IEEE Transactions on Energy Conversion, vol. 15 (3), 2000.
61. Mochamad Ashari, WL Keerthipala, Chernmangot V Nayar. A single phase parallely connected uninterruptible power supply/demand side management system. IEEE Transactions on Energy Conversion, vol. 15 (1), 2000.
62. Qing Liu, Tommaso Caldognetto. Review and Comparison of Grid-Tied Inverter Controllers in Microgrids. IEEE Transaction on Power Electronics, Vol. 35 (7), July 2020.
63. Alon Kuperman. Proportional-Resonant Current Controllers Design based on Desired Transient Performance. IEEE Transactions on Power Electronics 30(10):1-1. October 2015.
64. Masoud Yazdanian and Ali Mehrizi-Sani. Internal Model-Based Current Control of the RL Filter-Based Voltage-Sourced Converter. IEEE Transactions on Energy Conversion 29(4):873-881. December 2014.
65. Xiongfei Wang, Lennart Harnefors, Frede Blaabjerg. Unified Impedance Model of Grid-Connected Voltage-Source Converters. IEEE Transactions on Power Electronics, VOL. 33, NO. 2, February 2018.
66. Markku J. Lampien. Thermodynamic Analysis of Thermoelectric Generator. Journal of Applied Physics, 69, 4318. January 1991.
67. Sagi Samlas, Anilkumar S.H., Comparative Evaluation of Different Design Configurations for a Solid Waste Incinerator. International Confrence on

Green Computing, Communication and Conservation of Energy (ICGCE). 2013

PUBLICATIONS ARISING FROM THIS THESIS

Journal papers

1. M. Y. Fauzan, S. M. Muyeen, S. Islam, "Experimental Modelling of Grid-tied Thermoelectric Generator from Incinerator Waste Heat," International Journal of Smart Grid and Clean Energy, vol. 9, no. 2, March 2020, pp. 304-313.
2. M. Y. Fauzan, S. M. Muyeen, S. Islam, "Enhanced Power Extraction from Thermoelectric Generators Considering Non-uniform Heat Distribution," Journal of Energy Conversion & Management, Elsevier, 2021.

Conference papers

1. M. Y. Fauzan, S. Islam, S. M. Muyeen, A. S. Wardhana, Soedibyo, M. Ashari, "Experimental Modeling of Nano Power Generation using Thermoelectric Generator (TEG) from Incinerator Waste Heat," International Seminar on Intelligent Technology and Its Applications (ISITIA), Bali, Indonesia, 2019.

APPENDIX

Results from experiment with temperature differences varied are given in Fig. A to Fig. L

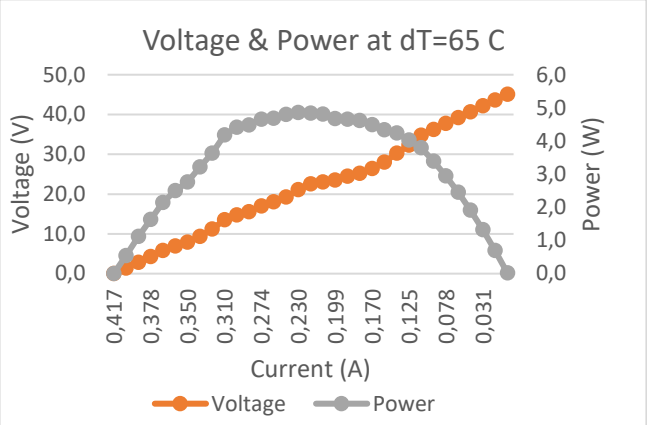

Fig. A. Volatge & power at ΔT 65C

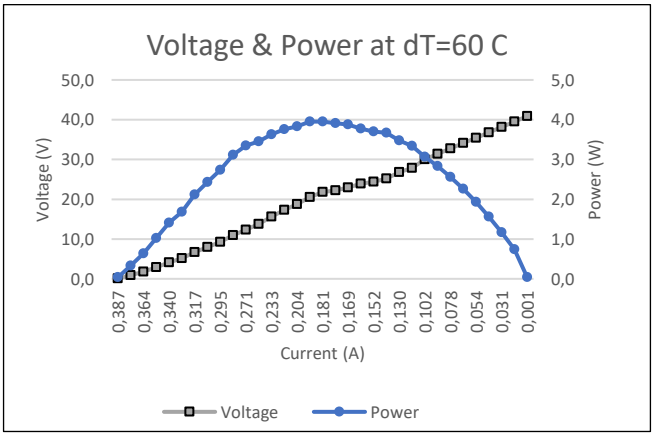

Fig. B. Volatge & power at ΔT 60C

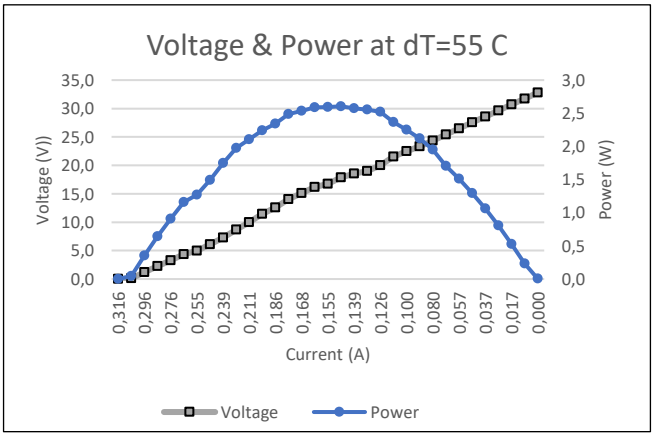

Fig. C. Volatge & power at ΔT 55C

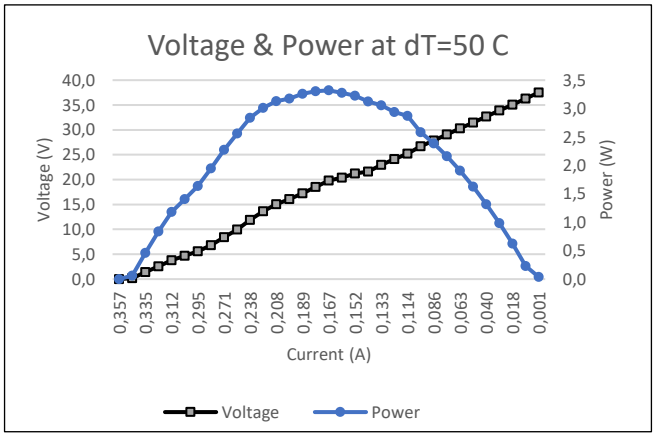

Fig. D. Volatge & power at ΔT 50C

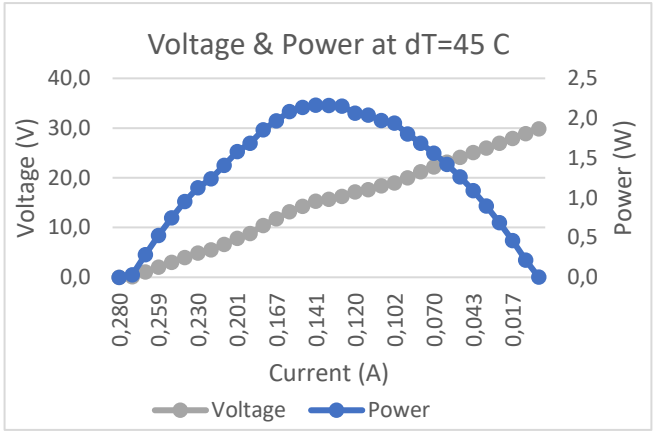

Fig. E. Volatge & power at ΔT 45C

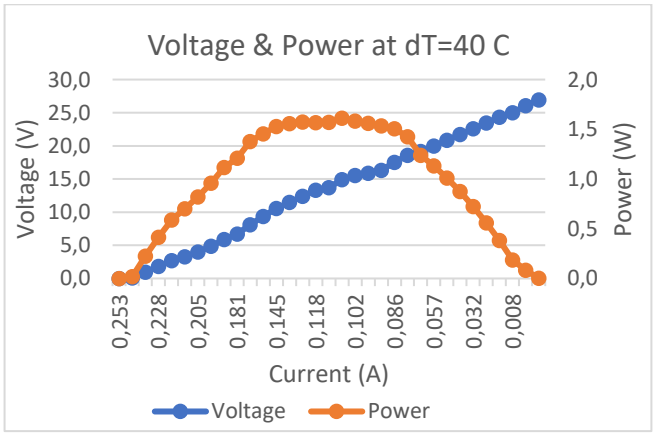

Fig. F. Volatge & power at ΔT 40C

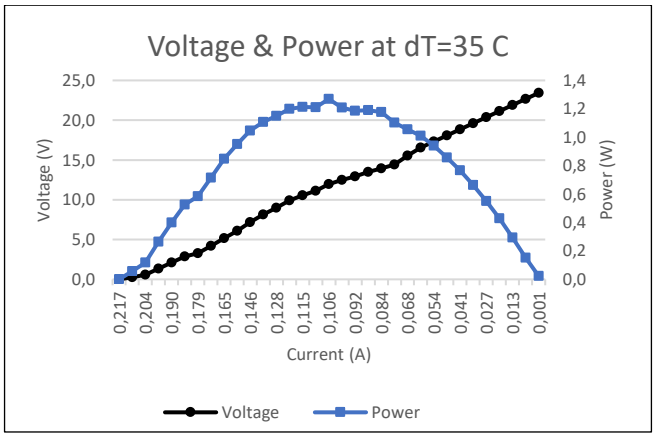

Fig. G. Volatge & power at ΔT 35C

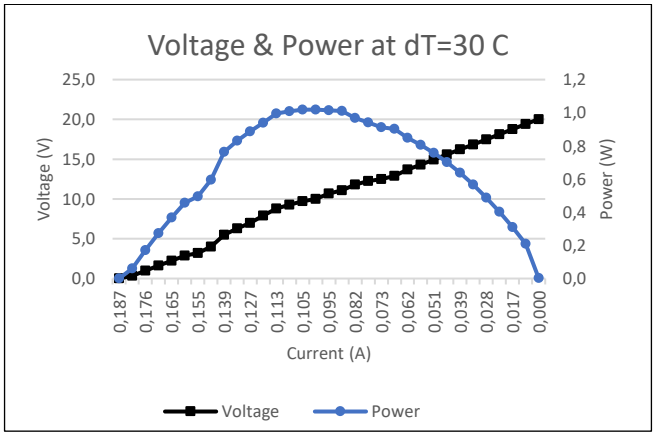

Fig. H. Volatge & power at ΔT 30C

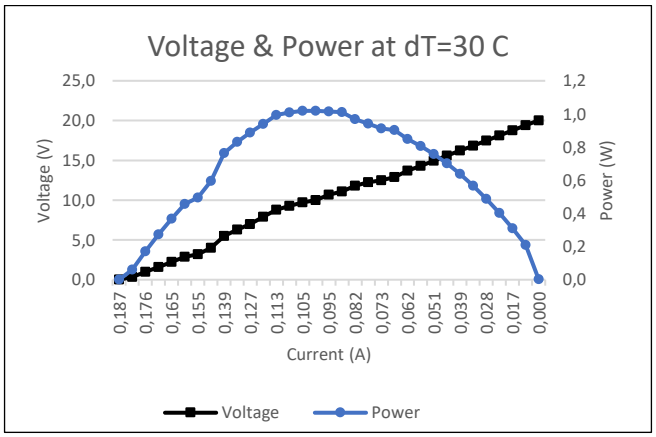

Fig. I. Volatge & power at ΔT 30C

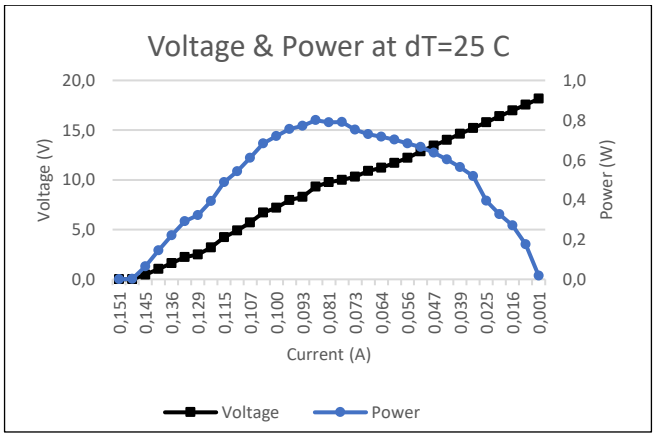

Fig. J. Volatge & power at ΔT 25C

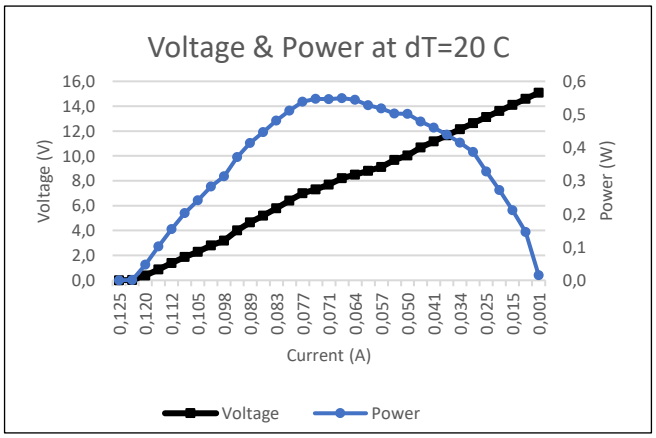

Fig. K. Volatge & power at ΔT 20C

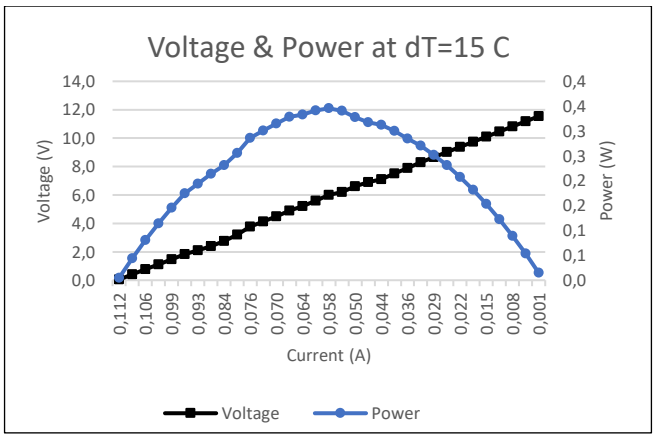

Fig. L. Volatge & power at ΔT 15C

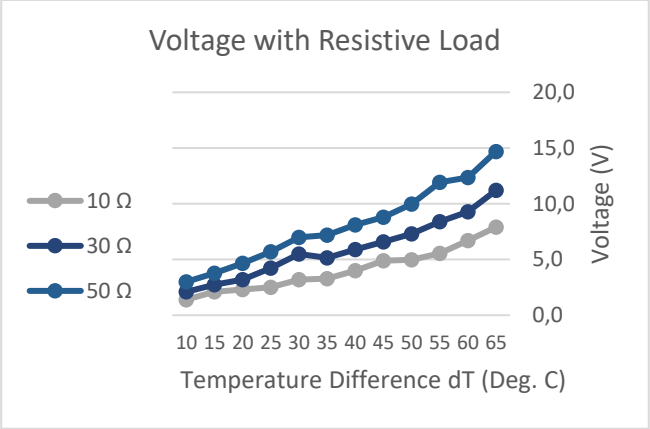

Fig. M. Volatge with resistive load at varied ΔT

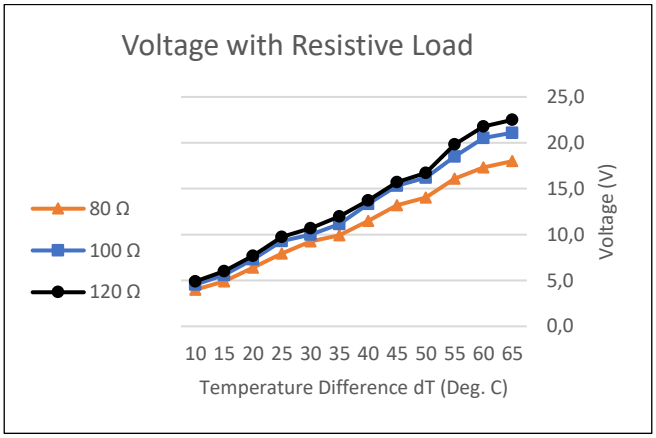

Fig. N. Volatge with resistive load at varied ΔT

To Whom It May Concern, I, Miftah Yama Fauzan, contributed the most parts of the papers including conceptualisation, experimentation, simulation, validation, and the writing to the paper/publication entitled “Experimental Modelling of Grid-tied Thermoelectric Generator from Incinerator Waste Heat”, published in International Journal of Smart Grid and Clean Energy, 2020, and “Enhanced Power Extraction from Thermoelectric Generators Considering Non-uniform Heat Distribution,” Journal of Energy Conversion & Management, Elsevier, 2021.

Miftah Yama Fauzan

I, as a Co-Author, endorse that this level of contribution by the candidate indicated above is appropriate.

S.M. Muyeen

Syed M. Islam